Bridging Research Gaps in Air Pollution Analysis: Methods, Models, and Low-Cost Solutions

Bujin Bekbulat

A dissertation

submitted in partial fulfillment of

the requirements for the degree of

Doctor of Philosophy

University of Washington

2024

Reading Committee:

Julian D. Marshall, Chair

Timothy V. Larson

Jessica Kaminsky

Program Authorized to Offer Degree:

Department of Civil and Environmental Engineering

University of Washington

Abstract

Bridging Research Gaps in Air Pollution Analysis:
Methods, Models, and Low-Cost Solutions

Bujin Bekbulat

Chair of the Supervisory Committee:
Julian D. Marshall
Department of Civil and Environmental Engineering

To address ambient and household air pollution, countries have implemented diverse strategies such as emissions regulations, fuel bans, and the adoption of cleaner cooking technologies. Although these efforts have markedly improved air quality, significant research gaps persist in quantifying the effects of these interventions and in forecasting outcomes to determine the most beneficial policies. This gap is largely due in part to the scarcity of accessible, user-friendly tools that can accurately measure and link changes in air pollution with specific initiatives.

This dissertation is structured around three main projects that employ innovative methods to advance our understanding of changes in air pollution exposure resulting from various interventions across different countries. It seeks to bridge these research gaps by enhancing data analysis techniques and developing cost-effective, low-maintenance air pollution sensors that can inform effective policy and technological solutions.

Chapter 1 provides an overview of current accountability analysis methods, outlining the motivation, objectives, and approaches of the dissertation.

Chapter 2 introduces a method for estimating "expected" or baseline concentrations to determine what air quality levels would have been if a specific event or intervention had not occurred. This methodology was used to evaluate changes in pollutant levels in the US during the initial months of the Covid-19 pandemic, when state governments issued stay-at-home orders. Comparing "expected" concentrations—calculated using this method— with the actual observed concentrations during the stay-at-home period, the analysis found that while $PM_{2.5}$ levels were slightly higher than anticipated, the levels of O_3, CO, NO_2, and PM_{10} were lower (though amounts varied by pollutant). This chapter highlights the significant impact of reduced human activity on air quality and emphasizes the critical role of methodological choices in shaping research findings.

Chapter 3 unveils the updated InMAP Source Receptor Matrix (ISRM), a comprehensive library of pre-run simulations using the reduced complexity model, InMAP. This innovative tool allows for rapid analysis of emission reduction scenarios and swift calculation of health outcomes; model runs that would require days or weeks with conventional approaches can require only a few minutes with the ISRM. The chapter uses the new ISRM to attribute air pollution-related mortality from 2002 to 2019 to various economic sectors. The findings indicate significant reductions in mortality attributable to decreased emissions primarily in the transportation and electricity sectors, yet with an emissions increase in the food and agriculture sector. This chapter corroborates the ISRM against conventional modeling and against measured concentrations and illustrates the practical utility of the ISRM.

Chapter 4 explores the development of the Washington Passive Sampler (WPS), an ultra-low-cost measurement tool designed to assess black carbon levels in resource-constrained, high-pollution settings. This innovative method involves image-based processing, wherein a cellulose fiber filter is photographed before and after deployment. The subsequent analysis of changes in pixel intensity on these images is used to estimate the amount of light-absorbing carbon. Field tests have quantified the method's precision and accuracy: it achieved an Intraclass Correlation Coefficient (ICC) of 90% for duplicate measurements, indicating good precision, and, indicating accuracy, a Root Mean Square Error (RMSE) of 21%, compared to 10% for gold-standard reference measurements. The chapter discusses how the WPS provides household air pollution researchers with an accessible, user-friendly tool for use in intervention studies, potentially transforming research approaches in low-resource high-pollution environments.

Overall, this body of work contributes valuable methodologies and tools to the field of air pollution research, supporting more effective policy-making and global health improvements. Chapter 5 summarizes the dissertation and suggests the next steps for this research.

Dedicated to Dad.

Acknowledgments

Reflecting on my years at the University of Washington, I am deeply aware that my achievements, particularly this dissertation, would not have been possible without the guidance of insightful mentors, the support of caring friends, and the unwavering encouragement of my family. While no words can truly capture the depth of my gratitude, I would like to humbly acknowledge those who have inspired me, guided me, and kept me grounded throughout this journey. Your impact on my life and work is something I will always cherish.

First and foremost, I want to express my heartfelt gratitude to my advisor, Professor Julian Marshall. Your exceptional mentorship, steadfast encouragement, and enduring positivity have been a guiding light throughout my academic journey. Your dedication to making a meaningful impact on the world and your generosity in sharing your ideas and expertise have profoundly shaped both my personal and professional growth. I am truly fortunate to have had you as my advisor and mentor, and I will always carry the lessons I've learned from you.

I am also deeply thankful to my thesis committee members—Professor Jessica Kaminsky, Professor Tim Larson, and Professor Dafeng Xu. Your thoughtful feedback, insightful questions, and constructive guidance have been invaluable in refining my work and helping me grow as a scholar. Your support and encouragement throughout this process have meant so much to me.

A special debt of gratitude goes to Jignesh Patel, Alper Unal, Chris Tessum, Sreekanth Vakacherla, Buyantushig Boldsaikhan, and Jargalsaikhan Galsuren. Your mentorship, collaboration, and patience in teaching me were instrumental to this work, forming the foundation for much of my research and growth. I am deeply grateful for your kindness and generosity in sharing your time and expertise.

To my colleagues in the Marshall and Apte Research Groups—Yuzhou Wang, Jiawen Liu, Arushi Sharma, Lara Clark, Matthew Bechle, Libby Koolik, Chirag Manchanda, and Lucas Mendoza—I am so grateful for your collaboration, support, and friendship. You have made this journey not only rewarding but also deeply enjoyable. Working alongside you has been an honor and a privilege.

Finally, my deepest gratitude goes to my family for your unwavering love and support. Your encouragement and belief in me have been the cornerstone of my accomplishments, providing me with the strength and inspiration to overcome every challenge.

Contents

List of Figures

List of Tables

Chapter 1

Introduction

On October 27, 1948, Donora, Pennsylvania was engulfed in a deadly haze. Residents found it difficult to breathe. Over five days, nearly half of the town's 14,000 residents suffered from severe respiratory or cardiovascular issues. At approximately 2:00 AM on October 30, the first death occurred, and within 12 hours, 17 more lives were lost. The town's streets were cloaked in a thick layer of gray smog as a warm air pocket passed overhead, sealing in pollution from the local steel and zinc smelters. Broad concern in the United States for "Clean Air" started here [1].

Researchers have since conducted thousands of studies on the fate and transport of air pollutants, as well as the health and environmental effects of both short- and long-term exposures. Governments have enacted hundreds of policies aimed at reducing emissions, exposure, and the economic costs associated with air pollution. Over the years, our knowledge of air pollution has grown significantly, with substantial evidence showing improvements in air quality over the past few decades. Yet, despite these advancements, air pollution was still responsible for more than 8.1 million deaths globally in 2021, maintaining its status as the largest environmental health risk [2, 3].

Addressing air pollution requires understanding several interconnected factors, including the chemical and physical properties of millions of pollutants, many of which remain unidentified; meteorology and other environmental conditions that affect pollutant dispersion; economic and social aspects that influence pollution sources and responses; and comprehensive management systems for monitoring pollution and evaluating the effectiveness of interventions. In this dissertation, I developed and applied multiple methods and tools that could help researchers and policymakers to effectively measure and attribute changes in air pollution to interventions, for both ambient and household air pollution.

1.1 Ambient Air Quality Management

1.1.1 Background

Ambient air pollution, commonly known as outdoor air pollution, refers to the contamination of the atmosphere by harmful chemicals, particulate matter, or biological substances. Common pollutants include particulate matter ($PM_{2.5}$ and PM_{10}), ozone (O_3), nitrogen dioxide (NO_2), sulfur dioxide (SO_2), and carbon monoxide (CO). These pollutants can originate from various sources such as vehicle emissions, industrial activities, power plants, construction sites, and natural events like wildfires. Depending on the pollutant, a substantial portion may be formed in the atmosphere rather than emitted directly. To mitigate the harmful effects of ambient air pollution on human health and the environment, regulatory authorities implement measures such as adopting ambient air quality standards (AAQS). As of 2021, the UN reported that 125 countries had incorporated some form of AAQS into their legislation [4]. The extent of this integration varies, and while there is no universal approach to managing air quality, robust governance systems are essential. These systems promote institutional responsibility, transparency, and accountability, and create administrative frameworks that support the effective implementation and enforcement of air quality standards.

Despite global progress in adopting AAQS, the structure and effectiveness of these standards can vary. The United States (U.S.), renowned for its relatively comprehensive and stringent air quality regulations, serves as a prime example of how a robust framework can protect public health and the environment [5]. The primary regulatory foundation for air quality management system in the U.S. is the Clean Air Act (CAA), which guides the development and enforcement many programs and rules, including ambient air quality standards [6]. According to the U.S. Environmental Protection Agency (EPA), this system operates as a dynamic cycle composed of five key steps [7]:

1. Establish Goals: The institution sets acceptable levels of air pollutants to protect public health. A common example is the U.S. National Ambient Air Quality Standards (NAAQS) [8].

2. Determine Emission Reductions: This step involves using emission inventories, air quality monitoring, and modeling to evaluate the spatial and temporal aspects of air pollution. This phase involves several tools and datasets, including the National Emission Inventory (NEI), the Air Quality System (AQS), which stores data from approximately 5,000 active monitoring stations, and air quality models such as the Community Multiscale Air Quality (CMAQ) model [9, 10].

3. Develop Control Strategies: Authorities devise pollution prevention and emission control techniques to reduce emissions effectively.

4. Implement Regulations and Incentives: Regulatory agencies enact and enforce rules or establish incentive programs to achieve air quality goals.

5. Evaluate Ongoing Efforts: The effectiveness of current regulations, policies, and programs is continuously assessed to ensure they meet air quality objectives and are adjusted as needed.

Each step of this process is grounded in scientific research that offers critical insights into the emission, transport, and transformation of air pollutants in the atmosphere and their impacts on human health and the environment. Publicly accessible tools, such as the National Emission Inventory (NEI), data from the Air Quality System (AQS) monitoring stations, and air quality models, support researchers in assessing emission reductions, developing effective control strategies, and evaluating the efficacy of current policies.

1.1.2 Policy evaluation

The Clean Air Act (CAA) serves as a critical benchmark for air quality policies in the United States, showcasing the profound impacts of comprehensive regulatory measures [6]. To assess the efficacy of the CAA over time, the EPA has conducted extensive retrospective and prospective cost-benefit analyses [11–13]. These analyses aim to quantify the broad range and scale of benefits resulting from emissions reductions by comparing two principal regulatory scenarios: the "control scenario," which reflects the actual outcomes following the CAA's implementation, and the "no control" scenario, which projects the conditions that would have prevailed without the 1970 Clean Air Act, where air pollution controls would have remained minimal in scope and stringency.

Similar studies and reports have been done for policies varying in size and scope - for example, analysis for National Clean Air Action Plan in China [14], Heavy Duty Emission Standards in Brazil [15], NO_2 Control Program in Japan [16], Energy Efficiency Obligation Scheme in Turkey [17], Diesel Vehicle Renewal Policy in Colombia [18], Low Carbon Transportation Program in California [19], and Air Quality Fee Rule in Washington [20]. These studies consistently employ air quality management tools to support their implementation and continuous improvement.

A critical component of these assessments is the estimation of health benefits, which include reductions in mortality and decreases in respiratory and cardiovascular diseases. Central to estimating these health benefits are the concentration-response or dose-response functions, which are derived from extensive scientific literature [21–25]. These mathematical models elucidate the relationship between exposure to pollutants and the range of associated health effects on the exposed population, spanning from negligible to severe or even lethal outcomes.

Air pollution concentration and population exposure are required to utilize the dose-response function. To quantify the changes in concentration empirical evidence grounded in a monitoring station is often required. Data from local and state air monitoring stations offer direct, real-time insights into pollutant levels across various locations. However, the number of monitoring stations is often limited and unevenly distributed due to the high capital and operational costs associated with regulatory grade instruments such as those meet Federal Reference Method (FRM) and Federal Equivalent Method (FEM) requirements [26, 27]. To enhance coverage and provide a more comprehensive assessment, additional approaches such as low-cost sensor networks, remote sensing technologies, mobile monitoring, and air quality models are sometimes employed [10, 28–32].

1.1.3 Air Quality Models

An air quality model is a mathematical representation used to predict the concentration and dispersion of air pollutants in the atmosphere. These models help assess the impact of emissions from various

sources on air quality, facilitate regulatory compliance, and support decision-making for air quality management. Air quality models vary greatly in complexity and application, depending on the specific pollutant of interest, geographic scope, and the time scale of predictions.

Table 1.1 presents examples of models commonly used in air quality management. Typically, in air quality policy evaluations, complex chemical transport models are designed to comprehensively represent the most critical processes influencing air quality and atmospheric chemistry, including advection, deposition, and solar radiation. For example, EPA has been using Community Multiscale Air Quality (CMAQ) as their premier modeling system for the last 25 years (See Figure 1.1) [33].

Table 1.1: Example of air quality model types and use cases

Type	**Examples**	**Brief Description**	**Common Use Case**
Chemical Transport Models (CTMs)	CMAQ [33], CAMx [34], GEOS-Chem [35], WRF-Chem [36]	Simulate the transportation and chemical reactions of pollutants, potentially over large geographic scales.	Regional air quality management and evaluation of policy measures.
Gaussian Dispersion Models	AERMOD [37]	Use Gaussian plumes to estimate the dispersion of pollutants, often from point sources.	Assessing local air quality impacts near industrial sites for regulatory compliance.
Lagrangian Models	HYSPLIT [38]	Track the advection and diffusion of air pollutants as they move through the atmosphere.	Studying short- or long-range transport of pollutants like dust, smoke, and chemicals.
Receptor Models	PMF [39]	Identify and quantify the contributions of various sources to pollution at a specific site based on sampled data.	Source apportionment.
Statistical Models	Regression models, Machine Learning models	Utilize statistical techniques to correlate air quality data with environmental and human factors for prediction.	Predicting how concentrations vary in space, or space and time, at excellent spatial resolution.
Integrated Assessment Models	RAINS [40], GAINS [41], BenMAP [42]	Combine physical, economic, and health data to assess the overall impacts of air pollution control strategies.	Evaluating the cost-effectiveness and benefits of air pollution reduction measures on a large scale.
Reduced Complexity Models	InMAP [43], EASIUR [44], APEEP [45]	Simplify complex interactions in air quality to provide faster, yet sufficiently accurate, predictions and assessments.	Used in policy analysis to quickly assess the health impacts of air pollution with fewer computational resources.

While state-of-the-art air quality models such as CMAQ provide robust estimates of pollutant concentrations, they demand significant computational resources and specialized expertise. Assessing the impact of air pollution on human health typically requires annual or at least seasonal averages of pollutant concentrations [22, 23, 46]. Consequently, generating these long-term average concentrations on a national scale with CMAQ can take several weeks to months, depending on the required grid resolution and computing power [47–51]. Therefore, running multiple scenarios to evaluate different policy impacts and estimating the resultant concentrations for each scenario becomes a complex and resource-intensive endeavor.

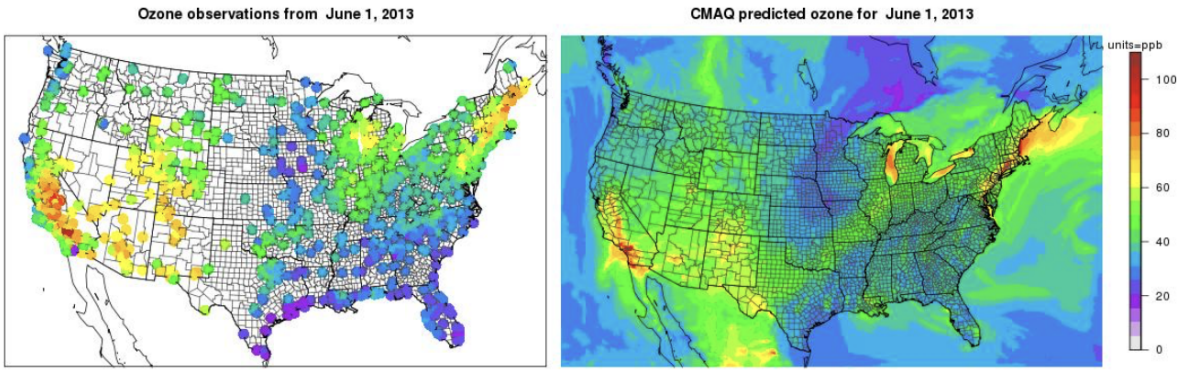

Figure 1.1: Example map of measured and CMAQ-modeled ozone concentrations in the US: max 8-hour concentration (ppb) on June 1, 2013. (Left) Measured concentrations at EPA monitoring sites. (Right) CMAQ-modeled output for each model grid cell [33]

To address these challenges, multiple reduced complexity models (RCMs) have been developed. RCMs employ simplified versions of the physical and chemical mechanisms to estimate pollutant concentrations from emissions sources. Although the accuracy RCMs may not be on par with full chemical transport models, their significantly reduced computational resource demands make them highly valuable for specific applications, including many types of policy analysis. Here, I focus on one RCM, the Intervention Model for Air Pollution (InMAP) [43]. InMAP utilizes preprocessed physical and chemical mechanisms from more complex models, such as WRF-Chem and WRF-CMAQ, to compute annual average concentrations of primary (i.e., directly-emitted) $PM_{2.5}$ and precursors of secondary (i.e., formed in the atmosphere) $PM_{2.5}$ such as NO_x, SO_x, NH_3, and VOCs resulting from marginal changes in emissions. In contrast to the extended computational times required by full-scale models (e.g., multiple days, weeks, or even months, on a high-performance computer), national-scale runs using InMAP can be completed in approximately 1 to 3 hours on a standard workstation. Figure 1.2 describes the performance evaluation of InMAP and WRF-Chem against ground measurements. InMAP modeling assumptions and performance evaluations against other models and measurements are described elsewhere [43, 52].

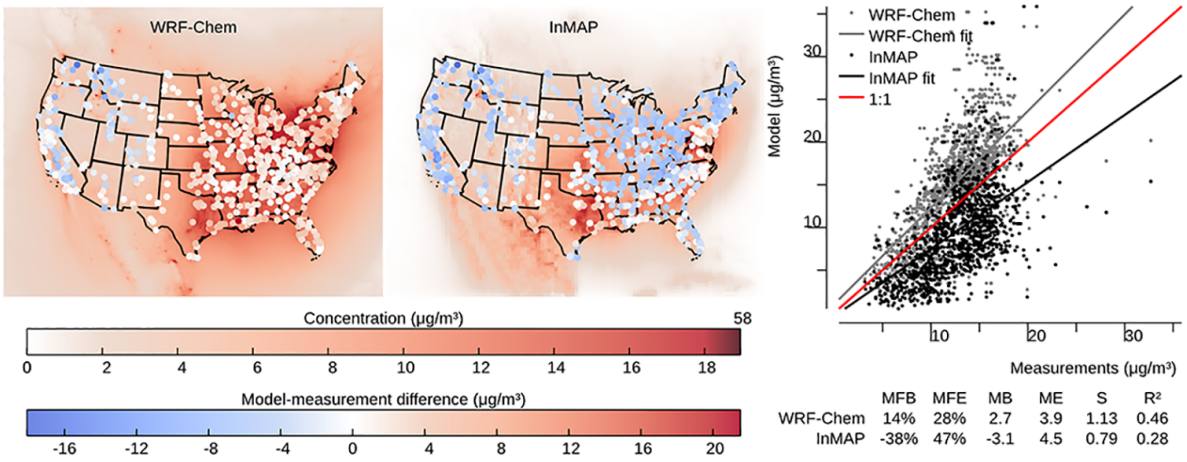

Figure 1.2: Comparison of WRF-Chem and InMAP performance in predicting annual average observed total $PM_{2.5}$ concentrations.The background colors in the maps represent predicted concentrations, and the colors of the circles on the maps represent the difference between modeled and measured values at measurement locations. For the comparison shown here, on average WRF-Chem overpredicts and InMAP underpredicts as compared to observations. Abbrevations: MFB = mean fractional bias; MFE = mean fractional error; MB = mean bias; ME = mean error; MR = model ratio; S = slope of regression line; R^2 = squared Pearson correlation coefficient [43]

To further enhance the efficiency of InMAP runs, the InMAP Source Receptor Matrix (ISRM)—a library of pre-run simulations—was developed [53]. The ISRM allows users to calculate changes in

annual total $PM_{2.5}$ concentrations on a national scale within minutes. Accessible through widely used programming languages such as R and Python, ISRM eliminates the need for specialized software. This advancement reduces simulation runtimes from hours (InMAP) to minutes (ISRM) and broadens accessibility for researchers and policymakers, facilitating rapid and comprehensive air quality assessments.

The first version of ISRM was produced in 2017 after running the initial version of InMAP approximately 150,000 times, each time simulating a 1-ton/year emission of primary $PM_{2.5}$, NO_x, SO_x, NH_3, and VOCs from various horizontal and vertical grid cells. This version has been widely adopted to explore air pollution in various contexts, including racial and income disparities, sectoral contributions to pollution, emission reduction strategies, and Environmental Justice (EJ) assessments, such as the Biden administration's Justice40 initiative [54–63]. In 2023, a new version of InMAP (InMAP 2.0) was released. However, prior to the present work, an updated version of ISRM (ISRM 2.0) had not been released, as running InMAP hundreds of thousands of times remains a resource-intensive process.

1.1.4 Our Contribution

This dissertation presents two methodologies and tools specifically designed for accountability studies:

- In Chapter 2, I employ Robust Differences, a method for estimating the "control" case that serves as a baseline for comparing observed pollutant concentrations following an event or intervention.
- In Chapter 3, I present an updated InMAP Source Receptor Matrix (ISRM 2.0), a comprehensive library of pre-run simulations using the updated reduced complexity model, InMAP 2.0. This updated matrix drastically reduces computational time (from hours (InMAP) to minutes (ISRM)) and improves user accessibility for conducting policy scenario analyses.

The first method, "Robust Differences", is applied here to ground-based measurements. It necessitates estimating a "control" or baseline concentration to assess the impact of an event on air pollution. This method is crafted to isolate the effects of individual interventions and policies, which may be obscured or misrepresented due to overlapping regulations and concurrent measures.

In Chapter 2, the "Robust Differences" method was applied to evaluate the impacts on air quality of the substantial disruption to day-to-day activities resulting from Covid-related stay-in-place rules. This investigation contributes to the broader body of accountability studies. The Covid-19 pandemic offered an unprecedented opportunity for such analysis due to its widespread and abrupt reduction in human activity. Government-mandated lockdowns and stay-at-home orders led to dramatic decreases in industrial operations, vehicular traffic, and other economic activities. This scenario created an unplanned but controlled experiment, allowing researchers to observe changes in air quality under conditions that would be difficult, if not impossible, to replicate through (air pollution-motivated) planned interventions.

The second tool, ISRM 2.0, is based on InMAP (described above). ISRM 2.0 is particularly well-suited for rapid policy analysis, enabling the assessment of various emission change scenarios and supporting environmental justice initiatives by estimating pollutant exposure across racial and ethnic groups. ISRM tracks source-receptor relationships for five key pollutants—primary $PM_{2.5}$ and precursors of secondary $PM_{2.5}$: NO_x, SO_x, NH_3, and VOCs—across 86,261 grid cells in the contiguous U.S. This detailed approach provides comprehensive insights into the impacts of emissions on air quality and population exposure on a national scale, yet the run time is $\sim$ minutes.

In Chapter 3, I applied ISRM 2.0 to estimate mortality linked to air pollution across various economic sectors from 2002 to 2019. Policies addressing these sectors in the US have shown significant variation in their scope and impact. For example, energy and climate policies have successfully reduced reliance on coal-fired power plants in the power sector, leading to a significant increase in the adoption of cleaner energy sources such as solar and wind. Similarly, government programs in the transportation sector have reduced tailpipe emissions and accelerated the adoption of lower-emitted vehicles. In contrast, for the years investigated, emissions have not dramatically reduced for the residential and agricultural sectors. Possible causes include the complexity of developing additional effective control technologies coupled with population growth and rising demands for food and consumer goods. Understanding these sector-specific trends is vital for identifying effective policies and establishing standards that will mitigate air pollution effectively.

1.2 Indoor Air Quality Management

1.2.1 Background

Indoor Air Pollution, also known as Household Air Pollution (HAP) for residential contexts, includes a wide range of pollutants including those originating from household activities and occupational activities, such as in factories, offices, and other workplaces. Common contaminants include particulate matter, carbon monoxide (CO), nitrogen dioxide (NO2), and various volatile organic compounds (VOCs). Despite the significant health and environmental risks posed by indoor air pollution—which, according to the Global Burden of Disease [64], are comparable to those of ambient air pollution—there is a notable lack of regulatory focus globally. According to a 2021 United Nations assessment, only 13 countries have enacted some form of general indoor air quality standards.

Current strategies for managing indoor air quality, implemented by local governments, researchers, and nongovernmental organizations, include:

1. Improved Cookstoves: In low-income settings, a primary source of indoor air pollution is the burning of biomass for cooking and heating. Improved cookstoves, which burn fuel more efficiently, can reduce emissions by using less fuel and producing fewer harmful byproducts, such as carbon monoxide and particulate matter.

2. Cleaner Fuels: Transitioning from solid fuels to cleaner alternatives, like liquefied petroleum gas (LPG), ethanol, or biogas, substantially reduces indoor air pollution. These fuels burn cleaner than coal or biomass, thus lowering the health risks associated with indoor smoke.

3. Ventilation Improvements: Simple ventilation solutions, such as creating smoke outlets or optimizing building designs for cross-ventilation, effectively reduce indoor pollutant concentrations. For instance, placing windows or vents above cooking areas can help direct pollutants outdoors.

4. Educational Programs: Educational initiatives that raise awareness about the health impacts of indoor air pollution and provide pollution reduction strategies empower individuals. These programs often emphasize the benefits of proper ventilation, cleaner fuels, and maintaining smoke-free interiors.

Despite significant efforts, household air pollution remains the second-highest environmental risk fac- tor for mortality (after ambient air pollution), emphasizing the critical need for comprehensive action and regulation on indoor air quality. This issue is particularly urgent in low- and middle-income countries, where women and children face disproportionate health risks due to prolonged exposure. The Covid-19 pandemic has further highlighted the link between indoor and outdoor air quality, underscoring their interconnected impacts on public health. However, regulating indoor air quality in private spaces—such as homes and small businesses—poses unique challenges. Many jurisdictions lack the authority or willingness to impose monitoring and control measures within private settings. Without systematic monitoring, it is nearly impossible to ensure that indoor pollutant levels remain within safe limits, leaving significant gaps in air quality management and public health protection.

1.2.2 Air quality monitoring

Air quality monitors are essential tools for assessing the effectiveness of interventions, such as improved cookstoves or cleaner fuels, in reducing household exposure to pollutants. While regulatory-grade monitors offer high accuracy, their substantial cost—often tens of thousands of dollars—restricts their widespread use. As a result, there has been considerable growth in the development of low-cost sensors tailored specifically for household air pollution monitoring. These sensors provide measurements of pollutant concentrations as well as ambient humidity and temperature, enabling more accessible and affordable monitoring solutions.

Many commercially-available low-cost sensors monitor particulate matter such as $PM_{2.5}$. That fact may reflect, in part, the importance of $PM_{2.5}$ for health: $PM_{2.5}$ exhibits a strong correlation with long-term health risks, including increased mortality. Table 1.2 lists examples of low-cost sensors on the market.

Table 1.2: Examples of Low-Cost Household Air Pollution Monitors

Device Name	**Air Pollutants Measured**	**Description**	**Approx. Cost (USD)**
UPAS [65]	$PM_{2.5}$, elemental and organic carbon	Personal sampling device for accurate $PM_{2.5}$ monitoring, widely used in occupational health studies	1,000
PurpleAir PA-II [66]	PM_1, $PM_{2.5}$, PM_{10}	Uses laser particle counters, provides real-time data, suitable for indoor and outdoor use	250
AirVisual Pro by IQAir [67]	$PM_{2.5}$, CO_2, temperature, humidity	Portable, user-friendly monitor with mobile app for real-time data, commonly used indoors	299
Uhoo Indoor Air Sensor [68]	$PM_{2.5}$, CO, CO_2, VOCs, NO_2, temperature, humidity	Comprehensive monitor covering multiple pollutants, with a mobile app for real-time data	399
Temtop M2000C [69]	$PM_{2.5}$, PM_{10}, CO_2, HCHO, temperature, humidity	Portable monitor ideal for high-pollution environments, tracks multiple pollutants	250
Atmotube Pro [70]	PM_1, $PM_{2.5}$, PM_{10}, VOCs, temperature, humidity	Compact and wearable for personal exposure monitoring; connects to a smartphone app	230
Sensirion SPS30 [71]	PM_1, $PM_{2.5}$, PM_4, PM_{10}	Laser-based sensor module, often used in custom-built air quality monitors	60 (sensor only)

While significantly more affordable than regulatory-grade monitors, low-cost sensors still pose financial challenges, with each unit typically costing several hundred dollars, which can limit large-scale deployment. In addition to the initial capital cost, these devices often incur ongoing expenses. For instance, PurpleAir sensors require a subscription to access historical data, and the Ultrasonic Personal Aerosol Sampler (UPAS) necessitates regular replacement of filters, which can be costly. Furthermore, these sensors demand consistent maintenance and strategic deployment planning. For example, PurpleAir sensors require a continuous power supply, while the UPAS requires battery recharging every 48 hours.

1.2.3 Our contribution

This dissertation contributes to the field of indoor air quality measurement by introducing the Washington Passive Sampler (WPS), an ultra-low-cost, passive sensor for light-absorbing carbon (LAC). LAC refers to the carbon components of fine particulate matter ($PM_{2.5}$), such as black and brown carbon, which strongly absorb visible light within wavelengths of 400–700 nanometers [72]. The WPS is relatively affordable, costing between USD 5–15, and is simple to deploy, requiring no electricity, costly laboratory equipment, or extensive maintenance. The device operates by measuring changes in the reflectance of a passively exposed paper filter, which is analyzed through digital imaging to quantify carbon accumulation.

In Chapter 4, we evaluated the accuracy and precision of the Washington Passive Sampler (WPS) by co-locating it with two reference methods: (A) quartz filters for elemental carbon (EC) analysis using the Ultrasonic Personal Aerosol Sampler (UPAS) as the gold standard, and (B) the PurpleAir sensor. This chapter aims to assess the potential of the WPS as a low-cost, user-friendly black carbon sampler for indoor air quality research.

Chapter 2

Application of "Robust Differences" in Accountability Study: Air Pollution Levels during Covid-19 Stay-at-Home Orders

Material in this chapter has been previously published in the following article:

Bekbulat, B., Apte, J. S., Millet, D. B., Robinson, A. L., and Marshall, J. D. (2021). Changes in criteria air pollution levels in the US before, during, and after Covid-19 stay-at-home orders: Evidence from regulatory monitors. *Science of The Total Environment*, 769, 144693. `https://doi.org/10.1016/j.scitotenv.2020.144693`.

2.1 Summary

Accountability studies in air pollution face significant challenges due to the absence of a true control or baseline concentration, especially when no specific event or intervention occurs. Typically, researchers only have access to concentrations recorded after such events, requiring sophisticated methods to estimate an "expected" or baseline concentration for meaningful comparisons. In this chapter, I introduce the "Robust Differences" method, designed specifically to estimate what concentrations would have been under normal conditions and to compare these with the observed concentrations. This method is then applied to assess changes in criteria air pollutants during the Covid-19 stay-at-home orders in the U.S.

The analysis revealed that during the stay-at-home period, average PM2.5 levels were slightly higher —about 10% of the multi-year interquartile range (IQR). In contrast, average levels of O_3, NO_2, CO, and PM_{10} were lower than anticipated—approximately 30%, 20%, 27%, and 1% of their respective IQRs. By 5–6 weeks following the stay-at-home orders, concentration anomalies generally returned to normal levels.

Similar studies using different approaches have consistently reported lower than-expected results for O_3, NO_2, and CO, although findings for $PM_{2.5}$ and PM_{10} have varied. These results underscore the pivotal role of methodological choices in shaping research outcomes and highlight the importance of a diverse array of analytical techniques for robust analysis.

2.2 Introduction

With the enormous and extremely rapid social and economic changes happening because of the novel coronavirus disease of 2019 ("Covid"), including stay-at-home orders enacted in nearly all US states, there is interest in quantifying the air pollution impacts of those orders. Changes in air pollution during Covid could reveal, for example, how changes in the economy affect air quality, and how those changes differ throughout the US. More broadly, responses to Covid create a unique opportunity to quantify the effect of human activity on air quality. Analogous investigations have been done multiple times at a more limited scale – for example, studying impacts of sudden industrial closure (e.g., a steel mill in Utah Valley [73]; copper smelters throughout the US [74], widespread power outage in the Northeastern US [75], new regulation such as a coal ban in Dublin [76] and a congestion charging scheme in London [77], and the 1996 Atlanta [78, 79] and 2008 Beijing Olympics [80, 81]. However, societal changes attributable to the Covid response are unprecedented in size, scope, and speed.

Air pollution concentrations at a given location vary on time scales from seconds to years; some variability is random or quasi-random, and other variability is systematic (i.e., non-random). Temporal variability is caused by changes in emissions and meteorology and their associated impacts on rates of transport, production, removal, and dilution. The net result is that because of random and systematic temporal variability, concentrations during Covid may be different than before Covid (e.g., one month or one year earlier) for reasons unrelated to the societal response to Covid. This Chapter adds to

the literature on changes in air pollution concentration associated with specific causes, including studies of the emissions, air pollution, or health benefits from environmental regulation ("accountability studies"). That literature addresses the random and systematic variability in pollution concentrations mentioned above via, e.g., detrending and counterfactual emissions scenarios [73–85].

This Chapter also adds to the existing literature exploring Covid-related impacts on air pollution and related activity levels [86–106]. Much of the news in the popular press regarding impacts of Covid on air pollution emphasizes that concentrations have improved during Covid [107–112]; our investigation aims to test those claims using a national dataset of in-situ concentration measurements. We present two approaches for deriving "expected" concentrations (i.e., in the absence of Covid responses publicly available compare observed concentrations: (1) our main approach is temporally corrected. (2) our secondary approach ("sensitivity analysis") is temporally and weather-corrected using regression techniques. We do not attempt to shed light on the specific causes of any changes nor on regulatory implications.

This Chapter uses nationwide, publicly-available monitoring data from the US Environmental Protection Agency (EPA) to investigate changes in criteria air pollutants, before, during, and after Covid stay-at-home orders. These data represent the largest source of publicly available and robust measurements of criteria air pollutants for the US. The methods we employed control for random and systematic variability on multiple time scales, and by state and nationally. There have been many investigations into how air pollution levels have changed during Covid; yet, to our knowledge, no prior research has systematically analyzed changes in in-situ measured criteria air pollution concentrations before, during, and after stay-at-home orders across the US.

2.3 Methods

2.3.1 General Approach

We use "before", "during", and "after stay-at-home orders" as general terms: "before stay-at-home orders" refers to weeks before stay-at-home orders, when, in 2020, Covid had little or no impact on activities in the US; "during stay-at-home orders" refers to a few weeks preceding the stay-at-home order dates and weeks during stay-at-home orders; "after stay-at-home orders" refers to weeks after the states have removed stay-at-home orders. Those labels are applied to specific weeks, as described in the analyses below. The scope of the stay-at-home orders varies from state to state. The term "stay at home" refers to a specific requirement (also called "shelter in place"), with a specific start and end date (A.1), announced by most state governments.

2.3.2 Data acquisition and selection

We employ publicly available daily average in-situ air pollution concentrations measured by EPA monitors. We downloaded data from the EPA AirData website (https://www.epa.gov/outdoor-air-quality- data/download-daily-data) on September 2, 2020. As of September 2, 2020, data for two pollutants are available from the EPA for the time- period of interest for Covid (March 2020 and later): fine particulate matter ($PM_{2.5}$, i.e., particles with aerodynamic diameter less than or equal to 2.5 μm) and ozone. Other pollutants or averaging times are currently unavailable from the EPA.

We also downloaded and analyzed NO_2, CO, PM_{10} data from the Environmental Sensor Data Repository (ESDR; https://esdr.cmucreatelab.org). ESDR data are EPA measurements that the EPA has provided in real-time but not yet in an archival or database format; ESDR saves ("scrapes") those real-time data and shares them in their raw form. (Available EPA data for SO_2 were too imprecise to support a robust analysis.)

We started by downloading all data (daily 24-hour average concentrations for $PM_{2.5}$ and PM_{10}, daily 8-h maximum for ozone and CO, daily 1-h maximum for NO_2; December 18, 2009 - December 31, 2019) for all monitors from EPA AirData. We then downloaded the year-2020 (January 1, 2020 - September 1, 2020) $PM_{2.5}$ and ozone data from EPA AirData and NO_2, CO, SO_2, and PM_{10} data from the ESDR website for all monitors with one or more days of data in year-2020. (As mentioned above, SO_2 data were downloaded but were too imprecise to support robust analysis.) Finally, we matched the historical and year-2020 data based on the monitor's latitude and longitude. We restricted the analysis to consider a specific window of days each year: for 2020, the window is January 1–September

1 (245 days); for years 2010–2019, the window is December 18–September 15 (Total: 273 days), i.e., the year-2020 range ± 2 additional weeks. Data outside of those windows were excluded from the analysis.

Analyses extend through September 1, 2020 (the 245th day of 2020 and the completion of the 35th week of the year). Weeks are sequential: week 1 is days 1–7 of the year, week 2 is days 8–14 of the year, etc. By stopping our analyses at week 35, we avoid the massive wildfires that occurred on the West Coast starting in week 36 (September 4 to September 10) [113, 114].

We carefully examined the completeness of data from each year and each monitoring site to determine whether it would be included in the study. As described next, these checks are performed as a two-step process for each monitor.

First, we tested each monitor year for data sufficiency. For years 2010–2019, if any monitor year contains more than 75% of the expected number of days in the target window (75%×273=206 days), then that year of data for that monitor is excluded. For year-2020, we checked the number of days of data pre-Covid (January 1–March 18; 78 days) and after the start of Covid (March 19–September 1; 167 days); if either period's data contains more than 75% of the expected days (75%×78 days=59 days; 75%×167 days=125 days), then that monitor is excluded.

Second, we ensure that a monitor has a sufficient number of years of valid data to calculate the temporal correction. This step employs the following three data requirements (Figure A.1): (1) monitors with fewer than 3 years of data are excluded. (2) Monitors without at least two of the last three years of data are excluded. (3) (i) For monitors with 8 or more years of data for 2010–2019, we calculate the 10-year slope from that monitor's available data. (ii) For monitors with under 8 years of data for 2010–2019, we determined if there are one or more monitors within 50 km. If there are, then we impute a slope using inverse distance weighting (IDW) of the slopes from up to 3 clos- est monitors within 50 km. This approach (3 nearest monitors within 50 km) has been adopted by prior articles [115]. Bravo et al. (2012) state, "A distance of 50 km was chosen because it represented a reasonable distance for extrapolation of observed air pollutant concentrations and has been used previously in epidemiological settings, but other distances could have been selected with similar justification [116]." Marshall et al. (2008) reported that this approach (3 nearest monitors within 50 km) yielded better results than two analogous approaches (all monitors within 50 km; and all monitors within 10 km) [117]. If there are no other monitors within 50 km, then we exclude that monitor from the analysis.

The AirData and ESDR websites provided year-2020 concentrations for 1141 $PM_{2.5}$, 1206 ozone, 436 NO_2, 270 CO, and 673 PM_{10} monitors. Our data completeness algorithm excluded a total of 583 (51%) $PM_{2.5}$, 543 (45%) ozone, 343 (79%) NO_2, 207 (77%) CO, and 565 (84%) PM_{10} monitors. Therefore, the results and discussion are based on data from 558 $PM_{2.5}$, 663 ozone, 93 NO_2, 63 CO, and 108 PM_{10} monitors. Each monitor is in a different location. State-specific results refer to states with monitors that met the inclusion criteria.

We downloaded meteorology data (hourly temperature, precipitation, mixing height, and dew point data for US; December 18, 2009 - September 1, 2020) from European Center for Medium-Range Weather Forecasts (ECMWF) ERA5 Reanalysis [118]. Then we extracted hourly meteorological data for each monitoring station and calculated the daily average values. We also analyzed US public transit mobility data from Google Community Mobility Reports (Figure A.9).

As a side-analysis, we examined the influence of upwind ozone entering the US (Figure A.10). In principle, upwind pollution levels could potentially enhance or offset the effects of changes in emissions in the US. We used observations from two remote upwind sites (Lassen Volcanic National Park, California [LAV] and Trinidad Head, California [THD]) operated by, respectively, the US National Park Service and the US National Oceanic and Atmospheric Administration Global Monitoring Laboratory (NOAA GMD) [119].

2.3.3 Main approach: temporal correction, using robust differences ("D")

We calculate a "robust differences" metric ("D"): the weekly median concentration for 2020, relative to the temporally-corrected historical median, normalized to the interquartile range (IQR).

$$D_i = \frac{C_{2020,i} - C_{h,i}}{I_{h,i}} \tag{1}$$

Eq.(1) is calculated for each week ("i") and for each monitor. D_i is the "robust differences" comparison metric for week i, $C_{2020,i}$ is the weekly-median concentration (i.e., the median of 7 daily-average

concentrations) for week i during year-2020, $C_{h,i}$ is the temporally corrected historical median concentration for week i plus/minus 2 weeks, and $I_{h,i}$ is the interquartile range (IQR, 75th percentile minus 25th percentile) for week i plus/minus 2 weeks. For example, to calculate D_i for week 10, we use $C_{2020,10}$ for week 10, and for $C_{h,i}$ and $I_{h,i}$, we use historical data (i.e., years prior to 2020) for weeks 8–12. The "plus/minus 2 weeks" approach for historical data increases the sample size for the comparisons (historic vs. year-2020), provides a broader historical comparison than just one week, and helps smooth atypical weeks in the historical dataset.

D_i is called a "robust" metric because it employs the median and IQR rather than the mean and standard deviation, so it is not impacted by outliers. $D_i = 0$ would indicate that the year-2020 median is equal to the "expected" value (i.e., the temporally corrected long-term average median). $D_i = 1$ would indicate that the year-2020 value is one IQR above the expected value; D_i = -2 would indicate two IQRs below the expected value. D_i reveals whether year-2020 concentrations are higher or lower than expected, for before, during, and after stay-at-home order weeks, but does not elucidate their cause nor inform regulatory aspects such as comparisons against national standards.

Temporal correction is needed because air pollutant concentrations exhibit systematic long-term (multi-year) trends that can vary by location (see example temporal correction in Figure A.2. The temporal correction for a monitor in week i is the 10-year slope (i.e., 2010–2019) of weekly-median historical concentrations at that monitor (Figure 2.1). In this manner, we compare actual year-2020 measurements to the "expected" level for week i in year-2020, accounting for 10-year trends for that week-of-year at that location. (As a sensitivity analysis, we used 5- rather than 10-year trends; results were similar (Figure A.3)) The interquartile range ($I_{h,i}$) is calculated using the prior 3 years of data (2017–2019); we employ this metric as a relatively recent measure of the typical spread in the data.

2.3.4 Sensitivity analyses: temporal and weather correction

As sensitivity analyses, we instead use linear (Eq.(2.1)) and spline (Eq.(2.2)) first-order multivariate autoregression to correct for temporal patterns and weather:

$$C_t = \beta_0 + \beta_1(m_t) + \beta_2\delta_{y,2020} + \beta_3(C_{t-1}) + \beta_4 y_t + \epsilon_t \tag{2.1}$$

$$C_t = \beta_0 + bs(m_t, y, \nu) + \beta_1\delta_{y,2020} + \beta_2(C_{t-1}) + \epsilon_t \tag{2.2}$$

Here, C_t is the concentration of the pollutant on day t, m_t is the daily average meteorology (temperature, precipitation, mixing height, and dew point) on day t, $\delta_{y,2020}$ is a dummy variable indicating if the day is in 2020, C_{t-1} is the concentration on the previous day (i.e., a 1-day lag), y_t is the year of the date the concentration was recorded, and ϵ_t is the error term, and bs is a B-spline function with degrees of freedom, ν (using the splines library in R). As above, data (concentrations, meteorology) are daily averages. Eqs. (2.1) and (2.2) are evaluated for each monitor and week (e.g., there are 44 weeks and 525 PM2.5 monitors, so Eqs. (2.1) and (2.2) are evaluated 23,100 times for PM2.5), and historical data (2010–2019) are "±2 weeks" (e.g., week 10 in year-2020 is matched to historical data from weeks 8–12). When analyzing results from Eqs. (2.1) and (2.2), and then aggregating across monitors, we define the time axis as the week number before, during, and after the stay-at-home order.

This analysis reveals whether year-2020 concentrations are different from the expected concentrations after temporal corrections and adjustments for meteorology. Eqs. (2.1) and (2.2) are autoregressive, explicitly accounting for temporal autocorrelation in the measurements (Figure A.4).

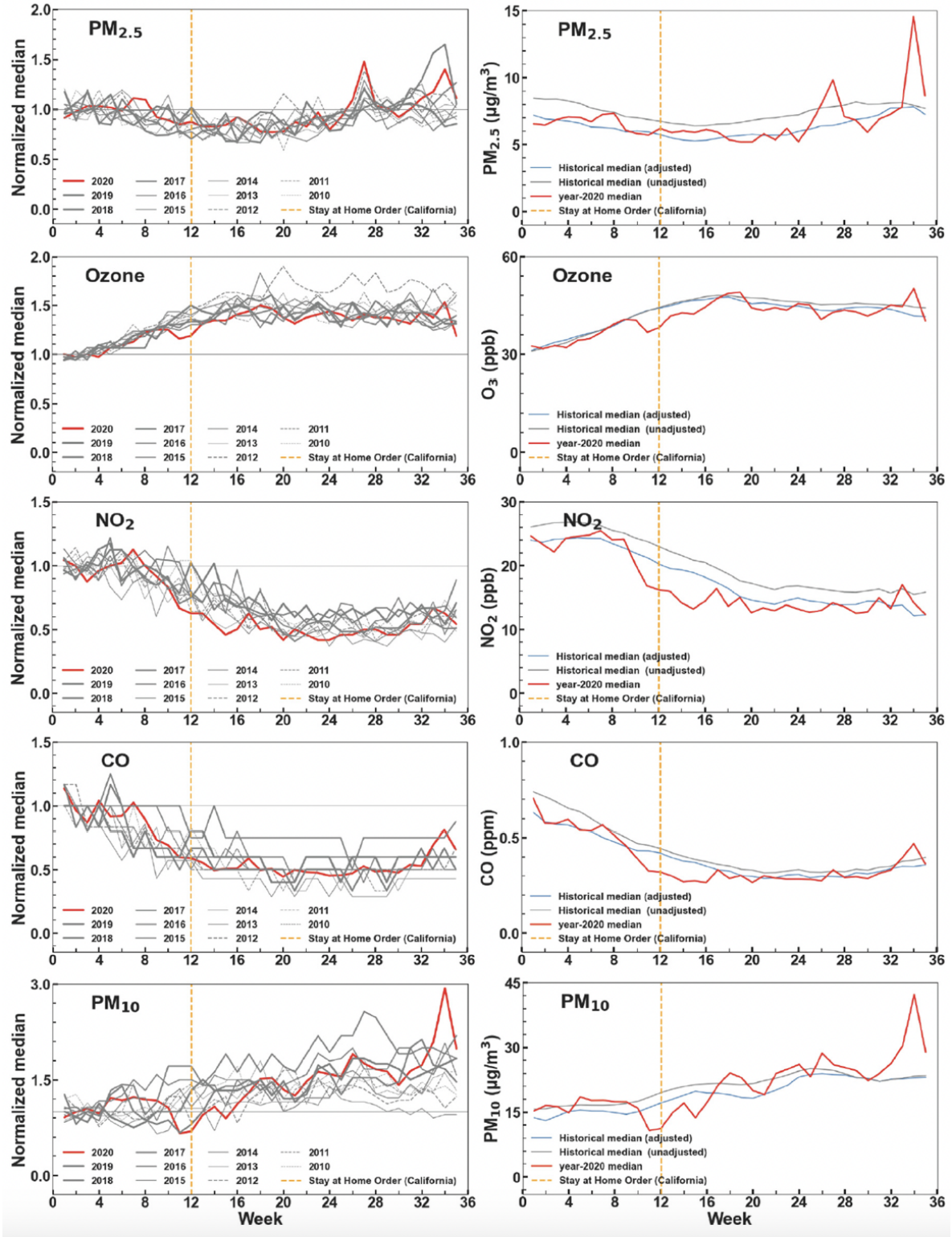

Figure 2.1: Year-2020 pollution levels (red lines) compared to 2010–2019 levels (grey/blue lines). The left panels show historical (2010–2019, unadjusted) and 2020 weekly median concentrations normalized to the January average for that year (i.e., dividing all weekly median concentrations by that year's January mean). Right panels show weekly 10-year median pollution levels with (blue line) and without (grey line) temporal correction, and the year-2020 median (red line). The orange vertical dashed line indicates the timing of the first stay-at-home order in the contiguous US: week 12 [CA]. These data indicate that except for $PM_{2.5}$, pollution levels exhibited a modest, temporary drop around the time of the first stay-at-home order.

2.4 Results

2.4.1 Temporal correction, using robust differences

As described next, concentrations during stay-at-home orders are slightly higher than expected for $PM_{2.5}$, and modestly lower than expected for ozone, NO_2, CO, and PM_{10}. The ozone anomaly was largest two weeks before the stay-at-home order; ozone levels returned to expected levels a few weeks after the stay-at-home orders were imposed. The anomalies for NO_2, CO, and PM_{10} are highest 2–3 weeks after the stay-at-home orders, and then levels returned to expected levels.

Figure 2.1 presents year-2020 and 2010–2019 pollution levels. After stay-at-home orders were imposed, $PM_{2.5}$ levels are towards the high end of the historical range, indicating, on average, a modest (3%) increase relative to expected concentrations. In contrast, average ozone, NO_2, CO, and PM_{10} levels are lower than expected, with the largest drop occurring during weeks 10–11 (i.e., March 4–18, 2020).

Historical $PM_{2.5}$, NO_2, CO, and PM_{10} concentrations are lower with temporal correction than without it (Figure 2.1, right) because pollution levels generally decrease each year. Ignoring that decrease (by comparing against uncorrected levels) would mean, on average, inappropriately concluding that most weeks are "lower than average" for any year. In contrast, temporally corrected results accounting for that long-term trend (Figure 2.1) suggest that $PM_{2.5}$ concentrations during stay-at-home orders are similar to or higher than expected concentrations.

For ozone, the temporal correction is minor (0.2% per year): ozone levels exhibit year-to-year variability but without a strong 10-year trend. Seasonally, ozone levels generally increase from January to April, reflecting increasing photochemical activity. Therefore, a direct comparison of weeks before versus during stay-at-home orders would incorrectly suggest that ozone levels are higher than expected; that conclusion fails to account for ozone's seasonal trend. Similarly, NO_2 and CO levels generally decrease from January to April. Hence, a direct comparison of pollution levels before versus during stay-at-home would exaggerate the effect of stay-at-home orders on NO_2 and CO levels.

General conclusions here are robust to the temporal correction method. Selecting an alternative temporal correction method might modestly shift up or down the corrected historical median concentrations (blue line, Figure 2.1, right panels), but that shift would not alter the year-2020 concentrations (red line, Figure 2.1, right panels) and so would be unlikely to suggest, for instance, that after stay-at-home orders, $PM_{2.5}$ concentrations are substantially lower than expected based on historical trends plus year-2020 concentrations before stay-at-home orders.

Figure 2.2 shows week-by-week robust differences before, during, and after the stay-at-home orders (adjusting the time axis to align with the date of a state's stay-at-home order). In this way, Figure 2.2 focuses directly on the impact of the stay-at-home order: before versus during the order (Figure 2.2, left) and during versus after the order (Figure 2.2, right). The number of states included in Figure 2.2 varies by week because states started and stopped stay-at-home orders on different dates.

The air pollution levels in states that have not initiated stay-at-home orders on a given date can be influenced by traffic and economic activity changes in the neighboring states that imposed a stay-at-home order or vice versa. Therefore, we also included week-to-week robust difference results where the time axis is calendar weeks of the year in 2020 (Figure A.5).

Noticeable declines in ozone, NO_2, CO, and PM_{10} start three weeks before stay-at-home orders, and the strongest ozone deviations occur two weeks before the stay-at-home order. The transit mobility analysis results (Figure A.9) indicate that transit mobility started to decrease from the baseline approximately three weeks before stay-at-home orders, which is consistent with this timing. In many locations, people curtailed social and economic activity starting before the official stay-at-home orders [120]. However, the pre-stay-at-home order reduction in ozone was not sustained; over time, D increases, and the size of the anomaly decreases. By six weeks after the stay-at-home orders, ozone concentrations were not significantly different from their expected levels.

We can summarize the differences in Figure 2.2 by considering "before" to be the average during weeks 4–14 before the stay-at-home orders, "during" to be the average of weeks 1–3 before and weeks 1–12 during the stay-at-home orders, and "after" to be the average during weeks 1–20 after the stay-at-home orders ended. Core results (Table 2.1) reveal that during stay-at-home, pollution levels were modestly lower than expected for ozone, NO_2, CO, and PM_{10}, but not for $PM_{2.5}$. Specifically, during stay-at-home orders, $PM_{2.5}$ levels were higher than expected by 10% of its IQR; ozone, NO_2, CO, and

PM_{10} levels were lower than expected by 1%–30% of their respective IQRs.

Pollution levels were also not precisely at expected levels before the stay-at-home orders; for PM_{10}, before stay-at-home levels were higher than expected by 32% of the IQR; remaining pollutants were between 10% of their IQR lower and 9% of their IQR higher than expected. After the states reopened, ozone and NO2 levels were close to expected levels (0%–1% of their IQR lower than expected), while $PM_{2.5}$, CO, and PM_{10} were higher than expected (8%–33% of their IQR).

Figure 2.3 shows results before, during, and after stay-at-home orders by state. (Alternative versions of this figure – including states that did not issue a stay-at-home order (Figure A.6) – reveal similar results.) The overall patterns described above (during stay-at-home orders, ozone, NO_2, PM_{10}, and CO levels, but not $PM_{2.5}$ levels, were modestly lower than expected) are observed in Figure 2.3; however, none of the patterns are ubiquitous. Considering each map in Figure 2.3 separately, some trends hold for most states, but none hold for all states.

2.4.2 Sensitivity analysis: temporal and weather correction using regression

As Eq.(2.1) corrects for temporal trends and meteorology, the estimated coefficients directly indicate whether year-2020 concentrations were higher (positive coefficients) or lower (negative coefficients) than expected. The results from the linear regression analysis mostly agree with the robust difference results (Table 2.1). Specifically, considering all 5 pollutants both before, during, and after stay-at-home orders (15 total comparisons), the sign of the result is the same between the two methods, with two exceptions. (The two exceptions are for before stay-at-home levels of $PM_{2.5}$ and CO; see **Table S5**. Specifically, the average robust difference before stay-at-home $PM_{2.5}$ and CO is 0.09, suggesting that $PM_{2.5}$ and CO were slightly higher than expected before stay-at-home orders. In contrast, the regression analysis indicates that before-stay-at-home $PM_{2.5}$ was, on average, 0.28 $\mu g/m^3$ lower than expected and CO was at the expected level.)

Furthermore, the trend in estimated coefficients aggregated by week is similar to the trend in robust differences by week before, during, and after stay-at-home orders. The concentration anomaly for all pollutants except $PM_{2.5}$ started 3–4 weeks before stay-at-home orders, and the anomaly decreased over time (Figs. 2.2 and A.8).

The results from the spline regression (Eq.(2.2)) are generally consistent. In some cases, the results vary with the degrees of freedom of the spline function. (Specifically, the results for during stay-at-home order PM_{10} and after stay-at-home ozone, NO_2, and CO varied among spline degrees of freedom)

2.4.3 Potential effects of upwind ozone entering the US

Two upwind background sites in California (LAV and THD) [121] exhibit lower-than-expected ozone concentrations around the time of the Covid response, but not to the same degree as seen above at the EPA sites (Figure A.10). Overall, additional analyses will be needed to ascertain how much of 2020 ozone anomalies seen over the US are due to Covid-related vs. transport effects. Our analysis suggests that the regional transport of ozone cannot fully explain the observed concentration patterns.

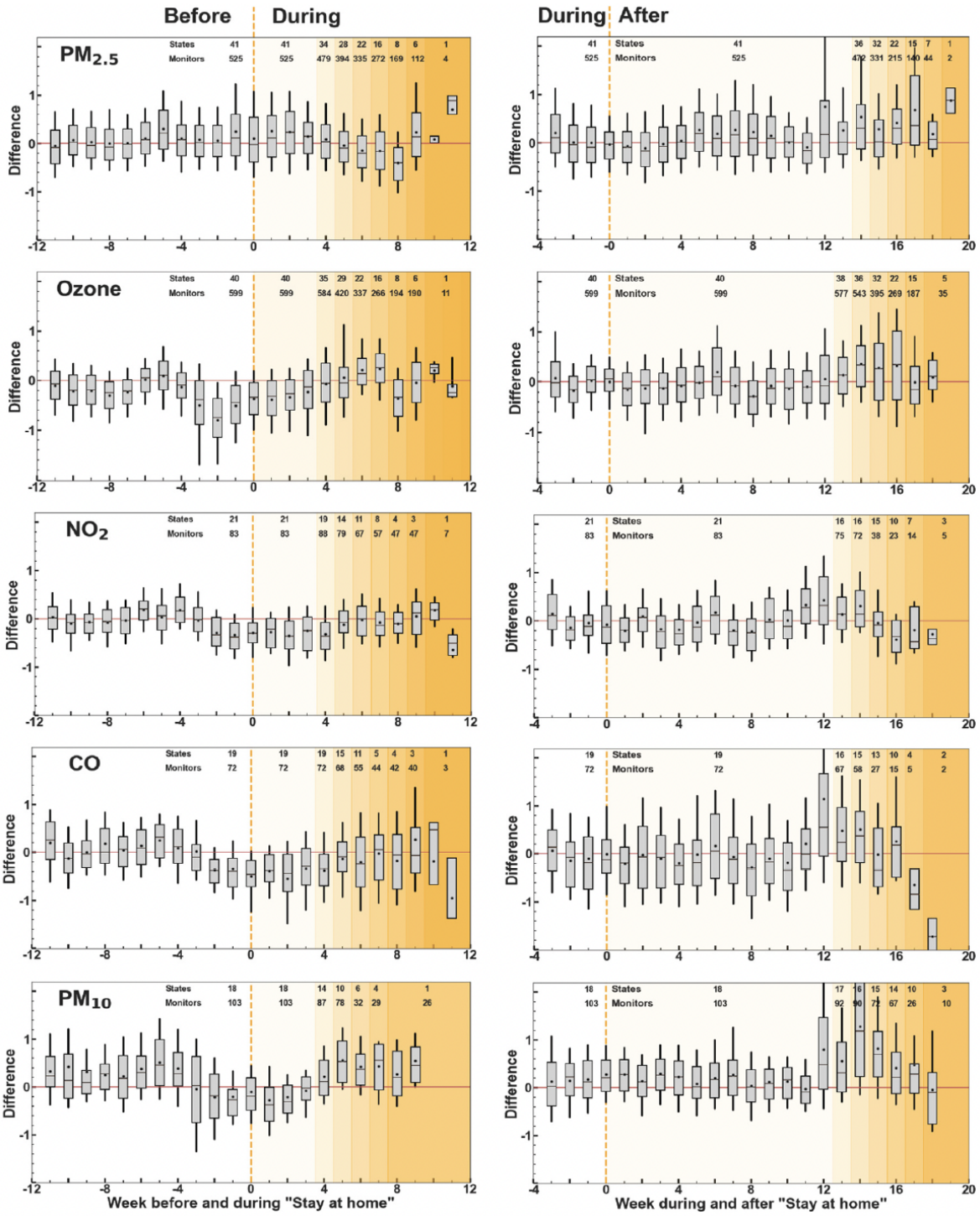

Figure 2.2: Robust differences (Eq.(1)) between year-2020 and the long-term average for that week, for $PM_{2.5}$, ozone, NO_2, CO and PM_{10} concentrations (top to bottom rows, respectively), with time adjusted to match each state's stay-at-home order. Left column: $time = 0$ reflects the day that stay-at-home started in that state. These plots compare before ($time < 0$) and during ($time > 0$) stay-at-home. Right column: time=0 reflects the day that stay-at-home stopped in that state. These plots compare during ($time < 0$) and after ($time > 0$) stay-at-home. Numbers inset near the top of each panel indicate the number of states and monitors with data in that range: 41 states enacted stay-at-home orders 4 or more weeks prior to week 35 of the year (i.e., the last week for which we have data), 34 states enacted stay-at-home orders 5 or more weeks before week 35, and 28 states enacted stay-at-home orders 6 or more weeks before week 35 (see Figure A.1). The change in number of states included in the analysis is indicated via the yellow shading. The box plots show 10th, 25th, 75th, and 90th percentiles, the 50th percentile (horizontal line), and the mean (dot); these are summary statistics of monitors throughout the US.

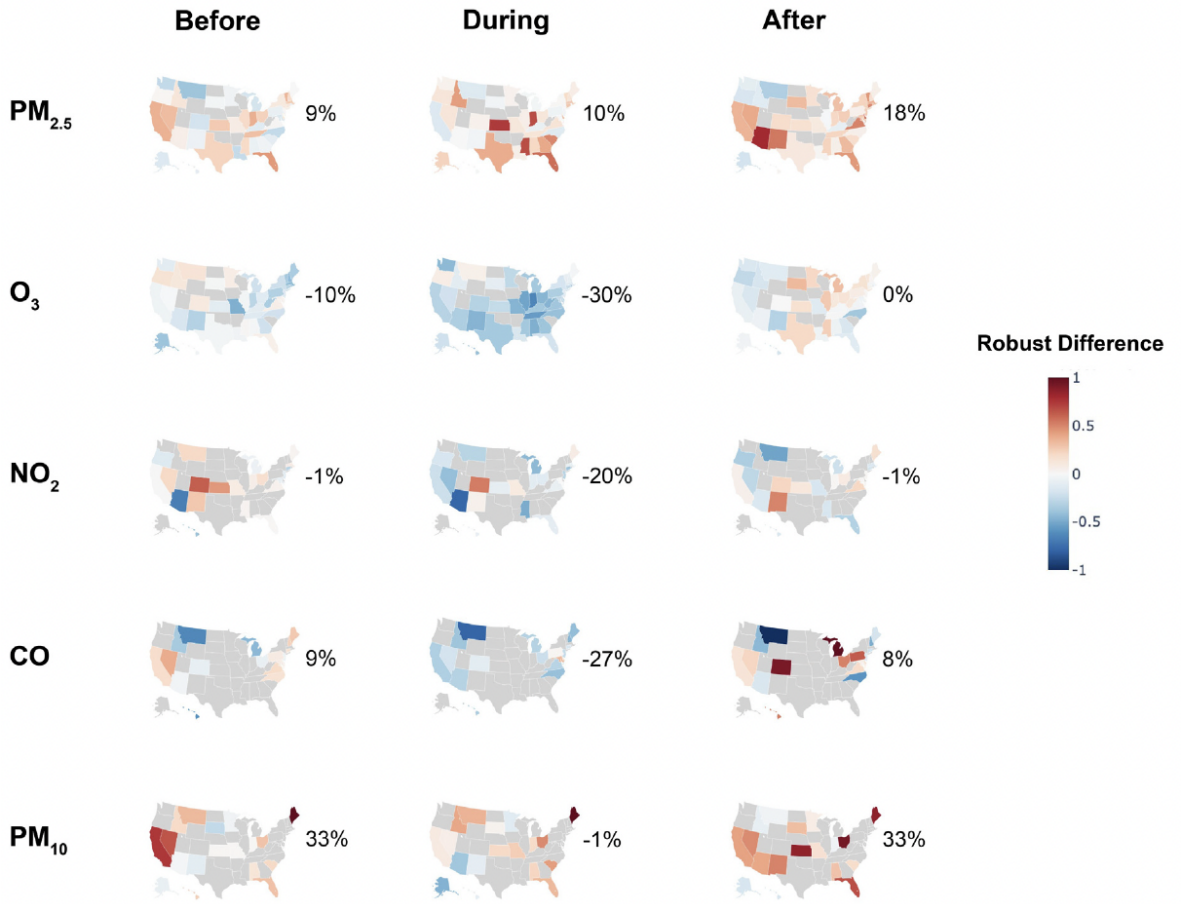

Figure 2.3: Robust differences (see Eq.(1)) by state and pollutant. Here, "before" is the average of weeks 4 to 14 before that state's stay-at-home order; "during" is the average of weeks 1 to 3 before and weeks 1 to 12 during that state's stay-at-home order; and, "after" is the average of weeks 1 to 20 after the end of that state's stay-at-home order. States shown in grey have no monitors that meet selection criteria and/or did not issue a stay-at-home order. The percentage numbers (right-side of each US map) indicate overall average robust differences (units: percentage of its IQR).

Table 2.1: Comparison of actual versus expected concentrations and D values.

Pollutant	Before (weeks −14 to −4)				During (weeks −3 to 12)				After (weeks +1 to +20)			
	Actual	Expected	Difference	D value	Actual	Expected	Difference	D value	Actual	Expected	Difference	D value
$PM_{2.5}$	7.04 $\mu g/m^3$	6.69 $\mu g/m^3$	5.1%	0.09	5.88 $\mu g/m^3$	5.58 $\mu g/m^3$	5.4%	0.10	7.42 $\mu g/m^3$	6.68 $\mu g/m^3$	10.0%	0.18
Ozone	34.79 ppb	35.54 ppb	−1.8%	−0.30	43.01 ppb	45.49 ppb	−5.3%	−0.30	43.62 ppb	43.82 ppb	−0.4%	0.00
NO_2	25.11 ppb	25.13 ppb	−0.1%	−0.01	16.47 ppb	19.16 ppb	−14.0%	−0.20	14.83 ppb	14.99 ppb	−1.8%	−0.01
CO	0.55 ppm	0.51 ppm	7.4%	0.09	0.30 ppm	0.36 ppm	−15.3%	−0.27	0.31 ppm	0.30 ppm	3.7%	0.08
PM_{10}	17.60 $\mu g/m^3$	14.83 $\mu g/m^3$	18.6%	0.32	17.27 $\mu g/m^3$	18.30 $\mu g/m^3$	−5.7%	−0.10	26.55 $\mu g/m^3$	22.66 $\mu g/m^3$	17.1%	0.33

2.5 Discussion

Covid's overall impacts are terrible, causing death, disease, job loss, economic loss, stress, and isolation. The societal response to Covid has caused enormous economic changes, likely shifting patterns of activity by people, governments, schools, companies, and industrial facilities. These changes create a unique opportunity to investigate the effects of human activity on air quality. To quantify these impacts, we analyzed criteria air pollution data from the EPA national monitoring network. We found that, during stay-at-home orders, levels of ozone, NO_2, CO, and PM_{10} were lower than expected, but the anomaly was modest and temporary. ($PM_{2.5}$ levels during stay-at-home orders were not lower than expected.) The decrease for ozone, NO_2, CO, and PM_{10} started approximately three weeks prior to the stay-at-home order, and the anomaly lessened over time. Four weeks after the stay-at-home orders, PM_{10} levels were at expected levels; five weeks after, ozone, NO_2, and CO levels were at expected

levels ($p > 0.10$). Most pollutants exhibited lower-than-expected levels of air pollution during the Covid response. However, the modest size of the drop (substantially less than one IQR) i.e., a drop substantially less than typical year-to-year variability) and the fact that the drop was not sustained over time were both somewhat unexpected given the large reductions in social and economic activity implied by "stay-at-home" orders. $PM_{2.5}$ did not exhibit a drop in pollution levels, which is another unexpected finding.

Air pollution concentrations depend on a complex mixture of sources, meteorology, and other factors. In order to isolate the effects of societal responses to Covid, one must control for non-COVID-response factors. We applied two methods to control for the effects of seasonal and longer-term patterns and meteorology. The two approaches reveal broadly consistent conclusions. While our results reveal patterns and trends, they do not indicate causation or regulatory impacts; additional research is needed to quantify the extent to which the observed changes are attributable to Covid-related changes (e.g., stay-at-home orders) versus other factors.

The results reveal important differences among pollutants. NO_2 and CO are primary (i.e., directly emitted) pollutants; as a result, connections between changes in activity, emissions, and concentrations are relatively direct. In contrast, ambient $PM_{2.5}$ includes both primary and secondary (formed in the atmosphere from chemical reactions) components. Ground-level ozone is secondary. For secondary pollutants, the connections between activity level, emissions, and concentrations are more complicated and, as discussed below, reflect nonlinear atmospheric chemistry and emissions. Traffic is a major source of NO_2 and CO; in contrast, emissions from many sources contribute to levels of $PM_{2.5}$, PM_{10}, and ozone.

This chapter contributes to the growing body of literature on the impacts of the Covid-19 response on air quality by examining data on a national scale, utilizing available in-situ measurements for multiple criteria pollutants, accounting for both random and non-random temporal variability, and performing sensitivity analyses that include explicit adjustments for meteorological factors. Furthermore, it investigates air quality before, during, and after the implementation of "stay-at-home" orders. Our results are largely consistent with studies that examined widespread changes in the United States. For example, a study examining $PM_{2.5}$ and NO_2 concentrations in 122 counties reported, for the US, a 25% decline in NO_2, and a statistically insignificant decline in $PM_{2.5}$ compared to 2017–2019 levels [98]. Another study found that in 20 US cities, after correcting for meteorology, NO_2 concentrations were 9% - 43% lower than in 2019 [99]. Analyses from individual locations, cities, or areas, can reveal different, potentially larger, impacts than the national-level trends reported here. At a near-road monitoring station in Seattle, WA, concentrations of $PM_{2.5}$, NO_2 and CO during Covid were 2–4% lower than pre-Covid concentrations [100]. Data from a low-cost sensor network in Pittsburgh, PA, suggest that levels of $PM_{2.5}$, NO_2, and CO were 30–50% lower during than pre-Covid [101].

Comparatively larger changes in air pollution have been reported in other countries. For example, in Barcelona, Spain, concentrations of NO_2 and black carbon were 50% lower during stay-at-home orders, but ozone concentrations increased by 50% [86]. In Delhi, India, measured concentrations of PM_{10}, $PM_{2.5}$, NO_2, and CO were substantially lower (for PM_{10} and $PM_{2.5}$, $\sim 2\times$ lower) during shelter-in-place [91]. In three cities in China, $PM_{2.5}$ and NO_2 levels in February 2020 were 30% and 61% lower than February 2017–2019 levels, respectively, but ozone levels were 14% higher than 2017–2019 levels [94]. $PM_{2.5}$ and ozone concentrations in the UK during April 2020 were not systematically different from average concentrations in 2015–2019, but NO_2 concentrations were 20–80% lower [96]. In general, many of these studies did not fully account for random and systematic temporal variability, for multiple time scales, as was done here.

Future research could usefully explore Covid-related changes in emissions and atmospheric chemistry [57, 85, 122], apply empirical modeling (e.g., national land use regression models) to understand spatial patterns in how pollution levels changed [123–125], analyze publicly-available networks of low-cost sensors such as PurpleAir [126, 127], and investigate changes to existing inequalities in exposure to air pollution [117, 128, 129]. First, there is substantial variability—random and systematic—which complicates finding a "signal" in changes in air pollution. We expect these effects would not completely hide large concentration changes, especially given the size of our dataset.

Second, ambient concentrations depend on the activity levels and emissions of many sources. Therefore, reducing emissions from one or a small number of source categories may or may not yield a large change in concentrations. For example, while major reductions in vehicle traffic occurred in many locations due to "stay-at-home" orders, traffic is but one of many sources. In addition, stay-at-home

orders could potentially increase some emissions (e.g., residential wood combustion, and backyard BBQ cooking). Emissions can also nonlinearly follow activity levels (e.g., if traffic reductions are primarily from newer, lower-emitting cars, while older and higher-emitting vehicles preferentially stay in use) or could be offset (e.g., if workplace electricity consumption declines but household electricity consumption increases, or increases at times-of-day when dirtier generators (coal) are more prevalent).

Third, concentrations of secondary pollutants (e.g., ozone and a large portion of $PM_{2.5}$) depend on complex and nonlinear atmospheric chemistry, involving, especially, NO_x and volatile organic compound (VOC) emissions [130]. NO_x is a key player in the photochemical cycle that produces ozone and is a precursor for $PM_{2.5}$ nitrate formation. For example, NO_x reacts with ozone; therefore, higher NO_x emissions can lead to lower ozone concentrations near the emission source, especially in urban areas. The VOC:NO_x ratio influences the radical chemistry that produces ozone and secondary organic aerosol (a major component of $PM_{2.5}$). For example, increasing VOC:NO_x ratios can increase secondary organic aerosol yields, leading to increased $PM_{2.5}$ concentrations [81, 131–133].

Changing NO_x and VOC emissions can alter hydroxyl radical concentrations, potentially leading to more rapid secondary PM and ozone production [134]. This nonlinear chemistry creates multiple ways in which lower emissions can lead to higher secondary pollutant concentrations. An excellent example is the well-known weekend ozone effect, whereby lower traffic emissions cause higher weekend ozone levels [135]. Similar phenomena may explain the increases in ozone concentration in response to Covid reported by some studies [86, 91]. Overall, the trends we observe are qualitatively consistent with known atmospheric chemistry.

Finally, the effects on air quality of societal responses to Covid may be lower in the US than in other countries, in part because of the comparatively cleaner air in the US [53, 136]. For example, because vehicle tailpipe emission factors are lower in the US than in many countries, reductions in driving, and the resulting reductions in tailpipe emissions, may have a smaller impact on air pollution levels for the US than for other countries.

2.6 Conclusion

We employed the "Robust Differences" method to examine the impacts of socio-economic changes resulting from Covid-19 stay-at-home orders on levels of criteria air pollutants across hundreds of EPA monitoring stations in the US. Additionally, a regression approach was used to derive "expected" pollution levels as part of a sensitivity analysis. Both methods controlled for random and systematic variability across multiple timescales, specifically by monitor-week, providing a robust baseline for comparison with observed pollution levels.

The findings indicate that during the stay-at-home orders, average $PM_{2.5}$ levels were consistently higher than anticipated. In contrast, average levels of ozone, NO_2, CO, and PM_{10} were slightly lower than expected. Shortly after the implementation of the stay-at-home orders, anomalies in pollutant concentrations ceased, with ozone, NO_2, and CO returning to expected levels, whereas $PM_{2.5}$ and PM_{10} remained higher than expected. These observations contrast with similar studies that typically reported reductions across all criteria pollutants, including $PM_{2.5}$. This chapter not only presents an alternative method to conduct an accountability study but also highlights how results can vary significantly depending on the analytical approach employed.

2.7 Appendix A: Supplemental Information for Chapter 2

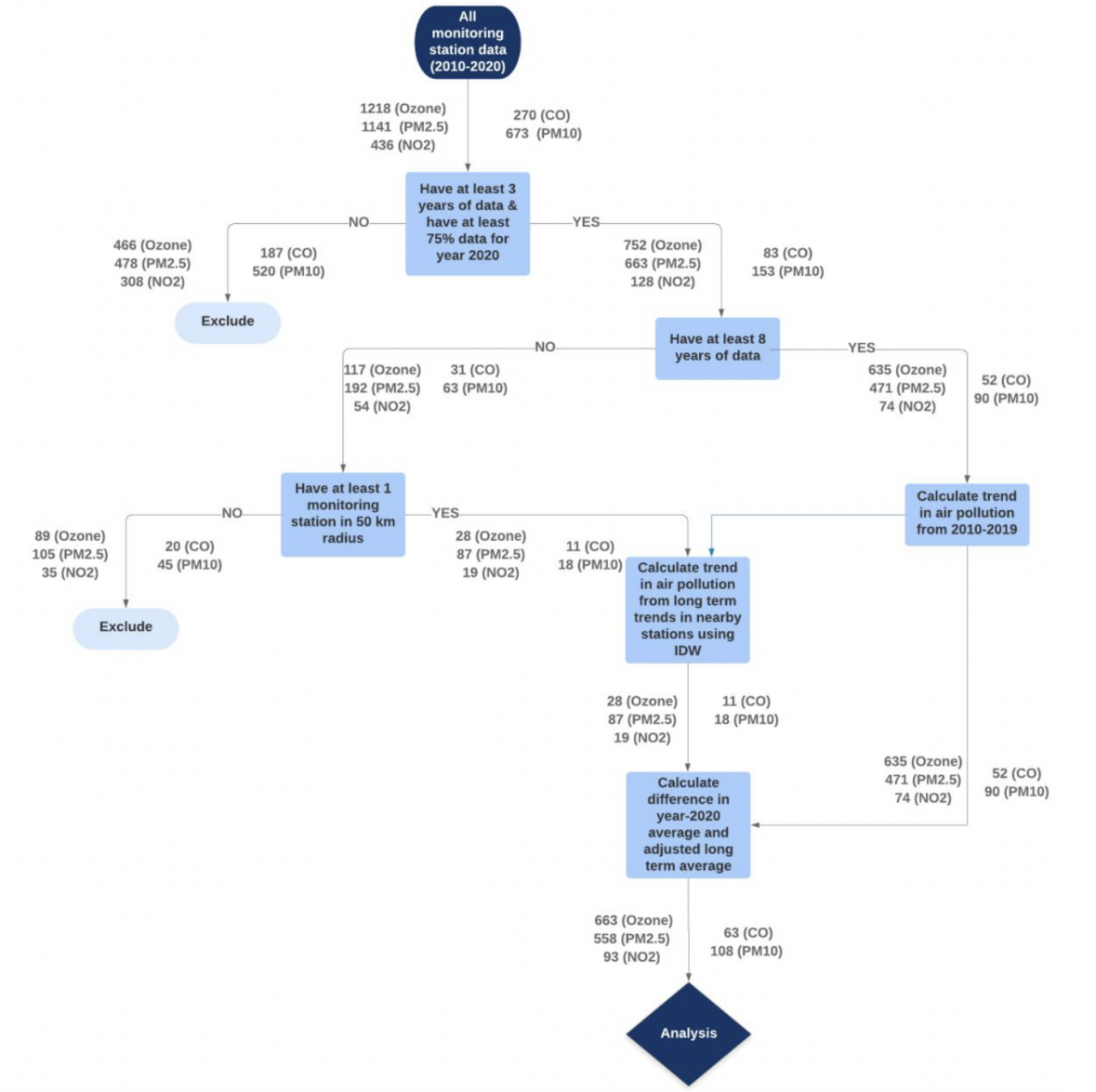

Figure A.1: Monitor inclusion rule flow diagram. Numbers indicate the number of monitors

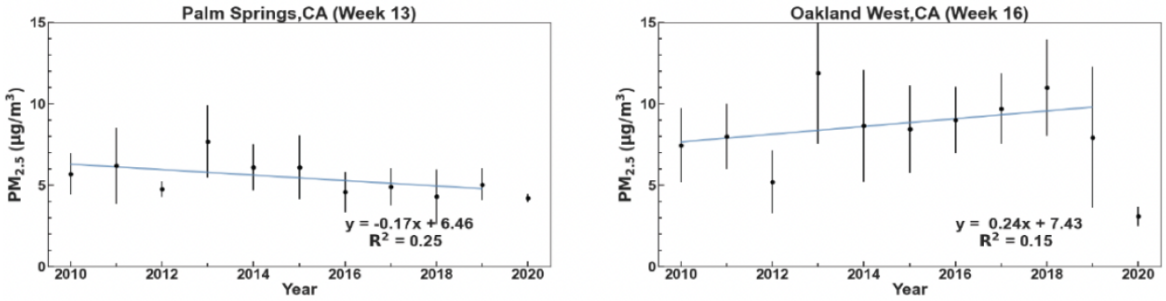

Figure A.2: Examples of temporal correction for $PM_{2.5}$Palm Springs, CA, monitor for week 13 (left) and Oakland West, CA, monitor for week 16 (right). Slopes (units: μg m^{-3} y^{-1}) are -0.17 (left), 0.24 (right). Temporal (10-year) corrections are used to adjust 2010–2019 pollution levels to an "expected" year-2020 level. These two monitor weeks were chosen as examples because their slopes have similar magnitude but opposite signs; the slope and R^2 for the left plot are approximately equal to the national medians. (Median temporal correction slopes and R^2 for all pollutants are shown in Table A 2.4.)

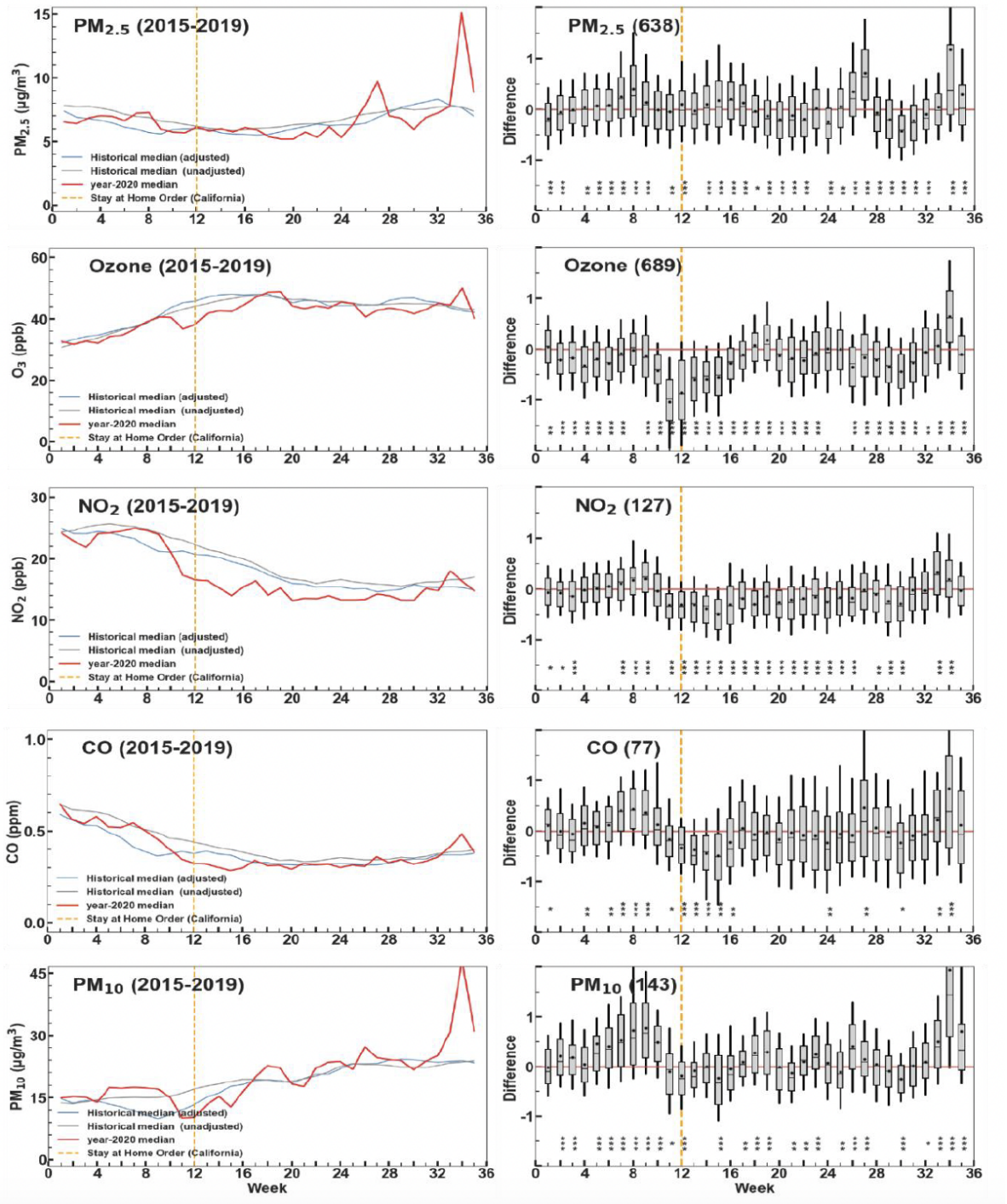

Figure A.3: This figure (left) is analogous to Figure 2.1 but uses historical trends derived from 5 years of data (2015-2019) instead of 10 years (2010-2019). (In the main text, the historical median is the 10-year median, here it is the 5-year median.)

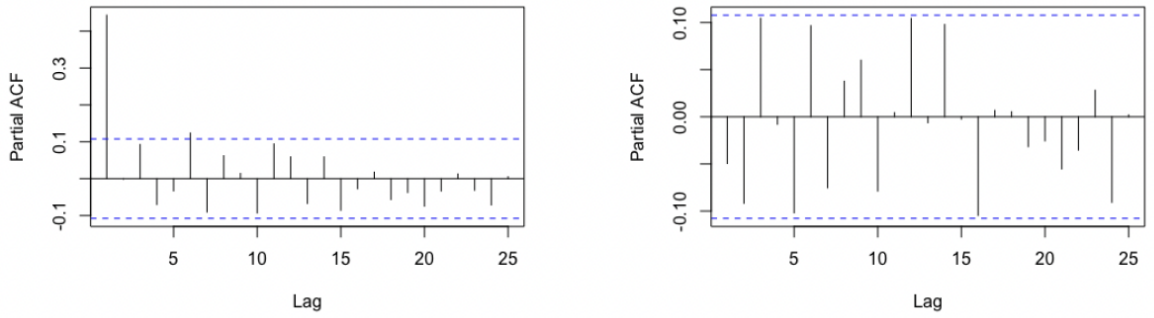

Figure A.4: Example of reducing autocorrelation using autoregressive analysis. Autoregression in PM2.5 monitor in Hawaii before (left) and after (right) using multivariate autoregressive analysis.

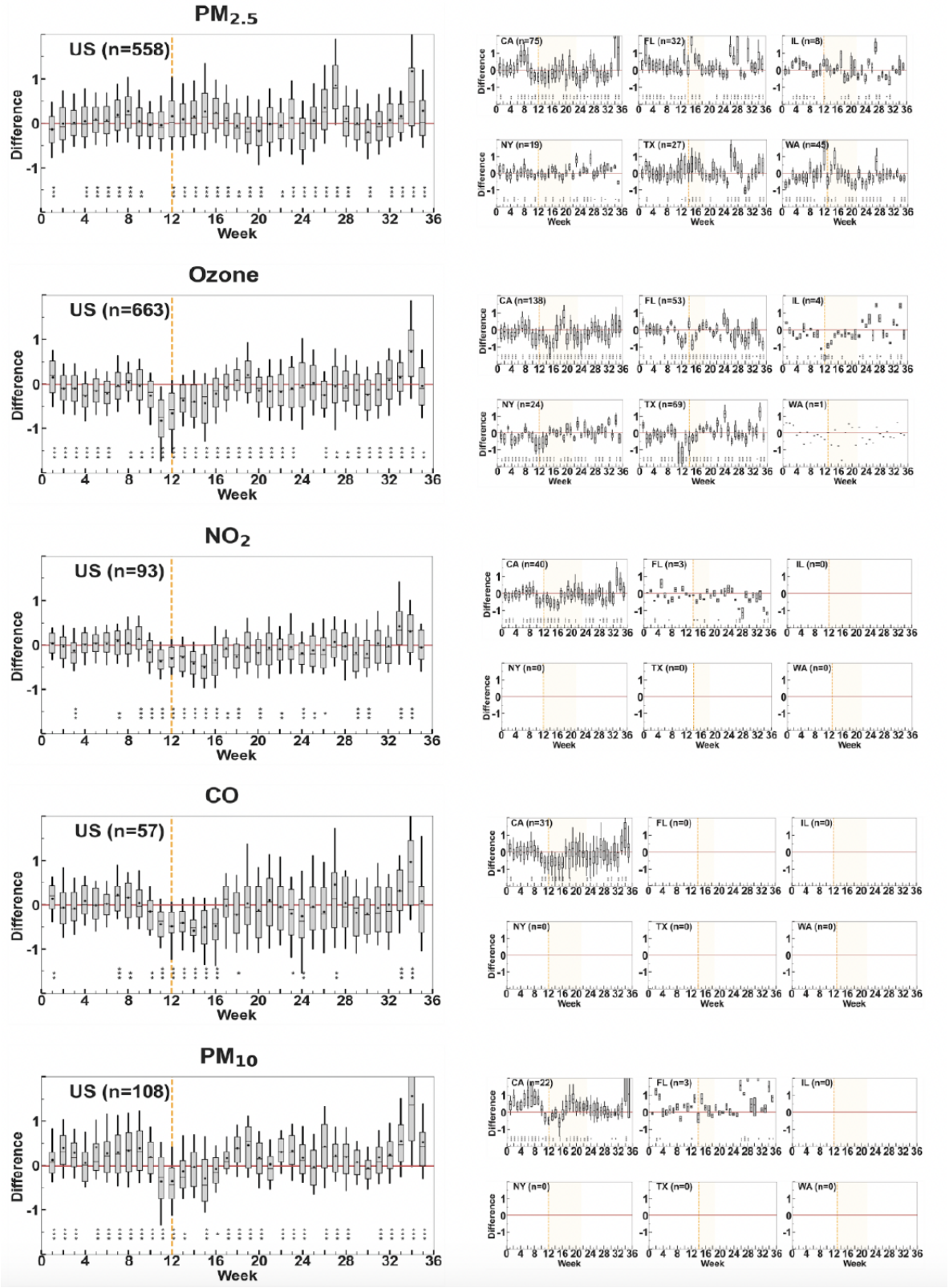

Figure A.5: Robust differences (equation 1) between year-2020 and the long-term average for that week, for $PM_{2.5}$, ozone, NO_2, CO and PM_{10} concentrations (from top to bottom rows, respectively), for the whole US (left column) and for 6 large US states (right columns): upper row: California (CA), Florida (FL), and Illinois (IL); lower row: New York (NY), Texas (TX), and Washington (WA). The start date for stay-at-home orders differs by state, as shown via the vertical dashed line for that state. (The vertical dashed line in the left plot [whole US] indicates the timing of the first stay-at-home order in the US: Week 12 [CA].

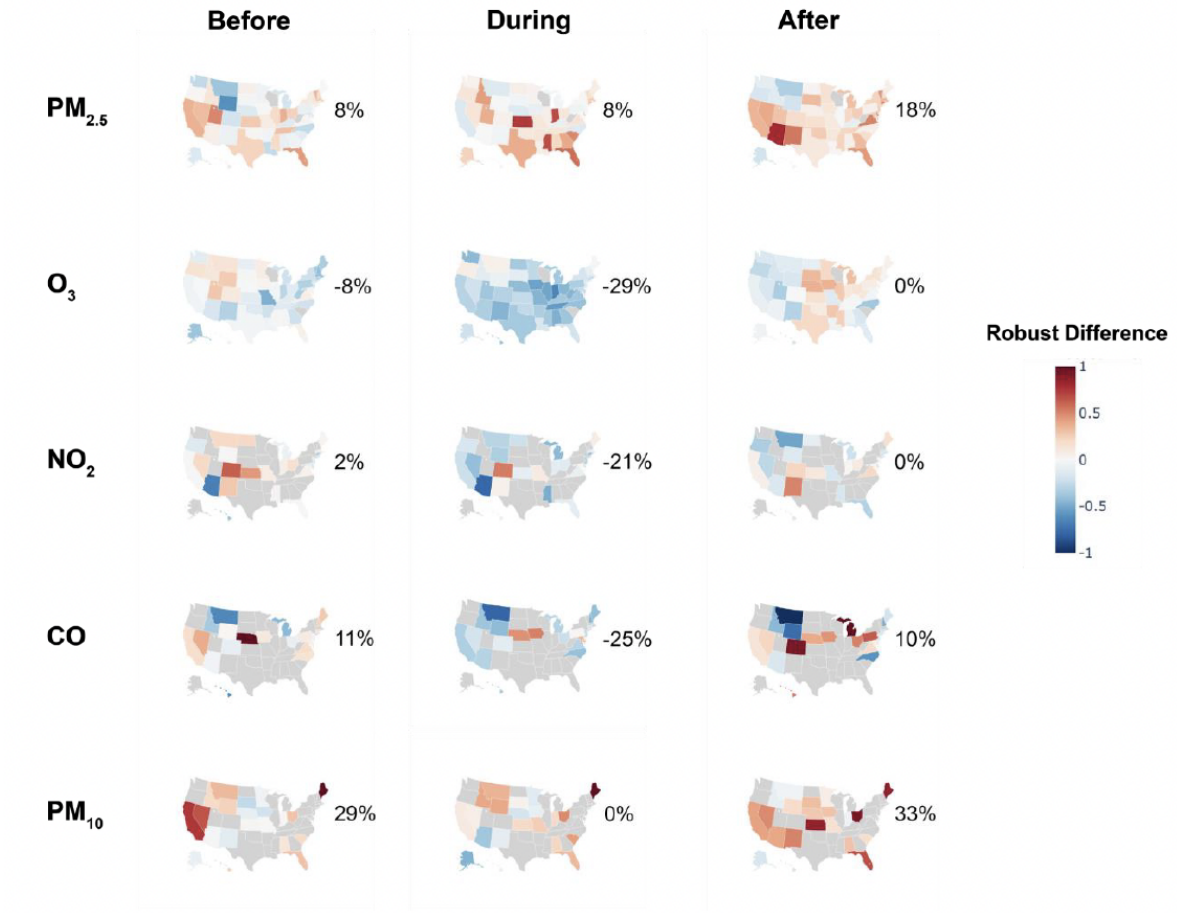

Figure A.6: This figure is analogous to Figure 2.3 but includes robust differences in states that did not issue a stay-at-home order. States shown in grey have no monitors that meet the selection criteria. The number of percentages (right-side of each US map) indicate overall average robust differences in the percentage of its IQR. Dates of shutdown and reopening of California were used for the states that did not issue a stay-at-home order.

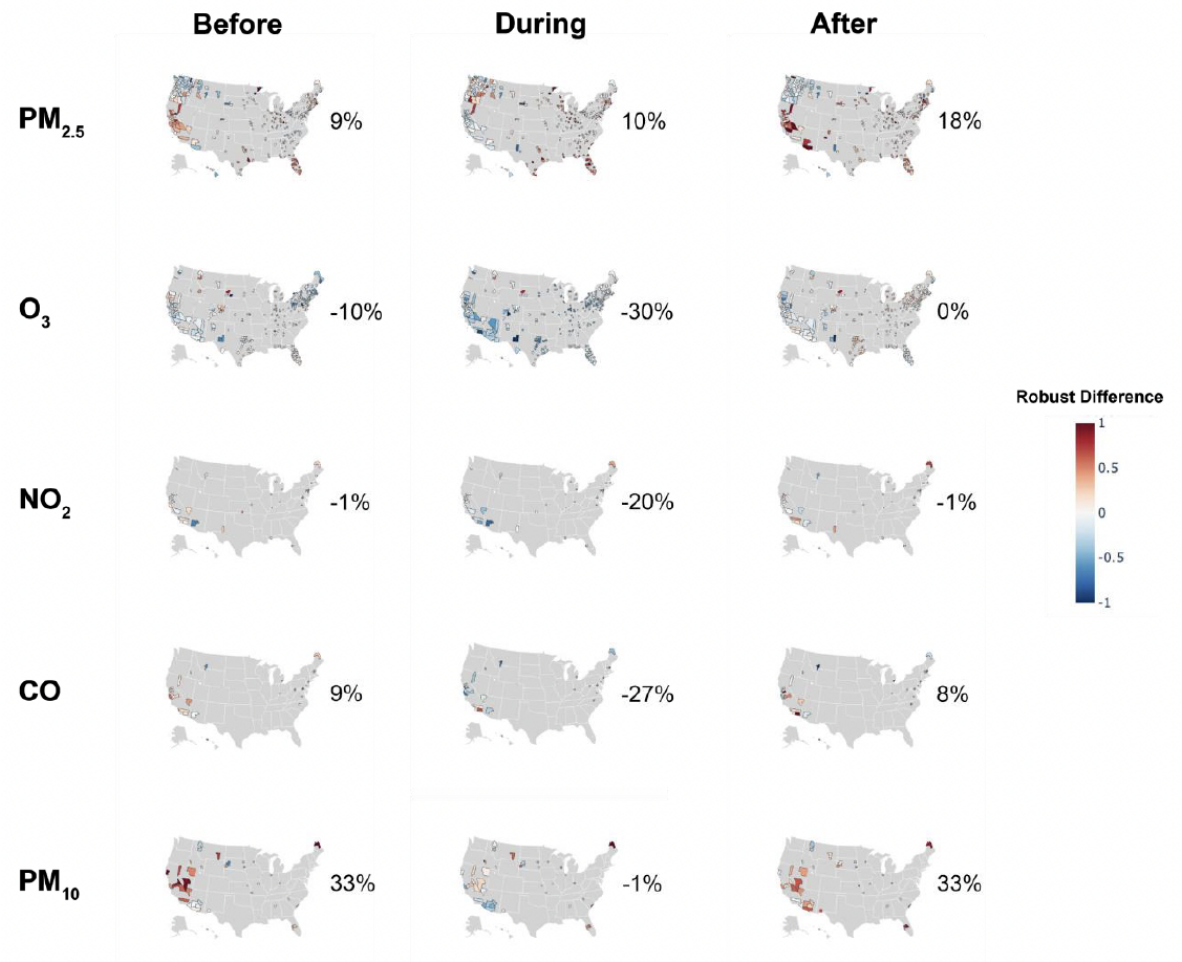

Figure A.7: This figure is analogous to Figure 2.3 but aggregated by counties. Counties shown in grey have no monitors that meet the selection criteria. The number of percentages (right-side of each US map) indicate overall average robust differences in percentage of its IQR.

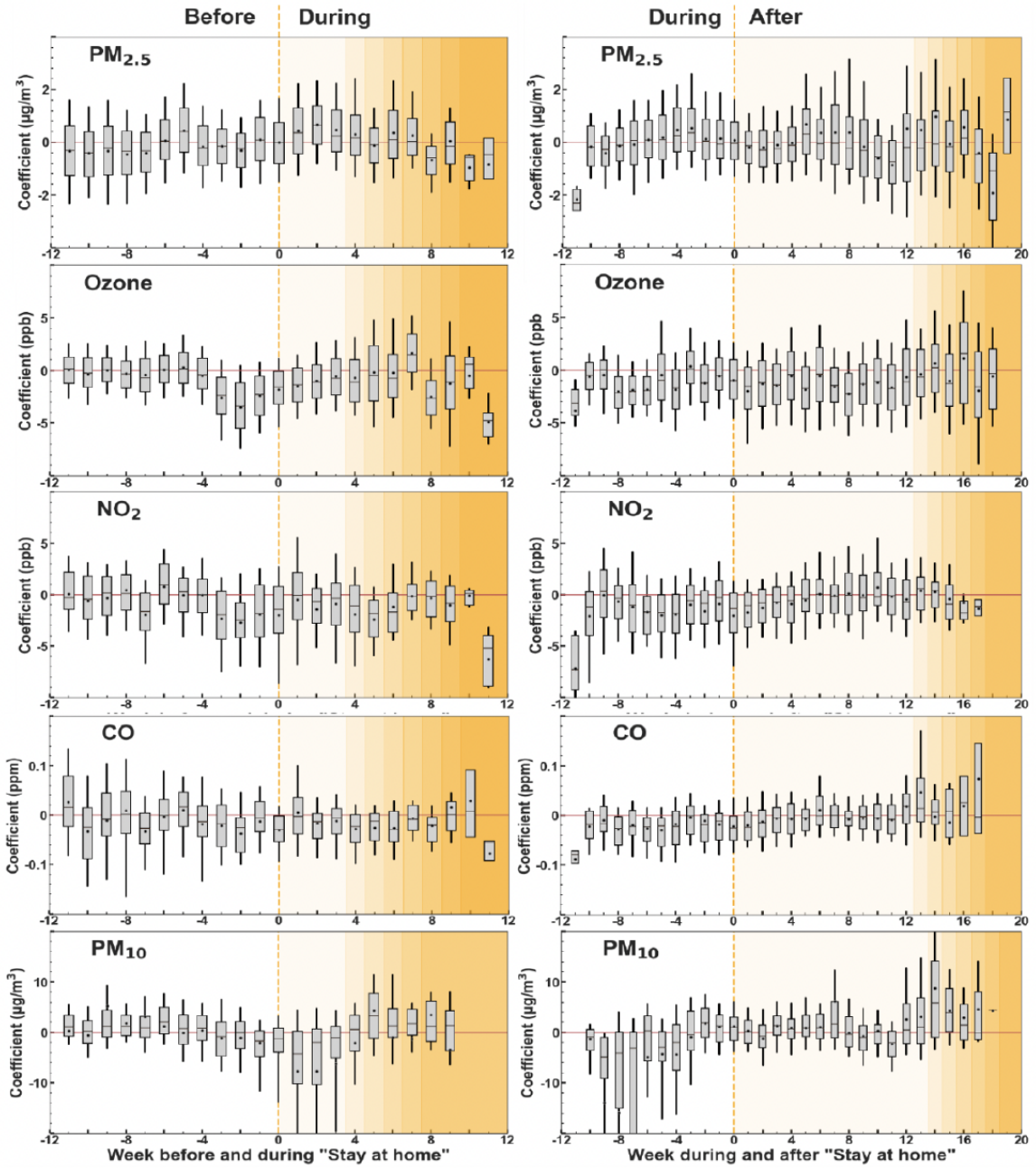

Figure A.8: Estimated coefficients (equation 2) of year-2020 concentrations after correcting for meteorology and temporal trend, for $PM_{2.5}$, ozone, NO_2, CO, and PM_{10} concentrations (top to bottom rows, respectively), with time adjusted to match each state's stay-at-home order. These plots are analogous to Figure 2.2, but using the results from the linear regression method (Eq.(2.2)). Left column: time = 0 reflects the day that stay-at-home started. These plots compare before (time<0) and during (time>0) stay-at-home. Right column: time = 0 reflects the day that stay-at-home stopped. These plots compare during (time<0) and after (time>0) stay-at-home.

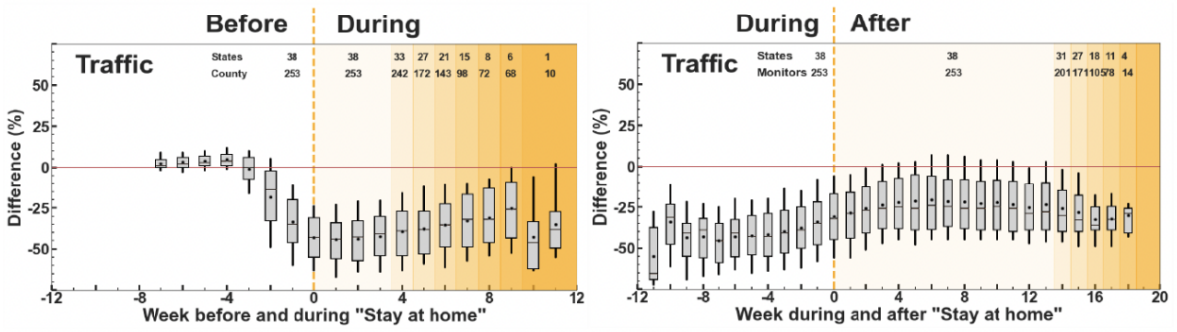

Figure A.9: Transit mobility changes in percentage from median base level (median traffic during 5 week period Jan 3 - Feb 6, 2020). Left column: time = 0 reflects the day that stay-at-home started. These plots compare before (time<0) and during (time>0) stay-at-home. Right column: time=0 reflects the day that stay-at-home stopped. These plots compare during (time<0) and after (time>0) stay-at-home. Numbers inset near the top of each panel indicate the number of states and counties with both mobility and monitoring data available.

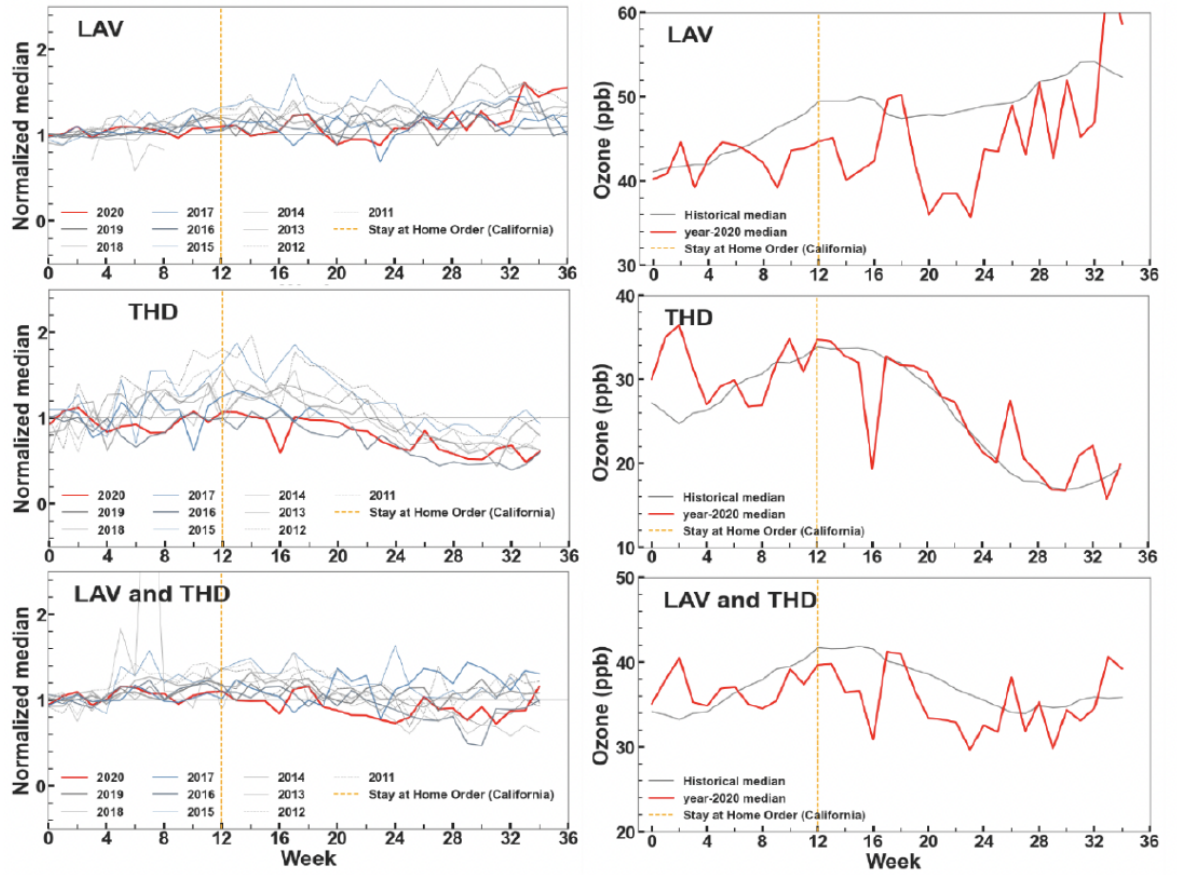

Figure A.10: Ozone concentrations at two upwind locations ((Lassen Volcanic National Park, California [LAV] and Trinidad Head, California [THD]) for 2010-2020, analyzed in the same manner as data in Figure 2.1.

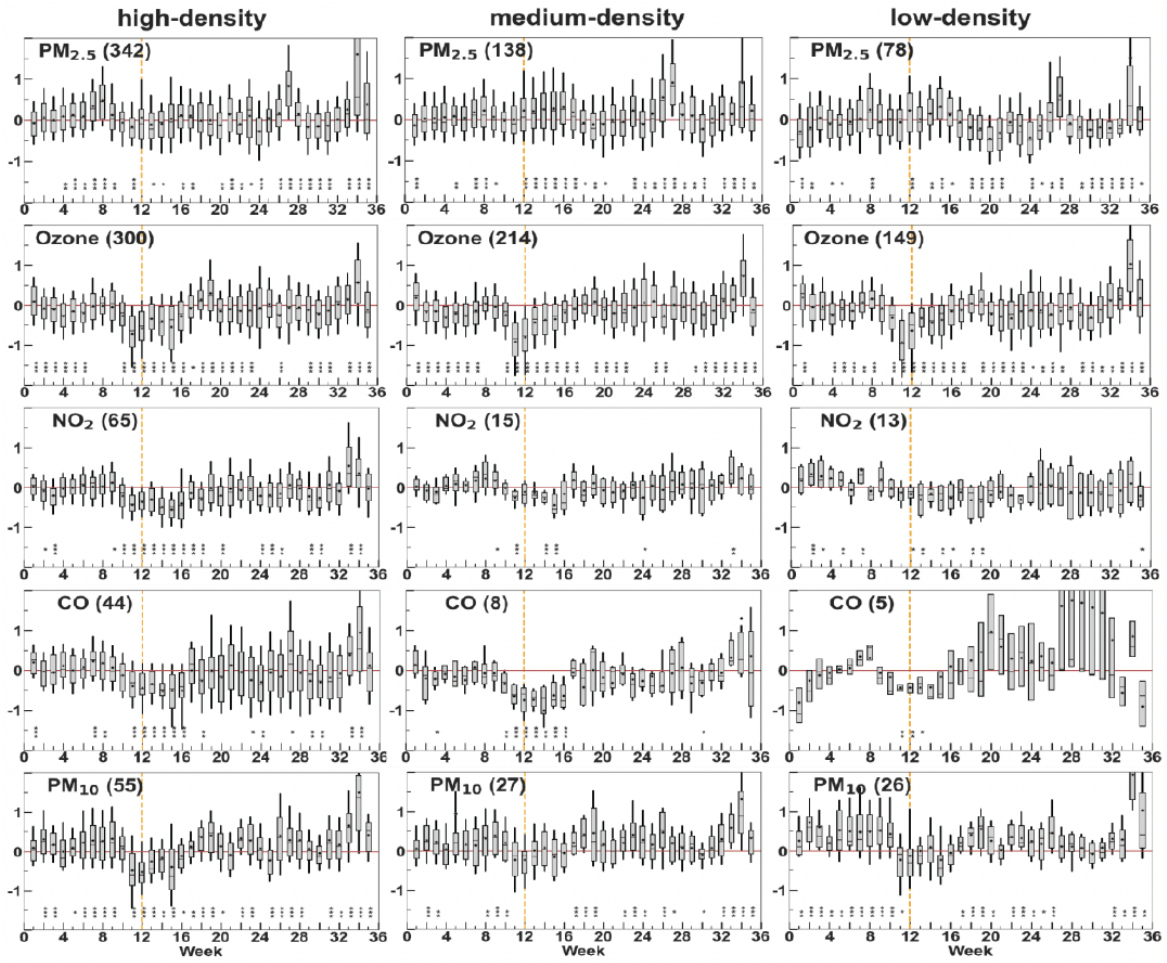

Figure A.11: Criteria pollutant level in low-, medium-, and high-density areas (categories, in people per square mile: <50, 50-1000, >1000). The number in parentheses is a number of monitors. The orange vertical dashed line indicates the timing of the first stay-at-home order in the contiguous US: week 12 [CA]

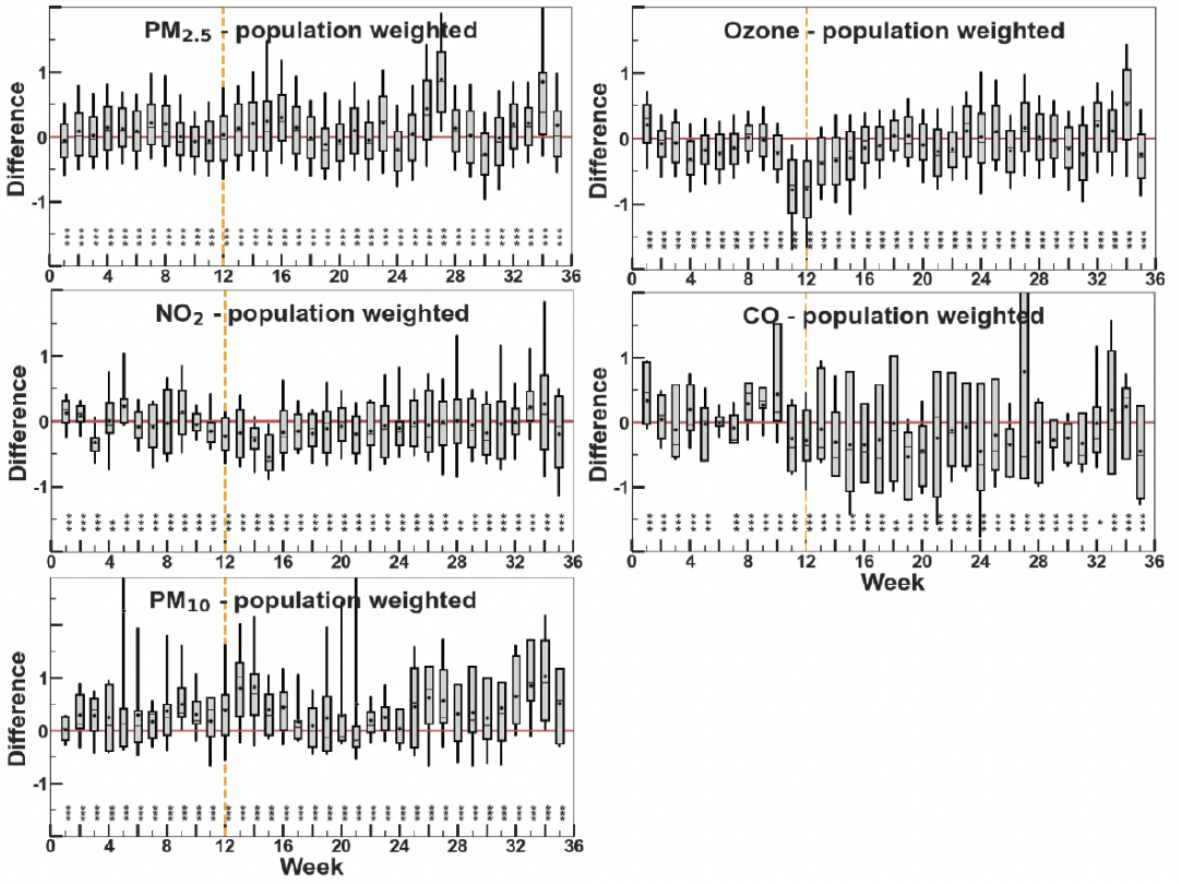

Figure A.12: Robust differences using population-weighting. The plots are analogous to Figure A2.5, but use population-weighting instead of the straightforward average of monitors. Population weighting is based on Census Tract population and centroids: for each Census Tract, we found the nearest monitor; we then calculated a population-weighted average of all Tracts, based on concentrations at the nearest monitor. In this manner, the unit of analysis here is a person (based on the nearest monitor), versus (in the main text) a monitor. The orange vertical dashed line indicates the timing of the first stay-at-home order in the contiguous US: week 12 [CA]

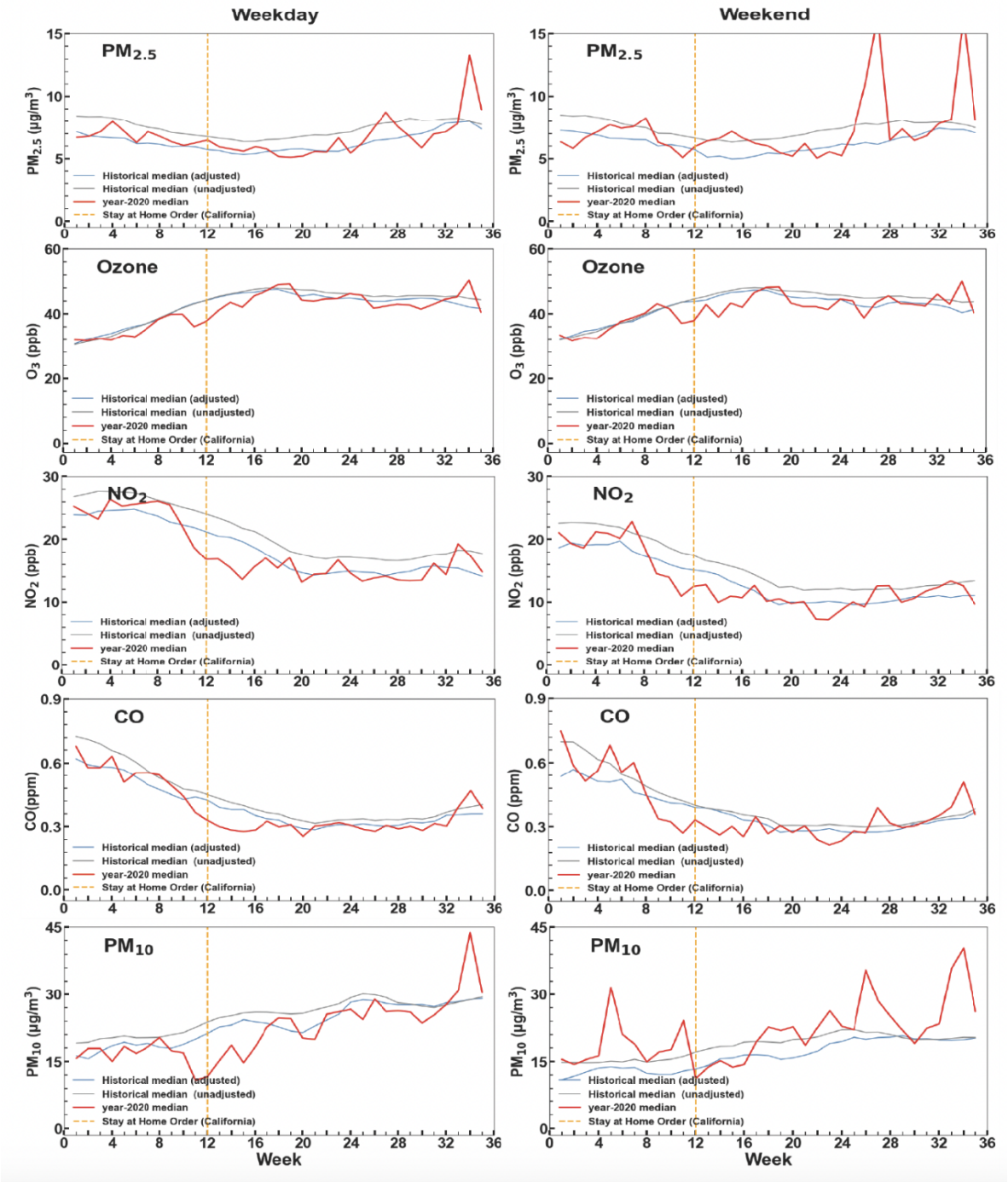

Figure A.13: This figure is analogous to Figure 2.1 but disaggregating weekdays and weekends. The orange vertical dashed line indicates the timing of the first stay-at-home order in the contiguous US: week 12 [CA]

Table A.1: Before, during, and after stay-at-home order periods by state

	Before stay-at-home		During stay-at-home		After stay-at-home	
State	Start	End	Start	End	Start	End
Alabama	1-Jan	3-Apr	4-Apr	30-Apr	1-May	1-Sep
Alaska	1-Jan	27-Mar	28-Mar	24-Apr	25-Apr	1-Sep
Arizona	1-Jan	30-Mar	31-Mar	8-May	9-May	1-Sep
Arkansas						
California	1-Jan	18-Mar	19-Mar	25-May	26-May	1-Sep
Colorado	1-Jan	25-Mar	26-Mar	27-Apr	28-Apr	1-Sep
Connecticut	1-Jan	22-Mar	23-Mar	20-May	21-May	1-Sep
Delaware	1-Jan	23-Mar	24-Mar	1-Jun	2-Jun	1-Sep
Florida	1-Jan	2-Apr	3-Apr	4-May	5-May	1-Sep
Georgia	1-Jan	2-Apr	3-Apr	24-Apr	25-Apr	1-Sep
Hawaii	1-Jan	24-Mar	25-Mar	7-May	8-May	1-Sep
Idaho	1-Jan	24-Mar	25-Mar	1-May	2-May	1-Sep
Illinois	1-Jan	20-Mar	21-Mar	29-May	30-May	1-Sep
Indiana	1-Jan	23-Mar	24-Mar	4-May	5-May	1-Sep
Iowa						
Kansas	1-Jan	29-Mar	30-Mar	4-May	5-May	1-Sep
Kentucky	1-Jan	25-Mar	26-Mar	20-May	21-May	1-Sep
Louisiana	1-Jan	22-Mar	23-Mar	15-May	16-May	1-Sep
Maine	1-Jan	1-Apr	2-Apr	1-May	2-May	1-Sep
Maryland	1-Jan	29-Mar	30-Mar	15-May	16-May	1-Sep
Massachusetts	1-Jan	23-Mar	24-Mar	18-May	19-May	1-Sep
Michigan	1-Jan	23-Mar	24-Mar	1-Jun	2-Jun	1-Sep
Minnesota	1-Jan	26-Mar	27-Mar	18-May	19-May	1-Sep
Mississippi	1-Jan	2-Apr	3-Apr	27-Apr	28-Apr	1-Sep
Missouri	1-Jan	5-Apr	6-Apr	4-May	5-May	1-Sep
Montana	1-Jan	27-Mar	28-Mar	26-Apr	27-Apr	1-Sep
Nebraska						
Nevada	1-Jan	31-Mar	1-Apr	9-May	10-May	1-Sep
New Hampshire	1-Jan	26-Mar	27-Mar	11-May	12-May	1-Sep
New Jersey	1-Jan	20-Mar	21-Mar	9-Jun	10-Jun	1-Sep
New Mexico	1-Jan	23-Mar	24-Mar	16-May	17-May	1-Sep
New York	1-Jan	21-Mar	22-Mar	29-May	30-May	1-Sep
North Carolina	1-Jan	29-Mar	30-Mar	8-May	9-May	1-Sep
North Dakota						
Ohio	1-Jan	22-Mar	23-Mar	12-May	13-May	1-Sep
Oklahoma						
Oregon	1-Jan	22-Mar	23-Mar	15-May	16-May	1-Sep
Pennsylvania	1-Jan	31-Mar	1-Apr	15-May	16-May	1-Sep
Rhode Island	1-Jan	27-Mar	28-Mar	9-May	10-May	1-Sep
South Carolina	1-Jan	6-Apr	7-Apr	20-Apr	21-Apr	1-Sep
South Dakota						
Tennessee	1-Jan	30-Mar	31-Mar	27-Apr	28-Apr	1-Sep
Texas	1-Jan	1-Apr	2-Apr	1-May	2-May	1-Sep
Utah						
Vermont	1-Jan	24-Mar	25-Mar	15-May	16-May	1-Sep
Virginia	1-Jan	29-Mar	30-Mar	15-May	16-May	1-Sep
Washington	1-Jan	24-Mar	25-Mar	26-May	27-May	1-Sep
West Virginia	1-Jan	23-Mar	24-Mar	4-May	5-May	1-Sep
Wisconsin	1-Jan	24-Mar	25-Mar	13-May	14-May	1-Sep
Wyoming						

Table A.2: Start and end date of each week during 2020 (a leap year)

Week Number	Start Date	End Date
1	01 January 2020	07 January 2020
2	08 January 2020	14 January 2020
3	15 January 2020	21 January 2020
4	22 January 2020	28 January 2020
5	29 January 2020	04 February 2020
6	05 February 2020	11 February 2020
7	12 February 2020	18 February 2020
8	19 February 2020	25 February 2020
9	26 February 2020	03 March 2020
10	04 March 2020	10 March 2020
11	11 March 2020	17 March 2020
12	18 March 2020	24 March 2020
13	25 March 2020	31 March 2020
14	01 April 2020	07 April 2020
15	08 April 2020	14 April 2020
16	15 April 2020	21 April 2020
17	22 April 2020	28 April 2020
18	29 April 2020	05 May 2020
19	06 May 2020	12 May 2020
20	13 May 2020	19 May 2020
21	20 May 2020	26 May 2020
22	27 May 2020	02 June 2020
23	03 June 2020	09 June 2020
24	10 June 2020	16 June 2020
25	17 June 2020	23 June 2020
26	24 June 2020	30 June 2020
27	01 July 2020	07 July 2020
28	08 July 2020	14 July 2020
29	15 July 2020	21 July 2020
30	22 July 2020	28 July 2020
31	29 July 2020	04 August 2020
32	05 August 2020	11 August 2020
33	12 August 2020	18 August 2020
34	19 August 2020	25 August 2020

Table A.3: Median (IQR) temporal correction and R^2 among all monitors and typical annual change represented by the temporal correction. Population weighting is based on Census Tract population and centroids: for each Census Tract, we found the nearest monitor; we then calculated a population-weighted average of all tracts, based on historical median concentrations at the nearest monitor. The typical annual change is calculated by dividing the median slope by the population weighted average concentrations.

Pollutant	Temporal correction Median (IQR)	R^2 Median (IQR)	Population weighted average concentration during 2010-2019	Annual change Median (IQR)
$PM_{2.5}$	-0.22 (-0.41 to 0.06) μg/m^3	0.21 (0.06 to 0.42)	7.2 μg/m^3	-3.0% (-5.2% to -0.8%)
Ozone	-0.08 (-0.3 to 0.2) ppb	0.10 (0.03 to 0.24)	43 ppb	-0.2% (-0.7% to 0.4%)
NO_2	-0.52 (-0.23 to -0.81) ppb	0.28 (0.10 to 0.48)	22.2 ppb	-2.1% (-1.3% to -3.9%)
CO	-0.007 (-0.02 to 0.0) ppm	0.13 (0.04 to 0.32)	0.5 ppm	-1.7% (-3.8% to 0.0%)
PM_{10}	-0.37 (-0.85 to 0.07) μg/m^3	0.15 (0.03 to 0.37)	21.2 μg/m^3	-2.2% (-3.8% to 0.3%)

Table A.4: Results from multivariate linear autoregression method, before, during, and after a state's stay-at-home order.

		Before stay-at-home orders (weeks -14 to -4)		During stay-at-home orders (weeks -3 to 12 of stay-at-home orders)		After stay-at-home orders (weeks +1 to +20 *after the removal* of stay-at-home order)		
Pollutant	**Population weighted average concentration (2010-2019)**	**Estimated coefficient**	**Effect before stay-at-home order**	**Estimated coefficient**	**Effect during stay-at-home order**	**Estimated coefficient**	**Effect after stay-at-home order**	**R^2 Median (IQR)**
$PM_{2.5}$	7.2 μg/m^3	-0.11μg/m^3	-1.6%	0.14 μg/m^3	2.1%	0.09 μg/m^3	1.2%	0.41 (0.34 to 0.49)
Ozone	43.0 ppb	-0.09 ppb	-0.2%	-1.4 ppb	-3.3%	-1.1 ppb	-2.5%	0.42 (0.35 to 0.49)
NO_2	22.2 ppb	-0.50 ppb	-2.3%	-0.81 ppb	-3.6%	-0.47 ppb	-2.1%	0.35 (0.24 to 0.45)
CO	0.5 ppm	0.00 ppm	0.1%	-0.02 ppm	-3.5%	0.01 ppm	2.1%	0.45 (0.34 to 0.57)
PM_{10}	21.2 μg/m^3	1.20 μg/m^3	5.7%	-2.94 μg/m^3	-14.0%	1.55 μg/m^3	7.4%	0.32 (0.19 to 0.44)

Table A.5: Results from multivariate spline autoregression (degrees of freedom = 2) method, before and after a state's stay-at-home order.

		Before stay-at-home orders (weeks -14 to -4)		During stay-at-home orders (weeks -3 to 12 of stay-at-home orders)		After stay-at-home orders (weeks +1 to +20 *after the removal* of stay-at-home order)		
Pollutant	**Population weighted average concentration (2010-2019)**	**Estimated coefficient**	**Effect before stay-at-home order**	**Estimated coefficient**	**Effect during stay-at-home order**	**Estimated coefficient**	**Effect after stay-at-home order**	**R^2 Median (IQR)**
$PM_{2.5}$	7.2 $\mu g/m^3$	-0.41$\mu g/m^3$	-5.8%	0.07 $\mu g/m^3$	1.1%	1.79 $\mu g/m^3$	24.9%	0.49 (0.41 to 0.51)
Ozone	43.0 ppb	-1.18 ppb	-2.8%	-1.71 ppb	-4.0%	-1.59 ppb	-3.7%	0.50 (0.45 to 0.53)
NO_2	22.2 ppb	-0.27 ppb	-1.2%	-2.07 ppb	-9.4%	0.58 ppb	2.7%	0.45 (0.38 to 0.50)
CO	0.5 ppm	0.01 ppm	2.0%	-0.01 ppm	-2.5%	0.04 ppm	8.0%	0.54 (0.4 to 0.6)
PM_{10}	21.2 $\mu g/m^3$	1.29 $\mu g/m^3$	6.1%	-1.15 $\mu g/m^3$	-5.5%	1.67 $\mu g/m^3$	8.0%	0.41 (0.23 to 0.47)

Table A.6: Results from multivariate spline autoregression (degrees of freedom = 3) method, before and after a state's stay-at-home order.

		Before stay-at-home orders (weeks -14 to -4)		During stay-at-home orders (weeks -3 to 12 of stay-at-home orders)		After stay-at-home orders (weeks +1 to +20 *after the removal* of stay-at-home order)		
Pollutant	**Population weighted average concentration (2010-2019)**	**Estimated coefficient**	**Effect before stay-at-home order**	**Estimated coefficient**	**Effect during stay-at-home order**	**Estimated coefficient**	**Effect after stay-at-home order**	**R^2 Median (IQR)**
$PM_{2.5}$	7.2 $\mu g/m^3$	-0.28 $\mu g/m^3$	-3.8%	0.08 $\mu g/m^3$	1.1%	0.01 $\mu g/m^3$	0.1%	0.49 (0.41 to 0.57)
Ozone	43.0 ppb	-0.20 ppb	-0.5%	-0.17 ppb	-4.0%	-0.16 ppb	-3.7%	0.50 (0.43 to 0.57)
NO_2	22.2 ppb	-0.52 ppb	-2.3%	-2.17ppb	-9.8%	-1.25 ppb	-5.6%	0.44 (0.33 to 0.55)
CO	0.5 ppm	-0.01 ppm	-2.9%	-0.02 ppm	-4.0%	0.05 ppm	9.8%	0.56 (0.44 to 0.66)
PM_{10}	21.2 $\mu g/m^3$	1.22 $\mu g/m^3$	5.8%	-0.60 $\mu g/m^3$	-2.8%	0.85 $\mu g/m^3$	4.0%	0.41 (0.29 to 0.53)

Table A.7: Results from multivariate spline autoregression (degrees of freedom = 4) method, before and after a state's stay-at-home order.

		Before stay-at-home orders (weeks -14 to -4)		During stay-at-home orders (weeks -3 to 12 of stay-at-home orders)		After stay-at-home orders (weeks +1 to +20 *after the removal* of stay-at-home order)		
Pollutant	**Population weighted average concentration (2010-2019)**	**Estimated coefficient**	**Effect before stay-at-home order**	**Estimated coefficient**	**Effect during stay-at-home order**	**Estimated coefficient**	**Effect after stay-at-home order**	**R^2 Median (IQR)**
$PM_{2.5}$	7.2 μg/m^3	-0.23.μg/m^3	-3.2%	0.30 μg/m^3	4.2%	0.54 μg/m^3	7.5%	0.51 (0.43 to 0.59)
Ozone	43.0 ppb	-0.20 ppb	-0.5%	-1.1 ppb	-2.7%	0.98 ppb	2.3%	0.51 (0.45 to 0.58)
NO_2	22.2 ppb	-0.66 ppb	-3.0%	-2.16ppb	-9.8%	1.44 ppb	6.5%	0.46 (0.39 to 0.58)
CO	0.5 ppm	-0.02 ppm	-4.3%	-0.01 ppm	-1.8%	-0.00 ppm	-0.8%	0.56 (0.44 to 0.67)
PM_{10}	21.2 μg/m^3	1.32 μg/m^3	6.3%	2.34 μg/m^3	11.1%	6.95 μg/m^3	32.8%	0.43 (0.32 to 0.55)

Table A.8: Results from multivariate spline autoregression (degrees of freedom = 5) method, before and after a state's stay-at-home order.

		Before stay-at-home orders (weeks -14 to -4)		During stay-at-home orders (weeks -3 to 12 of stay-at-home orders)		After stay-at-home orders (weeks +1 to +20 *after the removal* of stay-at-home order)		
Pollutant	**Population weighted average concentration (2010-2019)**	**Estimated coefficient**	**Effect before stay-at-home order**	**Estimated coefficient**	**Effect during stay-at-home order**	**Estimated coefficient**	**Effect after stay-at-home order**	**R^2 Median (IQR)**
$PM_{2.5}$	7.2 μg/m^3	-0.41μg/m^3	-5.8%	0.93 μg/m^3	12.9%	1.79 μg/m^3	24.9%	0.53 (0.46 to 0.61)
Ozone	43.0 ppb	-1.18 ppb	-2.8%	-0.42 ppb	-1.0%	-0.74 ppb	-1.7%	0.54 (0.47 to 0.60)
NO_2	22.2 ppb	-0.27 ppb	-1.2%	-5.34 ppb	-24.0%	0.91 ppb	4.1%	0.49 (0.38 to 0.60)
CO	0.5 ppm	-0.02 ppm	-3.7%	-0.07 ppm	-13.9%	-0.16 ppm	-32.4%	0.59 (0.47 to 0.70)
PM_{10}	21.2 μg/m^3	1.09 μg/m^3	5.1%	3.1 μg/m^3	14.7%	7.05 μg/m^3	33.3%	0.45 (0.33 to 0.57)

Chapter 3

Application of InMAP Source Receptor Matrix 2.0: Sectoral Impacts of Air Pollution on Mortality in the US (2002-2019)

3.1 Summary

Air pollution models are essential for understanding trends over time, offering insights into past, present, and future conditions. However, commonly used full-scale models require substantial computational resources and significant human effort, even for a single simulation, which complicates rapid analysis. In this chapter, we outline two main objectives: first, the development of a library of prerun simulations using the updated reduced complexity model, InMAP; and second, an analysis of air pollution mortality attributable to economic sectors in the U.S. from 2002 to 2019 using the developed matrix. InMAP, one of the most widely used reduced complexity models, can efficiently estimate annual average concentrations for five pollutants (primary $PM_{2.5}$ and the precursors of secondary $PM_{2.5}$, including NO_x, SO_x, NH_3, and VOC) from marginal changes in emissions. To further reduce the analysis run time, we introduce the updated InMAP Source Receptor Matrix (ISRM 2.0), a library of prerun simulations. This matrix allows researchers to estimate concentration changes that would result from emission changes; the run-time is typically ∼minutes, and the work uses widely accessible programming languages such as Python and R. We applied the ISRM to attribute air pollution-related mortality to specific economic sectors, activities, and processes over the period 2002 to 2019. The analysis highlighted significant reductions in mortality from the transportation and electricity sectors, while emissions from the food and agriculture sectors contributed to a modest increase in mortality. The total mortality estimates aligned well with findings from previous studies and were generated at least an order of magnitude faster than results from full-scale chemical transport models. These outcomes demonstrate the effectiveness of the ISRM as a practical tool for air quality management, enabling rapid and reliable assessments to support scenario analysis and policy evaluation.

3.2 Introduction

Air pollution—the second leading risk factor for premature death globally—represents a critical challenge for public health [137]. Most sources of ambient air pollution lie beyond individual control, necessitating coordinated efforts by policymakers at local, national, and regional levels. Over the past few decades, the United States has implemented various policies to mitigate the burden of air pollution, achieving mixed results.

This chapter examines changes in mortality linked to emissions affecting ambient fine particulate matter ($PM_{2.5}$) levels across the contiguous United States from 2002 to 2019. Using the categorization framework of Thakrar et al. (2020) [138], we attribute mortality changes across four dimensions: sector, activity, process, and pollutant. To assess sector-specific contributions, we categorize emissions into five main economic sectors: transportation, electricity, food and agriculture, residential, and industrial. Understanding trends within these sectors is critical for guiding future policies and establishing standards to reduce air pollution and associated health impacts.

The analysis is conducted using the Intervention Model for Air Pollution (InMAP), a widely applied reduced-complexity model [43]. InMAP leverages preprocessed physical and chemical mechanisms from more complex models, such as WRF-Chem and WRF-CMAQ, to estimate annual average concentrations of primary $PM_{2.5}$ and secondary $PM_{2.5}$ precursors (NO_x, SO_x, NH_3, and VOCs) resulting from marginal changes in emissions [36]. To reduce computational demands—approximately 120 national simulations per year—we developed a library of prerun simulations using an updated version of InMAP.

The InMAP Source Receptor Matrix (ISRM 2.0) developed in this study facilitates efficient and accurate estimations of annual mortality across sectors for the years 2002, 2010, and 2019. These

estimates are further disaggregated into 25 distinct activities within the sectors and 10 specific processes driving emissions. Additionally, we quantify mortality contributions from primary $PM_{2.5}$ and four key precursors of secondary $PM_{2.5}$.

This chapter advances the scope of air quality modeling tools and contributes to accountability research by offering detailed insights into the complex relationships between sector-specific emissions, air quality, and mortality. The ISRM 2.0 developed here serves as a practical and efficient resource for evaluating the effectiveness of emission reduction strategies for researchers and policymakers.

3.3 Methods

This section has two main components. First, we provide details on the development of the updated InMAP Source Receptor Matrix. Then, we outline the methods used to estimate mortality attributable to economic sectors, activities, and processes.

3.3.1 The updated InMAP Source Receptor Matrix

InMAP, a widely used reduced-complexity air quality models, is designed to estimate annual average $PM_{2.5}$ concentrations across the contiguous United States. It focuses on five key pollutants: primary $PM_{2.5}$, NO_x, SO_x, NH_3, and VOCs. By leveraging published simulation outputs from full chemical transport models, InMAP captures critical atmospheric properties while reducing computational complexity. The original model's assumptions and performance evaluations, including comparisons with other models and ground measurements, are detailed in prior studies [**?**, 43, 55]. While the first version of InMAP was based on 2005 WRF-Chem outputs, the latest iteration, InMAP 2.0, incorporates 2017 WRF-CMAQ outputs, retaining its core structure while integrating updated atmospheric data.

Despite InMAP's inherent efficiency in reducing the time and computational demands of national air quality simulations, its capabilities are further enhanced through the InMAP Source Receptor Matrix (ISRM). The ISRM is a library of precomputed simulations that enables users to estimate changes in pollutant concentrations resulting from a 1-ton-per-year emission change for the five pollutants. These results can be scaled to reflect actual emission changes, dramatically reducing simulation times from hours to minutes. Accessible through widely used programming languages such as R and Python, the ISRM eliminates the need for specialized software, making air quality assessments more accessible to researchers and policymakers.

Previously, the original ISRM (ISRM 1.0) was developed by running the first version of InMAP thousands of times and storing the outputs in a NetCDF file. In this work, we introduce ISRM 2.0, an updated version designed to improve usability and accuracy further. ISRM 2.0 incorporates both vertical and horizontal grid structures: two vertical layers (ground-level and elevated) aligned with atmospheric mixing heights and a horizontal grid comprising 86,261 cells (Figure 3.1). The horizontal grid is designed to vary in resolution, ranging from 1 km to 48 km, providing enhanced spatial granularity in densely populated areas where high accuracy is crucial. Further details on the vertical layers and grid structures are in Appendix B.

To construct the source-receptor matrix, InMAP was run for each grid cell, designating the cell as the source and calculating the resulting concentrations in each receptor grid cell. This process required running InMAP 86,261 times, corresponding to the total number of grid cells. Each run took approximately 1.5 hours on a 24-core machine, amounting to a total of around 130,000 hours (or roughly 15 years) if performed sequentially.

To significantly reduce computation time, we leveraged Google Cloud Kubernetes to deploy hundreds of virtual machines in parallel, completing the simulations within a few months [139]. The resulting 200 TB of raw data were stored in Google Cloud Storage and consolidated into five NETCDF files—one for each pollutant—containing information for all 86,261 sources and their corresponding receptors.

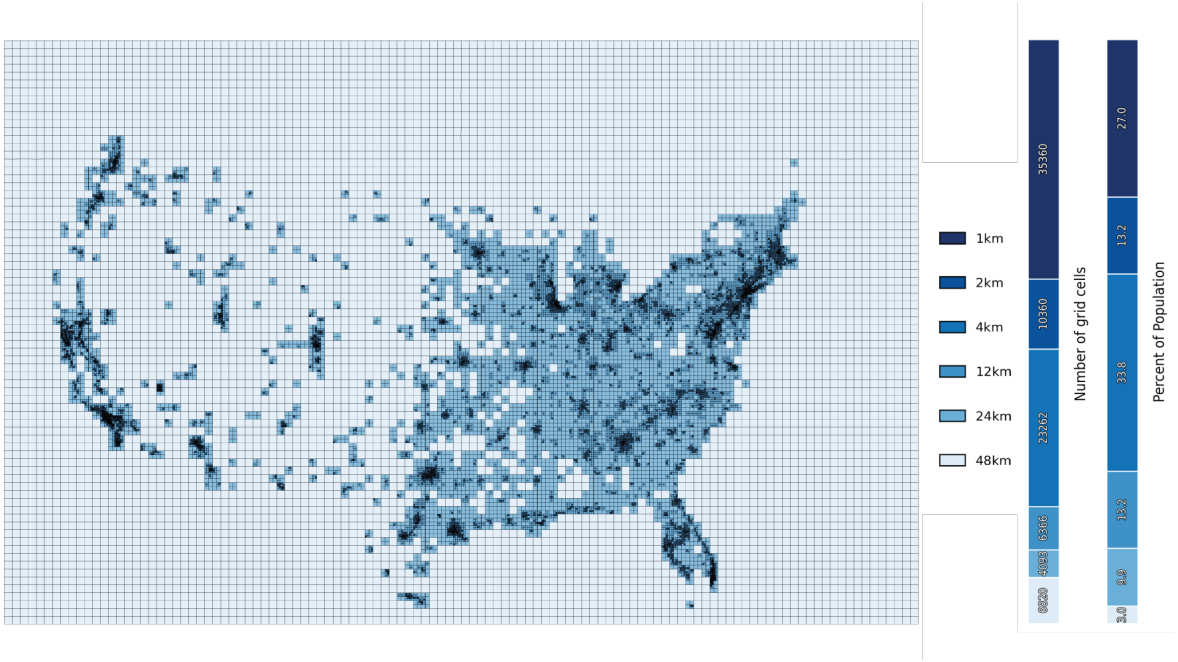

Figure 3.1: ISRM 2.0 horizontal grid cells covering the contiguous US, southern Canada, and northern Mexico, varying sizes of 1, 2, 4, 12, 24, and 48 km edge lengths. The size of the grid cells depends on population concentration, with more grid cells in areas of higher population density. The left column in the figure displays the number of grid cells corresponding to each grid cell size; the right column shows the population percentage for each size.

3.3.2 Mortality estimation utilizing ISRM

We utilized the updated ISRM developed in the previous section to estimate changes in mortality attributable to emissions from 2002 to 2019. Mortality was assessed across economic sectors, activities, processes, and pollutants for the contiguous United States using the following methodology:

1. Emission Aggregation: We aggregated annual emissions data from the EPA's Air Quality Time Series Project (EQUATES) into economic sectors, activities, and processes. This categorization was based on the Source Classification Code (SCC) framework used by the EPA [140] and methodology outlined by Thakrar et al. (2020) [138]. Emissions were analyzed for the years 2002, 2010, and 2019, representing the first and last available years and a midpoint for trend analysis.

2. Concentration Estimation: Using the ISRM developed in this chapter, we calculated annual average concentrations of primary $PM_{2.5}$ and secondary $PM_{2.5}$ from precursors (e.g., NO_x, SO_x, NH_3, and VOCs) based on the aggregated emissions data. This step involves spatially distributing the emissions into the ISRM 2.0 grid cells shown in Figure 3.1, and calculating the concentration changes in receptor grid cells from each of the source grid cells.

3. Population and Mortality Distribution: Population and baseline mortality rates were spatially allocated to each grid cell using data from the 2020 Census and mortality statistics. This step ensured that health outcomes were accurately linked to population exposure at the grid cell level.

4. Mortality Estimation: Finally, we estimated mortality attributable to air pollution emissions for each sector, activity, and process using dose-response relationships from Nasari et al. (2016) [141], Burnett et al. (2018) [142], and Krewski et al. (2009) [143]. This calculation combined concentration estimates, population distributions, and baseline mortality rates to determine the health impacts.

3.4 Results

Emissions of primary $PM_{2.5}$, NO_x, SO_x, and VOC have decreased from 2002 to 2019 with significant reductions observed in NO_x and SO_x. In contrast, NH_3 emissions showed a slight decrease from 2002 to 2010 but then increased, surpassing 2002 levels by 2019. Figure 3.2 illustrates the spatial distribution of emissions over these years, which remained largely consistent for $PM_{2.5}$, SO_x, and NH_3 while the spatial extent decreased for NO_x and VOC.

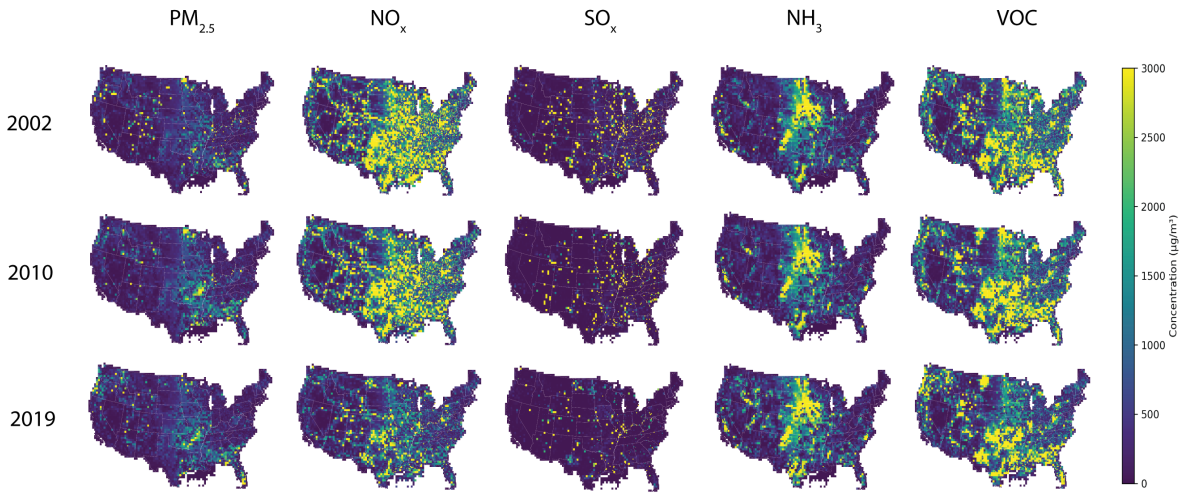

Figure 3.2: Annual Primary $PM_{2.5}$, NO_x, SO_x, NH_3, and VOC emissions in 2002, 2010, and 2019.

Figure 3.3 illustrates the estimated annual average concentrations derived from the emissions shown in Figure 3.2. Among the five pollutants analyzed, the largest reductions in population-weighted average concentrations were observed for NO_x and SO_x, which decreased by 70% and 86%, respectively (Table 3.1). Concentrations of primary $PM_{2.5}$ and VOCs also declined by 24% and 42%, respectively, while NH_3 concentrations remained largely unchanged. Overall, the population-weighted total $PM_{2.5}$ concentration decreased by nearly 50% during the study period, with the most significant reductions occurring between 2002 and 2010.

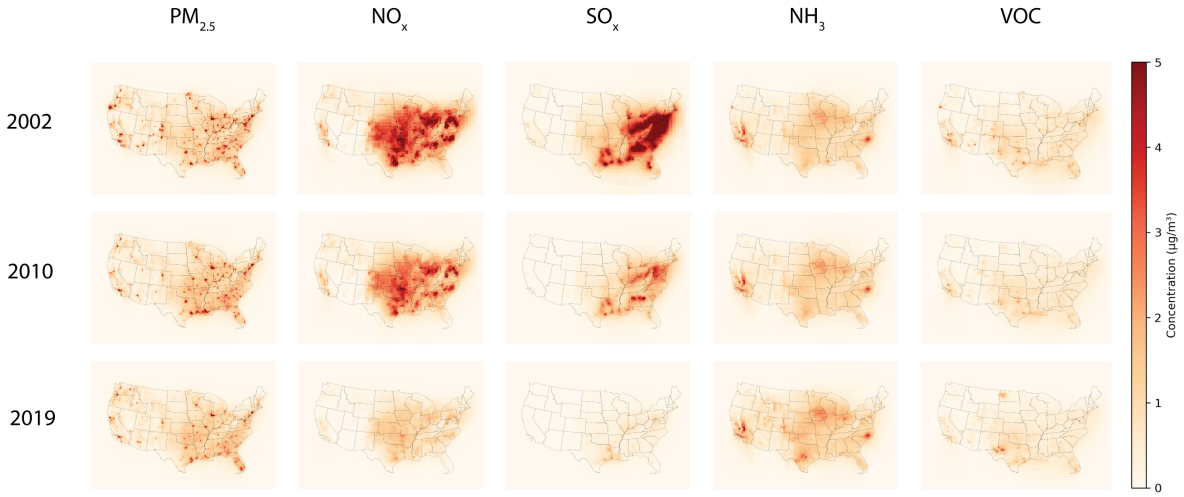

Figure 3.3: Annual average concentrations of Primary $PM_{2.5}$, NO_x, SO_x, NH_3,and VOC in 2002, 2010 and 2019

Table 3.1: Population-weighted annual average concentrations for Primary $PM_{2.5}$, NO_x, SO_x, NH_3, VOC and total $PM_{2.5}$

Year	Primary $PM_{2.5}$	NO_x	SO_x	NH_3	VOC	Total $PM_{2.5}$
2002	3.3	2.7	2.9	1.3	1.4	11.6
2010	2.9	1.7	1.1	1.2	1.0	7.9
2019	2.5	0.8	0.4	1.3	0.8	5.9

The changes in $PM_{2.5}$-related mortality, calculated from concentration reductions due to declining emissions, reveal a substantial decrease between 2002 and 2019. In 2002, air pollution contributed to approximately 147,000 premature deaths, which declined to 115,000 in 2010 and further to 67,000 in 2019 (Figure 3.4). This significant reduction was primarily driven by improvements in the transportation, electricity, and industrial sectors. Mortality associated with the transportation sector decreased by 35,000 deaths (a 64% reduction), the electricity sector by 24,000 deaths (an 88% reduction), and the industrial sector by 18,400 deaths (a 46% reduction).

The residential sector exhibited a more nuanced trend, with mortality increasing from 2002 to 2010 but declining between 2010 and 2019, resulting in an overall reduction of 5,200 deaths (46%). In contrast, the food and agriculture sector was the only one to show an overall increase in mortality. While deaths linked to this sector initially decreased between 2002 and 2010, they rose from 2010 to 2019, culminating in a net increase of 2,300 deaths (17%) over the study period.

Figure 3.4: Mortality from total $PM_{2.5}$ pollution by economic sector in 2002, 2010 and 2019.

Figures 3.5 and 3.6 illustrate mortality by sector, activity, process, and pollutant for 2002 and 2019, reflecting these shifts. Consistent with the emission reductions noted above, activities and processes within the transportation and electricity sectors show substantial declines in mortality. For instance, mortality associated with electricity generation from coal and passenger vehicle use decreased by 27,000 deaths (90%) and 14,600 deaths (70%), respectively, from 2002 to 2019. Similar downward trends are observed in specific processes, with the largest reductions occurring in coal, diesel, and gasoline fuel combustion.

Conversely, activities and processes related to the food and agriculture sector have seen increased mortality contributions from 2002 to 2019. Mortality attributions from commercial cooking food processing, and fertilizer application have risen by 57% and 40% respectively. Processes such as burning and losses and leaks associated with the agriculture sector have also shown an increase in mortality impacts.

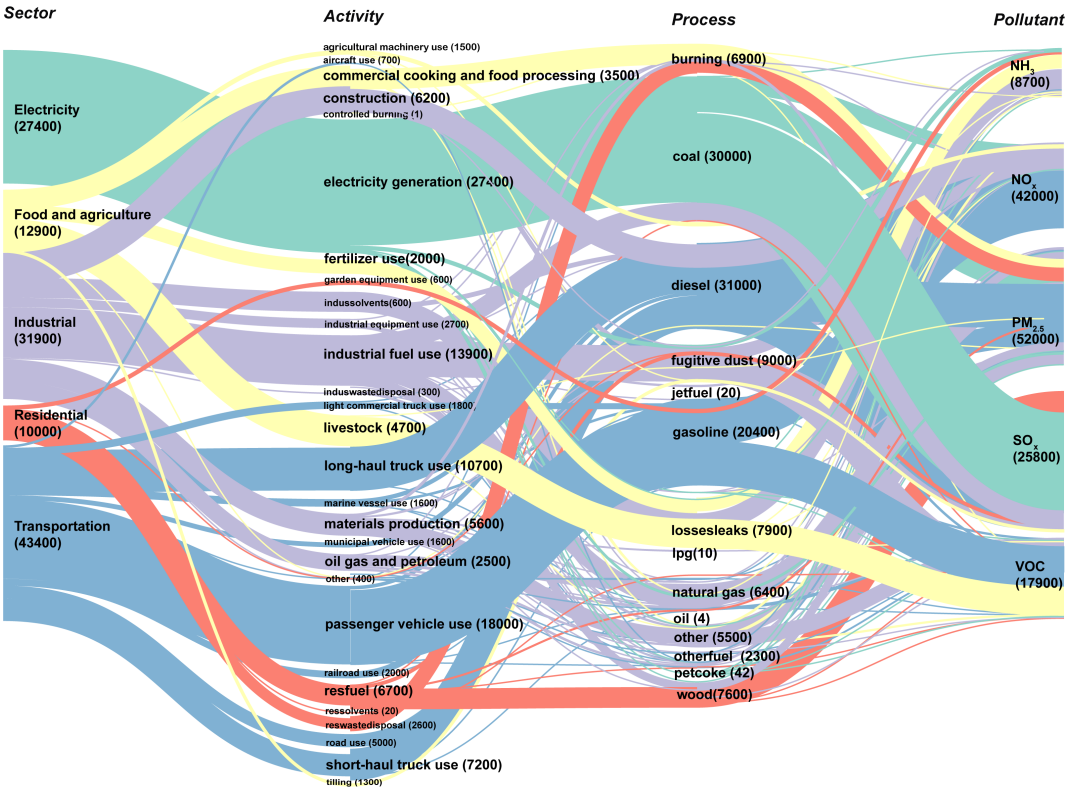

Figure 3.5: Mortality from $PM_{2.5}$ pollution by sector, activity and processes in 2002.

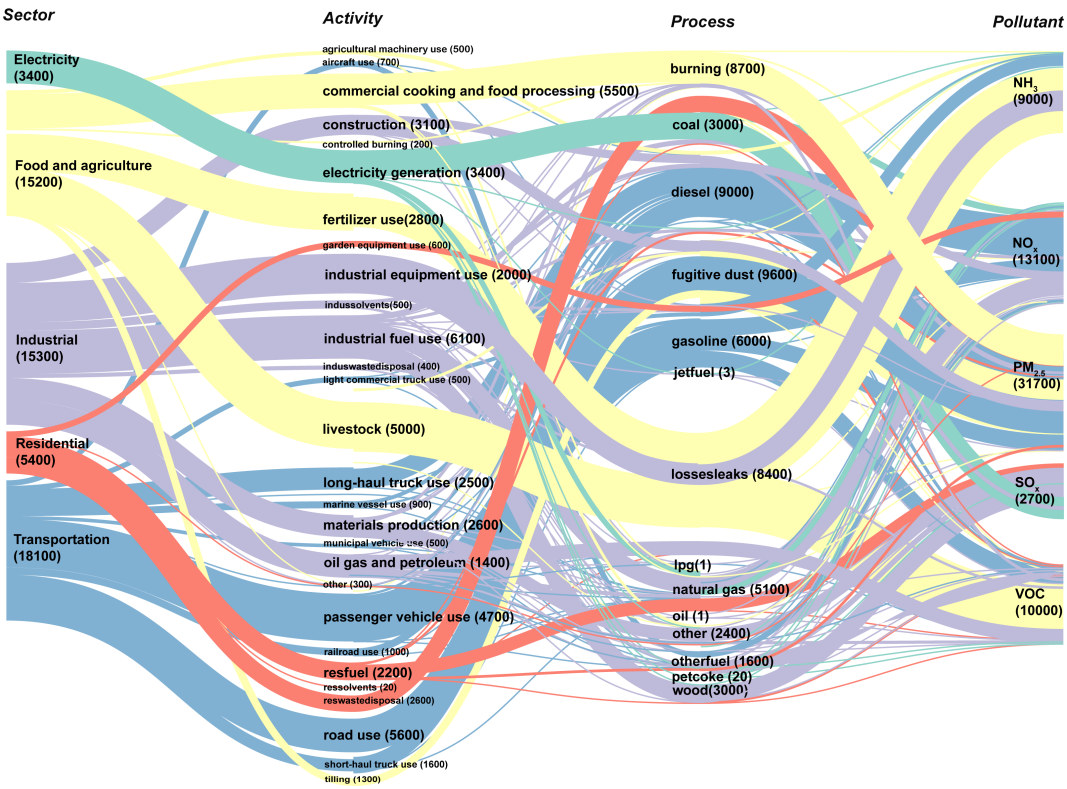

Figure 3.6: Mortality from $PM_{2.5}$ pollution by sector, activity and processes in 2019.

3.5 Discussion

Our findings reveal a significant reduction in overall mortality attributable to air pollution in the United States. Annual $PM_{2.5}$-related mortality decreased by approximately 80,000 deaths (a 54% reduction) from 2002 to 2019. This decline was primarily driven by substantial reductions in emissions from the transportation and electricity sectors. Once the leading contributors to $PM_{2.5}$-related mortality, these sectors are now among the least significant sources of such deaths. Conversely, the food and agriculture sector experienced a 17% increase in $PM_{2.5}$-related mortality, with approximately 2,300 additional deaths. While modest in absolute terms, this sector remains the only one without a decline in $PM_{2.5}$-attributed mortality; the proportion of deaths for this sector rose, from 10% (2002) to 31% (2019).

Our findings are consistent with previous studies. First, the annual estimated number of $PM_{2.5}$-related deaths falls within the 100,000 to 200,000 range reported by Burnett et al. (2018) [142] and Tessum et al. (2019) [55]. Second, the trends observed align closely with U.S. air quality policies implemented between 2002 and 2019. For instance, significant reductions in SO_x and NO_x emissions, and the corresponding mortality declines, can be attributed to landmark policies targeting the electricity sector. Programs like the Acid Rain Program [144] and the Cross-State Air Pollution Rule (CSAPR) [145] were instrumental in achieving these reductions. These efforts were complemented by state-level renewable energy mandates and tax incentives such as the Investment Tax Credit [146], which facilitated the electricity sector's transition to cleaner energy sources.

Similarly, the transportation sector has seen substantial reductions in emissions due to policies like the Tiered Vehicle Emission Standards [147], the Clean Truck Program [148], and the Diesel Emission Reduction Act [149]. Additional incentives, such as electric vehicle tax credits [150] and investments in public transit infrastructure, have further accelerated the adoption of cleaner technologies. Collectively, these measures have led to significant improvements in air quality and public health outcomes.

In contrast to the progress seen in the transportation and electricity sectors, emissions reductions in the food and agriculture sector have been limited. Programs like the Environmental Quality Incentives Program (EQIP) [151] and Precision Agriculture Technologies [152] aim to reduce emissions through

practices like cover cropping, improved manure management, and efficient pesticide and fertilizer application. However, these initiatives primarily focus on mitigating greenhouse gas emissions rather than addressing broader air pollutants such as $PM_{2.5}$ and NH_3.

The increase in $PM_{2.5}$-related mortality from the food and agriculture sector can likely be attributed to growing food demand driven by population growth, which has led to higher production of meat, dairy, and other agricultural goods. Additionally, controlling emissions from agricultural area sources remains complex and costly. For many agricultural operations, implementing advanced air pollution control technologies is neither practical nor economically feasible.

While substantial progress has been made in reducing $PM_{2.5}$-related mortality in the U.S., key challenges remain. Despite notable reductions, the transportation and industrial sectors still contribute significantly to air pollution-related deaths. The agriculture sector, in particular, requires more targeted policies and innovative technologies to address its unique challenges. Achieving further reductions in mortality will necessitate additional regulatory efforts, financial incentives, and advancements in pollution control.

This chapter provides a detailed analysis of changes in air pollution-attributed mortality from 2002 to 2019, disaggregated by sector, activity, and process. Aggregating mortality by sector and linking it to emission trends offers critical insights for developing effective strategies to improve public health through air pollution mitigation. The updated InMAP Source Receptor Matrix introduced in this chapter equips policymakers and analysts with a powerful tool to identify and prioritize these strategies, enabling a data-driven approach to air quality management. Future research should explore the integration of climate and air quality models to assess the co-benefits of mitigation strategies.

3.6 Appendix B: Supplemental Information for Chapter 3

Emissions Groups Used

The emissions groups in this paper follow the EPA NEI source categories but are simplified to better suit the analysis. Below are definitions of some key emissions groups, clarifying their scope and meaning [138].

- **Sector:** Broad categories of polluting activities, generally based on EPA NEI source classifications.
  - **Industrial & Commercial:** This sector includes most industrial and commercial sources as defined by the EPA NEI categories, excluding sources covered by other sectors (e.g., commercial cooking, which is included in the Food & Agriculture sector).
  - **Transportation:** Largely aligns with the EPA NEI transportation category but excludes transportation sources assigned to other sectors (e.g., off-road agricultural machinery, which falls under the Food & Agriculture sector).
  - **Food & Agriculture:** Encompasses emissions from agricultural activities, including farms, as well as emissions from commercial food processing and cooking.
- **Activity:** Specific human actions that directly lead to pollution.
  - **Crop Burning:** Refers exclusively to agricultural crop burning. Excludes land management burning for wildfire risk reduction or burning of logging residue.
  - **Road Use:** Includes emissions primarily from dust disturbance on roads, as well as from brake and tire wear, with minor contributions from oil spills.
  - **Commercial Cooking & Food Processing:** Includes emissions from food processing for retail, as well as emissions from restaurants.
  - **Oil, Gas & Petroleum Production:** Includes emissions from petroleum and oil/gas industry activities as defined by the EPA NEI. Covers emissions from flares and product volatilization in storage tanks.
  - **Solvent Use:** Emissions from using solvents (e.g., paint application, printing), excluding emissions from solvent production or storage.
  - **Waste Disposal:** Emissions from site remediation and waste burning for disposal purposes, excluding combustion of waste as fuel.
  - **Materials Production:** Includes emissions from the production of materials (e.g., glass, paper, ceramics) and may also include emissions from mining and smelting.
  - **Municipal Vehicle Use:** Emissions from public transportation vehicles, such as buses, and vehicles used for road cleaning.
- **Process:** The specific mechanism through which pollution is generated in each activity.
  - **Fuel Combustion:** Refers to fuel burning specifically for energy generation (e.g., heating, mechanical work).
  - **Burning:** Non-energy-use burning, including waste burning, crop residue burning, and fires in residential or vehicle settings.
  - **Losses and Leaks:** Inadvertent releases of gaseous or aerosol products (e.g., NH_3 volatilization, NMVOC evaporation) but excludes dust emissions.

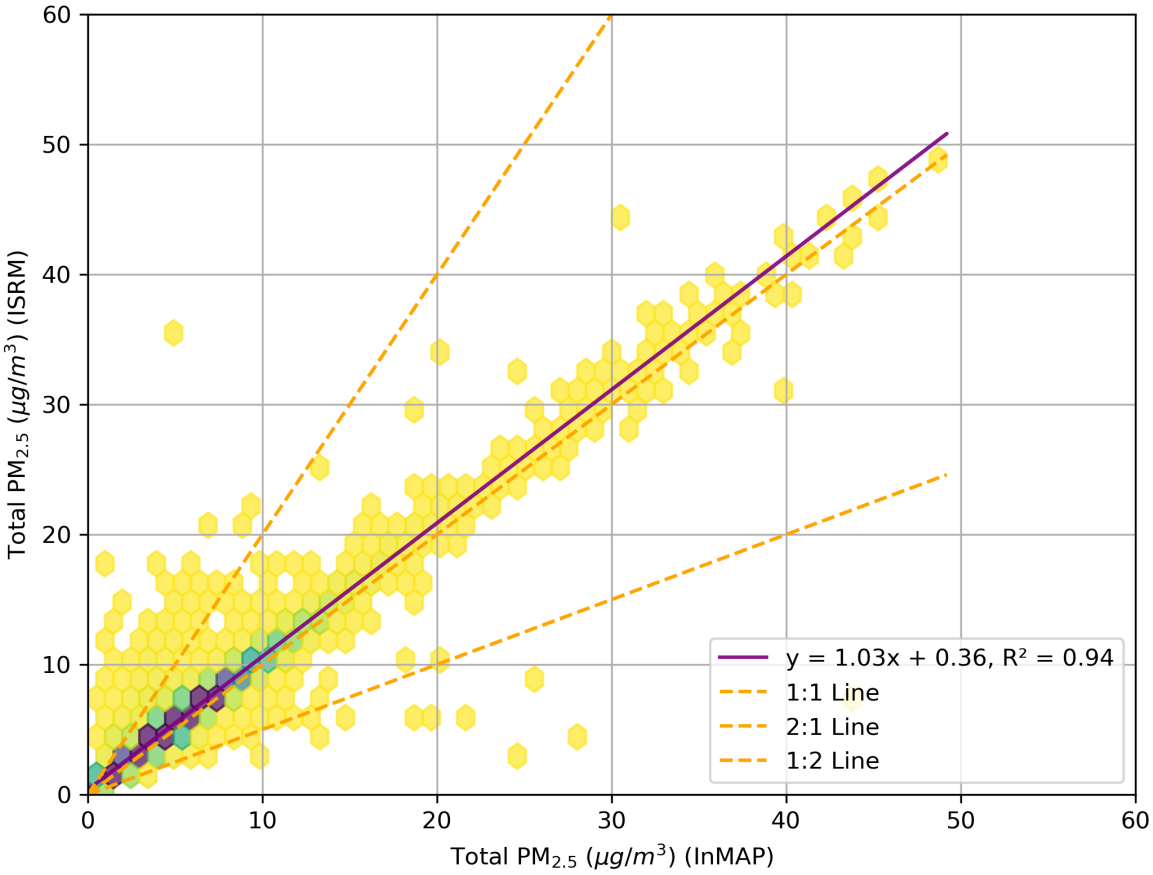

Figure B.1: Total PM2.5 Concentration correlation between running InMAP 2.0 and ISRM 2.0 with 2019 emissions.

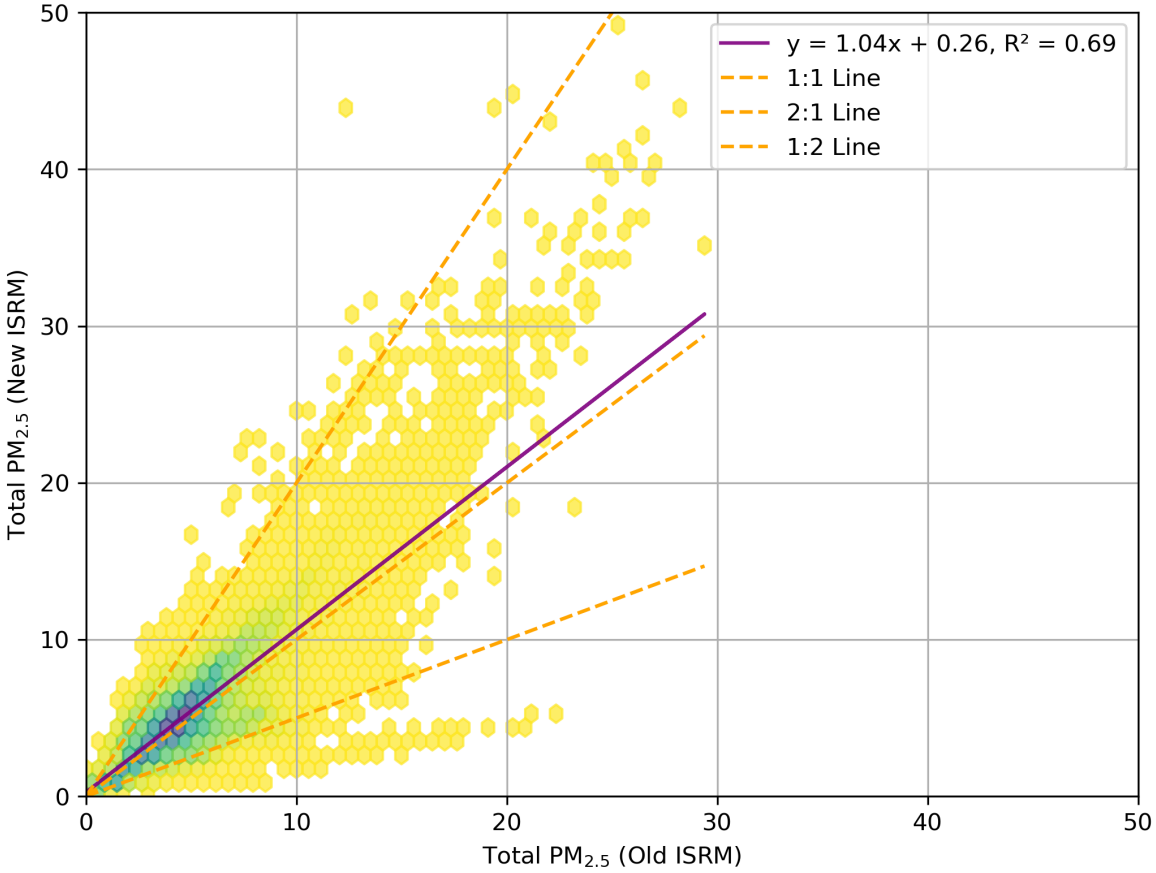

Figure B.2: Total $PM_{2.5}$ Concentration correlation between running ISRM 1.0 and ISRM 2.0 with 2019 emissions. (The number of grid cells is 65% more for ISRM2.0 than for ISRM 1.0. Run time for ISRM2.0 is 3-4 times faster than ISRM 1.0.)

Figure B.3: $PM_{2.5}$ related mortality by pollutants. This figure is similar to Figure 3.4, but aggregated by pollutant

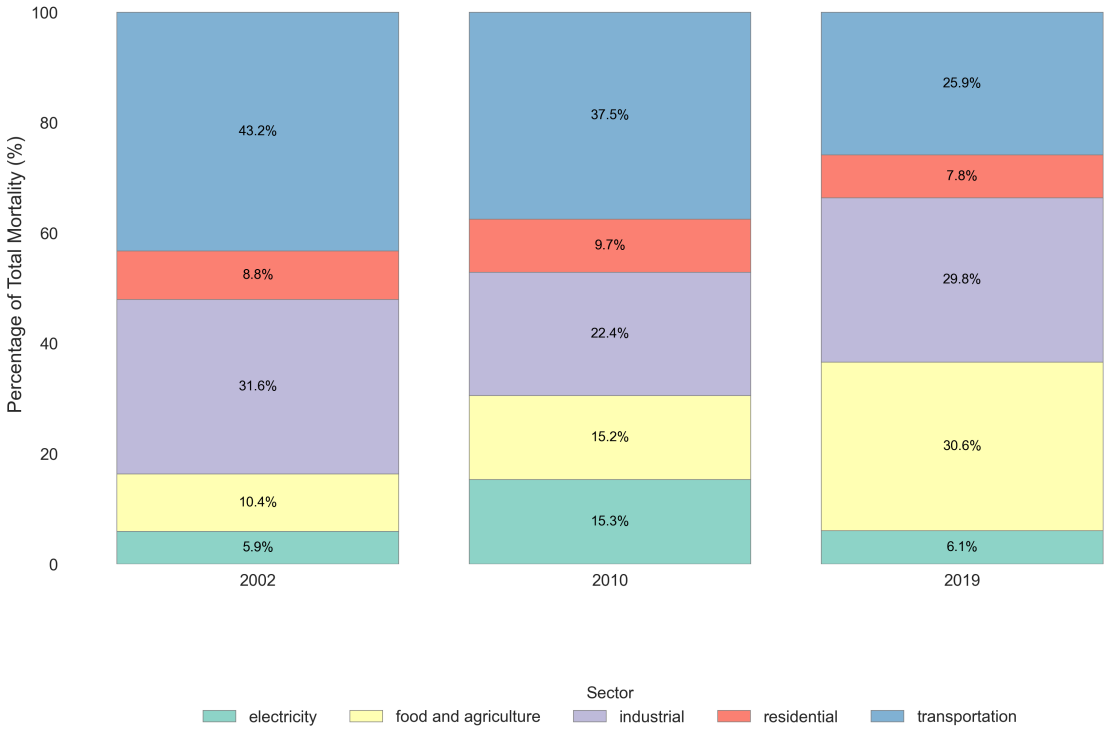

Figure B.4: Percentage of total mortality by each sector. This figure is similar to Figure 3.4, but displayed as percentage of total $PM_{2.5}$ related mortality

Chapter 4

Application of an ultra-low-cost passive sampler for light-absorbing carbon in Mongolia

Material in this chapter has been previously published in the following article:

Bekbulat, B., Agrawal, P., Allen, R. W., Baum, M., Boldbaatar, B., Clark, L. P., Galsuren, J., Hystad, P., L'Orange, C., Vakacherla, S., Volckens, J., and Marshall, J. D. (2023). Application of an Ultra-Low-Cost Passive Sampler for Light-Absorbing Carbon in Mongolia. *Sensors*, 23(21), 8977.

4.1 Summary

Monitoring household air pollution presents significant challenges, including the high costs and maintenance demands of monitoring equipment, as well as the intrusive nature of regularly entering private spaces to collect samples. In this chapter, I introduce the Washington Passive Sampler (WPS), an ultra-low-cost passive sampler designed for resource-constrained and highly polluted environments. Priced between 5 to 15 USD, the WPS can estimate long-term average black carbon concentrations in households with minimal maintenance and disruption to the host household.

The WPS utilizes an image-based analysis method, where concentrations are estimated by photographing a filter before and after deployment and calculating the change in pixel intensity. To assess its precision and accuracy in the field, we collocated duplicate WPS units with a gold-standard method (UPAS with a quartz filter) and PurpleAir in ten households in Ulaanbaatar, Mongolia, over four months.

Field test results showed an Intraclass Correlation Coefficient (ICC) of 90% for duplicate measurements, and a Root Mean Square Error (RMSE) of 21%, compared to 10% for the gold-standard reference measurements. Our findings suggest that the WPS provides a viable option for long-term studies in resource-constrained settings, offering a reliable, practical, and cost-effective solution for monitoring black carbon concentrations.

4.2 Introduction

Household air pollution is a major risk factor for death and disease, annually responsible for 3.5 million premature deaths and 92 million disability-adjusted life years (DALYs) [64, 153–156]. Most premature deaths occur in low-income countries, where households have relatively higher exposure to air pollution (e.g., $PM_{2.5}$, black and brown carbon) due to household combustion of solid fuels for cooking and heating [157–160]. Two major challenges associated with studying indoor air pollution are cost and logistics [161–163]. Air pollution samplers can range in price from a few hundred to several thousand US dollars, depending on factors such as their accuracy, efficiency, robustness, and user-friendliness [164–166]. Deployments of these samplers often require detailed planning associated with deploying and collecting equipment including tasks such as charging equipment between deployments, coordinating visits with residents, ensuring safe and secure locations, and having access to laboratory facilities. Passive samplers can lower costs and simplify logistics associated with in situ air quality measurements; the Washington passive sampler (WPS) aims to do so for measuring the long-term average levels of light-absorbing carbon (LAC) air pollution [167]. "LAC" refers to the carbon components of fine particulate matter ($PM_{2.5}$), such as black and brown carbon, which strongly absorb visible light (wavelengths: 400–700 nanometers) [72]. The WPS is comparatively ultra-low-cost (∼USD 5-15) and logistically straightforward to use (no electricity, expensive lab equipment, or extensive maintenance required). The WPS uses digital images to measure the change in the reflectance of a passively exposed paper filter.

Here, we build on a previous study that tested the reproducibility and precision of the WPS in 20 households in Hyderabad, India [167]. The present study aimed to determine the accuracy and uncertainty of the WPS by co-locating it with (A) quartz filters for elemental carbon (EC) analysis using an ultrasonic personal aerosol sampler (UPAS, Access Sensors Technologies, Fort Collins, CO, USA), and (B) the PurpleAir sensor (PurpleAir, Draper, UT, USA) [65, 66]. This investigation is the first to compare results between the WPS and other methods, including comparison against a thermal-optical analysis, which is the gold-standard measurement method for elemental carbon.

4.3 Materials and methods

In this section, we outline the methodology employed to intercompare three distinct measurement methods: the Washington passive sampler (WPS), a reference method utilizing elemental carbon thermal-optical analysis, and the PurpleAir sensor.

4.3.1 The Washington Passive Sampler (WPS)

As stated above, the WPS is an ultra-low-cost passive sampler for light-absorbing carbon. As deployed in the field, it consists of a downward-facing cellulose filter (Whatman 1002110 qualitative circle cellulose filter paper, GE Healthcare, Chicago, IL, USA), a filter holder, and a protective case for deployment (Figure S1) [72]. Before and after deployment, the cellulose filter was photographed in a lightbox using a Basler acA3800-14 um monochrome camera (Basler acA3800-14um, Basler AG, Ahrensburg, Germany). Each photo in the lightbox was taken of two filters: the sample and a field blank. The lightbox was lit by light-emitting diode (LED) strips located on the lid, ensuring uniform lighting conditions; trays for the sample and the blank were in a fixed position, immediately below the LEDs. The lightbox was sealed to eliminate any outside light. As described below (Section 3.2), the blank filters were used to correct for potential variance in the light intensity between the pre-and post-deployment photos.

Image analysis was conducted using MATLAB's `imread` function (MATLAB and Statistics Toolbox Release 2023A, MathWorks, Inc., Natick, MA, USA) to measure the pixel intensity (PI), which serves as a metric for image "blackness". A PI value of 65,535 represents the whitest or lightest point, while a PI of 0 corresponds to the darkest point in the image. The difference in the PI (DPI) between the post-exposure and pre-exposure images serves as a quantification of the reflectance change, attributed to the deposition of light-absorbing carbon on the filter during deployment. For ease of interpretation, we consider the change in PI to be positive when the filter darkens. Consequently, all DPI values presented in this study utilized the MATLAB result multiplied by a negative one.

The average cost of each WPS measurement is approximately USD 5–15, dependent on the deployment details. The WPS itself does not require electricity or lab equipment and is relatively easy to assemble, deploy, and maintain. For further information about the design and application of WPS and the light box, please see Clark et al. (2020) [167].

Each cellulose filter within the WPS was subjected to photography both before and after each deployment period to assess the change in pixel intensity (DPI), denoting "blackness", during that specific period. Subsequently, following each deployment period, the WPS devices were redeployed in households to accumulate further darkening, alongside freshly exposed WPS units. To investigate the impact of filter loading, we progressively increased the number of WPS devices in each sampling period. The total number of WPS devices within each household during each period is detailed as follows: two WPS units in period 1, four WPS units (comprising the original two and two newly deployed units) in period 2, six WPS units (including two from period 1, two from period 2, and two newly deployed units) in period 3, and eight WPS units in period 4 (refer to Table S1). Additionally, for quality assurance, a total of 10 field blanks were photographed and stored within a vacuum environment during each deployment. These field blanks were matched with sample sets from individual households to correct for potential issues, such as fluctuations in camera performance or lighting conditions. For example, if both the sample and the blank exhibited darkening, we employed the change in the pixel intensity of the blank to correct the sample's change in pixel intensity (see Section 3.3.2 for results related to field blanks).

4.3.2 Reference Method

To determine the accuracy of the WPS, we compared the changes in the reflectance of the WPS against a "gold-standard" reference method, in this case, elemental carbon (EC) and organic carbon (OC) aerosol analysis. The EC/OC aerosol analysis method is a thermal-optical analysis, which leverages differences in the thermal refractivity of elemental and organic carbon to separate and quantify these components on a quartz-fiber filter [168]. There are several EC/OC analysis protocols, each with a different temperature plateau, residence time, carrier gas, and/or optical charring correction. The uncertainty of each protocol may reflect the composition of the aerosol samples, the filter loading effect, and the occurrence of inorganic compounds that may enhance charring and lead to erroneous determinations [168–170]. For details about the NIOSH5040 protocol employed here, see Karanasiou et al. (2015) [169]. We used the elemental carbon concentration as a proxy for light-absorbing carbon, as has been carried out and suggested in several studies [170–175].

To obtain samples for elemental carbon analysis, we utilized the UPAS [65]. The UPAS is a time-integrated active sampler that can record the mass flow (MZBD001, 0.5–3.0 L/min, accurate within 5%), temperature, pressure, relative humidity, light intensity, and acceleration. To avoid the possible saturation of the filters in active samplers, such as the UPAS, we used quartz filters and a 5% duty cycle for the UPAS, meaning that the UPAS ran 5 s every 100 s. After each deployment, the UPAS samples were collected and subsequently sent to the Center for Energy Development and Health (CEDH) at Colorado State University (CSU) in Fort Collins, CO, for thermal-optical analysis. This analysis enabled us to determine the mass of elemental carbon collected on the filter. By combining this elemental carbon mass with the mass flow data recorded by the UPAS, we calculated the average elemental carbon concentration for each household during each deployment period. We compared this elemental carbon concentration against the WPS-measured average pixel intensity change recorded during the corresponding deployment period, allowing us to establish the calibration curve.

4.3.3 PurpleAir

To compare the light-absorbing carbon and elemental carbon concentrations with $PM_{2.5}$ concentrations, we employed PurpleAir sensors, which continuously measure the PM concentration, temperature, and relative humidity. These sensors are equipped to transmit real-time data to the cloud when connected to Wi-Fi, a feature that we utilized to monitor any disruptions during deployment, such as electricity outages, and to visit the households after such disruptions.

The $PM_{2.5}$ concentrations reported by PurpleAir sensors demonstrate a strong correlation with reference methods, such as the EPA federal reference methods and federal-equivalent methods ($R^2 > 0.9$). However, PurpleAir readings can occasionally overestimate or underestimate concentrations by as much as a factor of 2, primarily due to environmental variables, such as high relative humidity [176–180]. In our study, PurpleAir sensors were deployed without prior calibration, a common practice even though it may compromise the precision of PurpleAir measurements. Consequently, we utilized PurpleAir data for comparative purposes but excluded them from some analyses, including the establishment of the calibration curve.

4.3.4 Study Design

The study was conducted in 10 households in Ulaanbaatar, Mongolia, from December 2020 to April 2021 (4 months). The households had a similar size and geometry, and each used government-subsidized charcoal as the main fuel source for cooking and heating. In each household, we utilized three devices (WPS, UPAS, and PurpleAir; see Table 1). As described in Table C.1, the 4 months consisted of a total of 4 deployments (i.e., sampling periods) of 21–35 days each.

Table 4.1: Deployment details.

Device	Design	Sampling Type	Filter/Sensor Type	Measuring Species	Comments
WPS		Passive, time integrated. Ultra-low cost.	Cellulose (Whatman)	Light absorbing carbon (LAC)	Each WPS was photographed before and after deployment.
UPAS		Active, time integrated. Reference method.	Quartz (37 mm)	Elemental carbon (EC)	Each UPAS was connected to electricity and continuously sampled at a 5% duty cycle during the deployment period.
PurpleAir		Active, real-time. Medium-cost.	Continuous sensors [1]	$PM_{2.5}$	Electricity outages were determined with PurpleAir Map.

4.3.5 Data Analysis

Given the study's design, the potential maximum number of elemental carbon measurements would have been 40 duplicates (10 households over 4 deployment periods). However, this maximum data point count was not achieved due to various maintenance issues, such as UPAS shutdowns due to high temperatures, battery depletion during electricity outages, and other unexplained factors. To ensure data quality, we enforced a requirement that all UPAS measurements ran for a minimum of 24 h per deployment (i.e., the maximum sampling duration for UPAS at a 5% duty cycle was 25–42 h). As a result, the final count of elemental carbon measurements amounted to $N = 21$, with 10 duplicates and the rest representing single measurements, owing to the deployment issues mentioned above. Our data analysis encompasses four main components:

1. *Precision and reproducibility of WPS and UPAS:* We utilized the intraclass correlation coefficient (ICC) to determine the same-method agreement between paired duplicate WPS samples and (separately) paired duplicate UPAS samples. We also compared the precision of both methods [181]. The ICC measures how strongly the duplicate samples resemble each other; ICC = 1 means that the duplicate samples perfectly match, signifying the perfect/infinite precision of the sampler. The ICC is more appropriate than R^2 for understanding the consistency of duplicate measurements because the paired duplicate measurements are mathematically equivalent. (In contrast, R^2 is used when the pairs have differentiation: one measurement is necessary "x", and the other is necessarily "y".)
2. *Comparing the WPS against the gold standard:* In this step, we assessed the performance of the WPS against the gold-standard method and established a calibration curve for the light-absorbing carbon relative to the elemental carbon. Deming regression (Deming package in R (R version 4.1.2, R Foundation for Statistical Computing, Vienna, Austria)) was used to derive the calibration curve due to the uncertainties in both the elemental carbon and the light-absorbing carbon measurements. The accuracy of the WPS was then computed as the root-mean-square error (RMSE) between the observed change in reflectance (utilizing the gold-standard method) and the predicted change in reflectance (using the WPS with the empirically determined calibration curve)
3. *Correlations across methods:* This component involved examining the correlations among all three measurement methods for each household during each deployment period.
4. *Comparing WPS measurements across deployments:* This component aimed to investigate potential filter-loading effects by comparing the WPS measurements across different deployment periods (i.e., across duplicate samples made using different ages of the filter and filter paper).

4.4 Results

4.4.1 Measurement Completeness

The measurement completeness, which represents the percentage of successfully executed samples out of the intended samples, was notably higher for the Washington passive sampler (WPS), with a rate

of 80% (32 out of 40 intended samples) compared to 55% for the ultrasonic personal aerosol sampler (UPAS) (21 out of 40 intended samples). When focusing on duplicate-sample completeness, i.e., the percentage of intended paired duplicates that were successfully obtained, the WPS achieved a rate of 70% (28 out of 40 intended samples), while the UPAS showed a lower rate of 25% (10 out of 40 intended samples). These results underline the reliability and lower failure rate of the WPS in comparison to the UPAS, particularly during longer measurement periods.

4.4.2 Precision of WPS and UPAS

Figure 1 reports duplicate samples collected by the WPS, and (separately) the UPAS. Both methods demonstrated relatively good self-agreement. As measured by the intraclass correlation coefficient (ICC), the precision was higher for the UPAS (ICC = 0.96) than the WPS (ICC = 0.88).

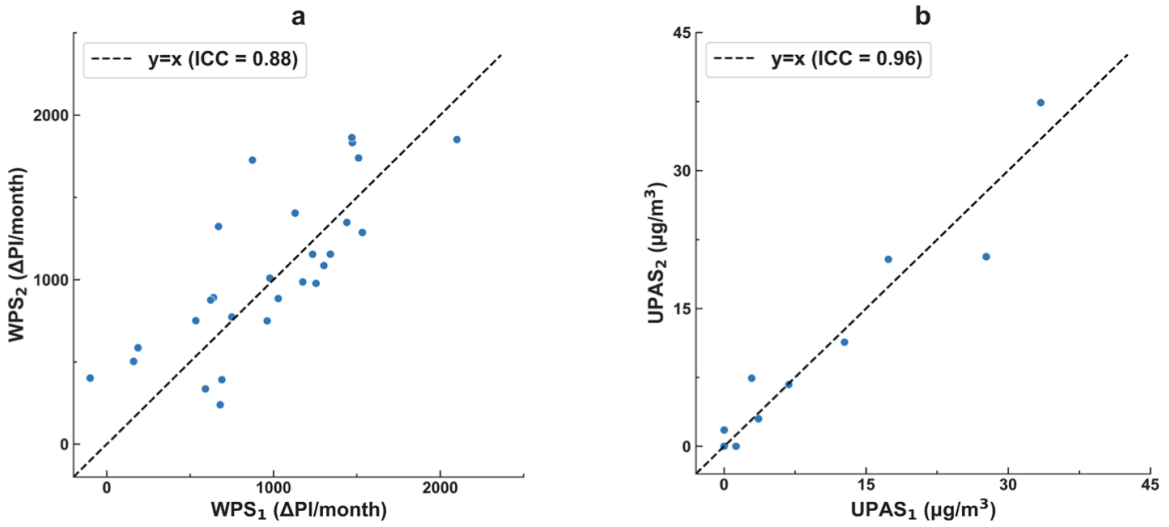

Figure 4.1: Correlation between duplicate samples: (a) Washington passive samplers (WPS), which measure the passive deposition of light-absorbing carbon (LAC), and (b) filter samples collected via an ultrasonic personal aerosol sampler (UPAS) and thermo-optically analyzed for elemental carbon (EC). ICC is the intraclass correlation coefficient, a measure of how strongly the duplicate measurements resemble each other. The elemental carbon collected by the UPAS measurement is considered the "gold standard"; the light-absorbing carbon collected by the WPS measurement is the new method investigated here. The plots show that the duplicate WPS and UPAS each exhibited strong within-method agreement (ICC $>$ 0.88), but precision was higher for the UPAS than the WPS. There are more measurements shown for the WPS than for the UPAS ($n = 28$ vs. $n = 10$), reflecting that the WPS is simpler and less failure-prone than the UPAS; the percentages of intended duplicate samples that were successfully obtained were 70% for the WPS and 25% for the UPAS.

4.4.3 Field Blank and Calibration Curve

The mean change in the reflectance for the 10 field blanks was 77 (standard deviation of 20) PI per month. Before establishing the calibration curve, we adjusted the change in the reflectance for the exposed filters by subtracting the mean change in the field blanks. The Deming regression analyses to calibrate the light-absorbing carbon to the elemental carbon measurement indicate that, on average, 1 μg of elemental carbon (EC) per cubic meter corresponds to 62 PI per month (as shown in Figure 2). Applying that conversion to all WPS measurements to predict the elemental carbon concentrations from the passive light-absorbing carbon measurements, for a one-month measurement, the root-mean-square error is 3.1 μg/m^3 EC. That value corresponds to 21% of the average elemental carbon concentration.

In summary, the average concentrations were 180 μg/m^3 for $PM_{2.5}$ (PurpleAir, uncalibrated) and 14.1 μg/m^3 for elemental carbon (measured by the UPAS) from the 21 samples collected across various households during each deployment period. The light-absorbing carbon measurements, expressed in their original, uncorrected units, reflect the rate of change in the filter color, denoted in units of change

in pixel intensity per month, which depends on the deposition of the light-absorbing carbon over time. The average value for the change in pixel intensity (ΔPI) was 1052 PI per month for all 32 samples collected, and 952 for the samples collected from the same subset of households where elemental carbon samples were successfully obtained. Using the calibration value (1 μg of EC per m^3 corresponds to 62 PI per month), 1052 PI per month would correspond to an average of 17.0 μg/m^3. Alternatively, when using the calibration curve shown in Figure 2 ($y = 62.1x + 75.1$), 1052 PI per month would correspond to 15.7 μg/m^3. These two values suggest that if the number of successful samples for elemental carbon analysis were 32 instead of 21, the average concentration would have been greater than 14.1 μg/m^3.

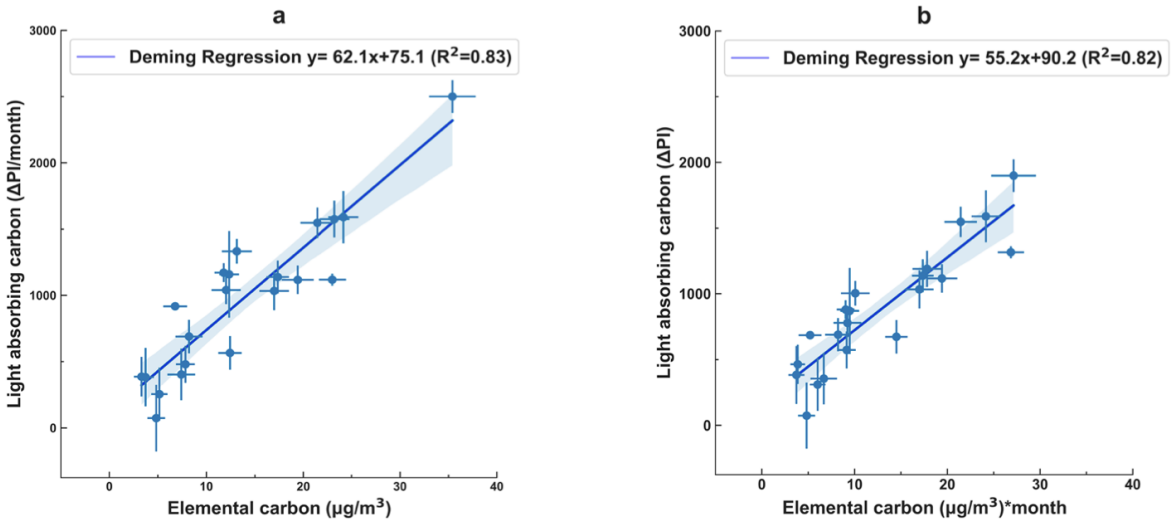

Figure 4.2: Correlation between the "gold standard" (x-axis: EC) and the WPS (y-axis: LAC), displayed using the native units of (a) the elemental carbon measurements and (b) the light-absorbing carbon measurements. (The two plots represent the same data, displayed in different units; the plots are similar but not identical because the deployment duration differed by the sampling period.) The y-error bars represent the range of the duplicate WPS, and the x-error bars represent the uncertainties from the elemental carbon analysis. The change in the filter color, denoted in units of change in pixel intensity per month, depends on the deposition of the light-absorbing carbon over time. The average value for the change in pixel intensity (ΔPI) was 1052 PI per month for all 32 samples collected, and 952 for the samples collected from the same subset of households where elemental carbon samples were successfully obtained. Deming regression was utilized (R, Deming package), reflecting that both measurements have uncertainties.

4.4.4 PurpleAir

In our comparison of the $PM_{2.5}$ concentration in households with both light-absorbing carbon and elemental carbon, the results, as depicted in Figure 3, indicate that both light-absorbing carbon and elemental carbon exhibited strong correlations with $PM_{2.5}$. Specifically, the UPAS (measuring elemental carbon) demonstrated a slightly stronger correlation with $PM_{2.5}$, with an R^2 value of 0.88, in comparison to the WPS (measuring light-absorbing carbon), with an R^2 value of 0.77. This observation likely reflects the diverse sources and chemical composition of $PM_{2.5}$, as well as, perhaps more significantly, the slightly lower precision of the WPS compared to the UPAS in this context.

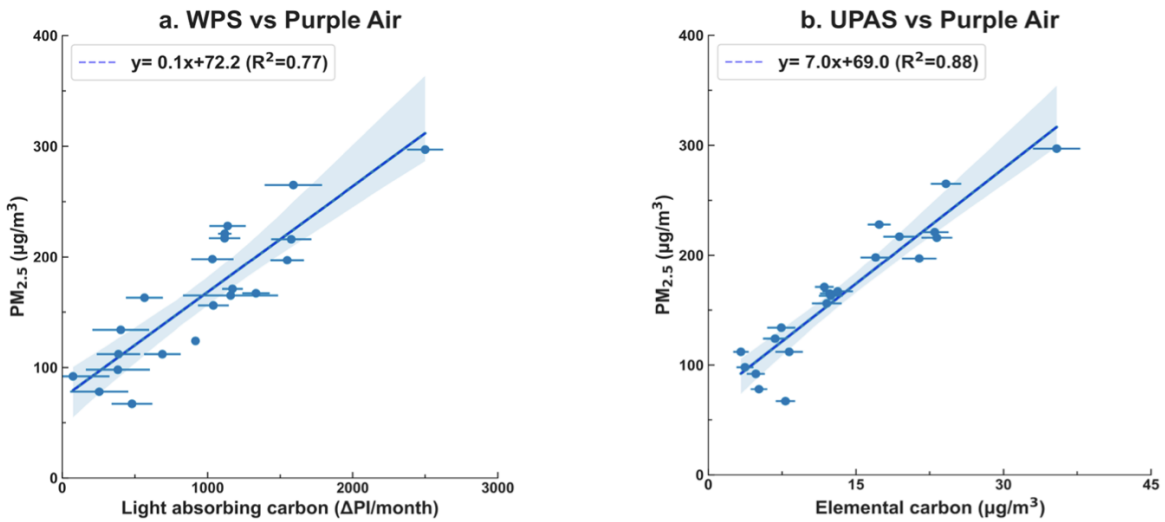

Figure 4.3: Correlation between PurpleAir (uncalibrated) with WPS (a) and elemental carbon analysis (b). The x-value error bars represent the difference between the duplicate WPS results (a) and the elemental carbon analysis uncertainties reported by the lab (b).

4.4.5 Darkening Rate of Fresh and Aged Filters

Here, we compare the darkening rates of aged (exposed for more than 4 weeks) and fresh (exposed for 4 weeks) filters. The darkening rates were similar but not identical (ICC = 0.90); the 95% CI on the best-fit line includes the 1:1 line. There is moderate evidence of a modest difference in the filter darkening rate for the aged and fresh filters (slope = 1.06 ± 0.05). This "filter loading" effect is well-documented for micro-aethalometers [182], which use similar principles to the WPS.

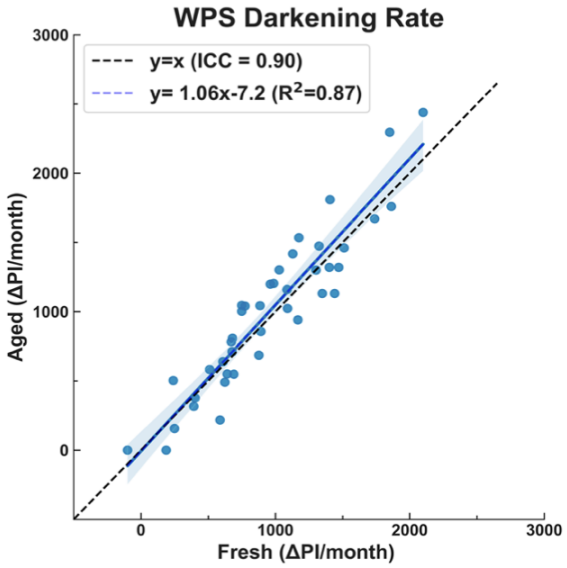

Figure 4.4: Darkening rate difference between fresh and aged filters. Fresh filters were photographed before deployment and 4 weeks after exposure in the household; aged filters were photographed after being exposed for a certain period, then photographed after 4 more weeks of exposure, i.e., aged filters represent the delta pixel intensity of already exposed filters after more exposure. The results here are similar to the "filter loading" effect, which is well-documented for micro-aethalometers.

4.5 Discussion

The objective of this study was to assess the performance and uncertainty of the Washington passive sampler (WPS), an innovative, cost-effective passive sampler designed for measuring light-absorbing carbon. The precision and accuracy of the WPS were determined through the deployment of multiple duplicate samples and co-location with a $PM_{2.5}$ proxy method (PurpleAir), as well as duplicates of the "gold-standard" reference method (UPAS with elemental carbon analysis). Notably, unlike the active PurpleAir and the gold-standard UPAS method, the WPS is a passive sampler. The study's findings indicate that changes in the reflectance measured by the WPS can effectively predict the long-term average elemental carbon concentration with a relatively good level of accuracy, as indicated by a root-mean-square error (RMSE) of 21%.

The reported accuracy of the Washington passive sampler (WPS) with an RMSE of 21% is consistent with the accuracy levels reported for other methods used to measure black carbon or elemental carbon [183–188]. For instance, low-cost black carbon samplers available on the market exhibited similar accuracy, such as an RMSE of 25% reported for ABCD, and approximately 10% for another image-based reflectance method [182, 184]. Chiappini et al. (2022) [189] conducted a study involving three sets of duplicated co-located samples, each analyzed using three different protocols for elemental carbon (EC) analysis. They reported overall uncertainties of 14%, 39%, and 20% for the respective sets (averaging 24%) for samples #1, #2, and #3, indicating that elemental carbon analysis can have variable uncertainties across different protocols. Several inter-laboratory comparison studies have also reported relative standard deviations of 6–26% for elemental carbon analysis across various widely used thermal-optical analysis protocols in different laboratories (see Table C.2) [169, 185–187, 189–192]. It is important to note that the RMSE, a measure of accuracy, is the combination of the standard deviation (a measure of precision) and absolute bias [193]. Therefore, the RMSE, as reported here for the WPS, is expected to be higher than the standard deviation. The accuracy of the WPS aligns with the levels reported in the literature for other methods, including the gold-standard reference methods, underscoring its reliability and effectiveness for measuring light-absorbing carbon. The correlation between the $PM_{2.5}$ and light-absorbing carbon, indicated by an R^2 value of 0.77, was slightly lower than the correlation between the $PM_{2.5}$ and elemental carbon, which had an R^2 value of 0.88. This implies that the relationship between the $PM_{2.5}$ and elemental carbon is slightly stronger. Additionally, the darkening rates of the aged and fresh filters exhibited good correlations, as reflected by an intraclass correlation coefficient (ICC) of 0.90. The 95% confidence interval (CI) region of the best-fit line includes the 1:1 line, and the slope of the line for the aged versus fresh filters was 1.06 ($\pm$0.05). The minor difference observed, with the darkening rates being slightly lower for the aged filters (i.e., darker) compared to the fresh filters (i.e., less dark), aligns with the well-documented filter-loading effect observed for micro-aethalometers [182].

A recent study by Jeronimo et al. (2020) [184] also developed a low-cost method for estimating the concentration of black carbon using a digital camera. They compared the image-based reflectance method to several existing reference methods, including thermal-optical analysis, and found a good correlation with a normalized RMSE of less than 10% for all comparisons. Both studies (ours; Jeronimo et al. (2020) [184]) developed a digital image-based method and compared it against a gold-standard method; the main differences include the sampling method (Jeronimo et al. (2020) [184] employed active sampling instead of passive samplers), filter type (Jeronimo et al. (2020) [184] used more expensive PTFE filters, whereas our method utilized cellulose filters), and sampling time (in Jeronimo et al.'s study, the sampling duration ranged from 24–48 h, whereas our study extended over 21–35 days). Nevertheless, the results of Jeronimo et al.'s study offer consistent and reassuring evidence that an image-based reflectance method can deliver accurate estimates.

Relative to the gold-standard method (thermal-optical analysis of active filters), the WPS offers important advantages in scalability, ease of use, utility, lower measurement failure rate, and cost. Most studies of indoor air pollution effects on human health are based on exposure data collected for 24–48 h, owing to the high cost of measurement devices and the logistics of measurements [176, 194]. Thus, the results of these studies rely on short-term average concentrations of black carbon, which can be different with changing environments and household behavior. In some cases, studies with filters employ multiple visits (e.g., three samples of 24 h each, for an 18-month period), thus providing a small number of snapshots. In contrast, the WPS can be deployed for months or potentially years without requiring extensive maintenance, and it allows for the collection of long-term levels of LAC

concentrations. For many investigations, the lower cost of measurement and the greater ease of use of the WPS relative to the gold-standard measurements, combined with the opportunity of using the WPS to obtain long-term rather than short-term averages, may offer important advantages for exposure and health studies in households that use solid fuels.

Recent studies comparing low-cost methods on the market to reference methods all suggest that the readings of low-cost sensors are sensitive to environmental factors, such as the relative humidity, and performances against reference monitors change with the weather [191, 192, 194, 195]. Light-absorbing carbon estimates using image-based methods for reflectance may be sensitive to the site, season, pollution source (e.g., fuel type), and/or reference method selected for calibration. Further testing needs to be carried out to determine (i) the correction factor under different environmental conditions, (ii) the calibration curve of light-absorbing carbon against $PM_{2.5}$, and (iii) the upper and lower thresholds of the detection limit in terms of concentration and time.

4.6 Conclusions

This study evaluated the Washington passive sampler (WPS) as a novel, ultra-low-cost sensor for assessing the levels of light-absorbing carbon. A prior field campaign [167] investigated the precision of this method; the present campaign aimed to investigate its accuracy. To do so, we compared duplicate samples of the WPS against co-located duplicate samples using a gold-standard method, thermal-optical analysis.

Our results indicate that the root-mean-square error (RMSE) of the WPS was 21%, which is comparable to the literature-reported values for other methods, including gold-standard methods. This level of accuracy is surprisingly high, given the ultra-low cost and the ease of use of this method. The two main differences between the WPS and the gold-standard measurements are the measurement type (image analysis versus chemical analysis) and passive versus active samples (i.e., without versus with a pump).

The strong correlation with elemental carbon ($R^2 = 0.88$) and $PM_{2.5}$ ($R^2 = 0.77$), along with the consistency observed in the darkening rates of aged and fresh filters (i.e., no strong filter-loading effect), further corroborates the WPS's reliability. The WPS offers advantages in terms of its scalability, ease of use, cost-effectiveness, and a prolonged deployment approach, which enables collecting data on long-term levels of light-absorbing carbon pollution. In our study, the percentage of successful samples collected over the intended sample number was notably higher for the WPS (80%) compared to the UPAS (55%) in total. When considering duplicate samples, the difference remained substantial, with the WPS achieving a success rate of 70% versus the UPAS's 25%. While these challenges encountered during data collection may be unique to our study, issues such as unintentional shutdowns due to factors like high temperatures, battery depletion from extended power outages, and unexplained operational disruptions, could be encountered universally in field conditions, especially in regions like rural India. Based on our findings, the WPS appears to be a well-suited choice for long-term studies in rural locations, offering a reliable, practical, and inexpensive solution for measuring light-absorbing carbon pollution.

This paper represents only the second publication regarding the WPS [167]; additional testing of its robustness and methods for deployment would be helpful. For example, further research on the sensitivity of the WPS to environmental factors, the detection limit, and the calibration curve against elemental carbon and $PM_{2.5}$ would usefully shed light on the WPS's reliability across diverse environmental contexts.

4.7 Appendix C: Supplemental Information for Chapter 4

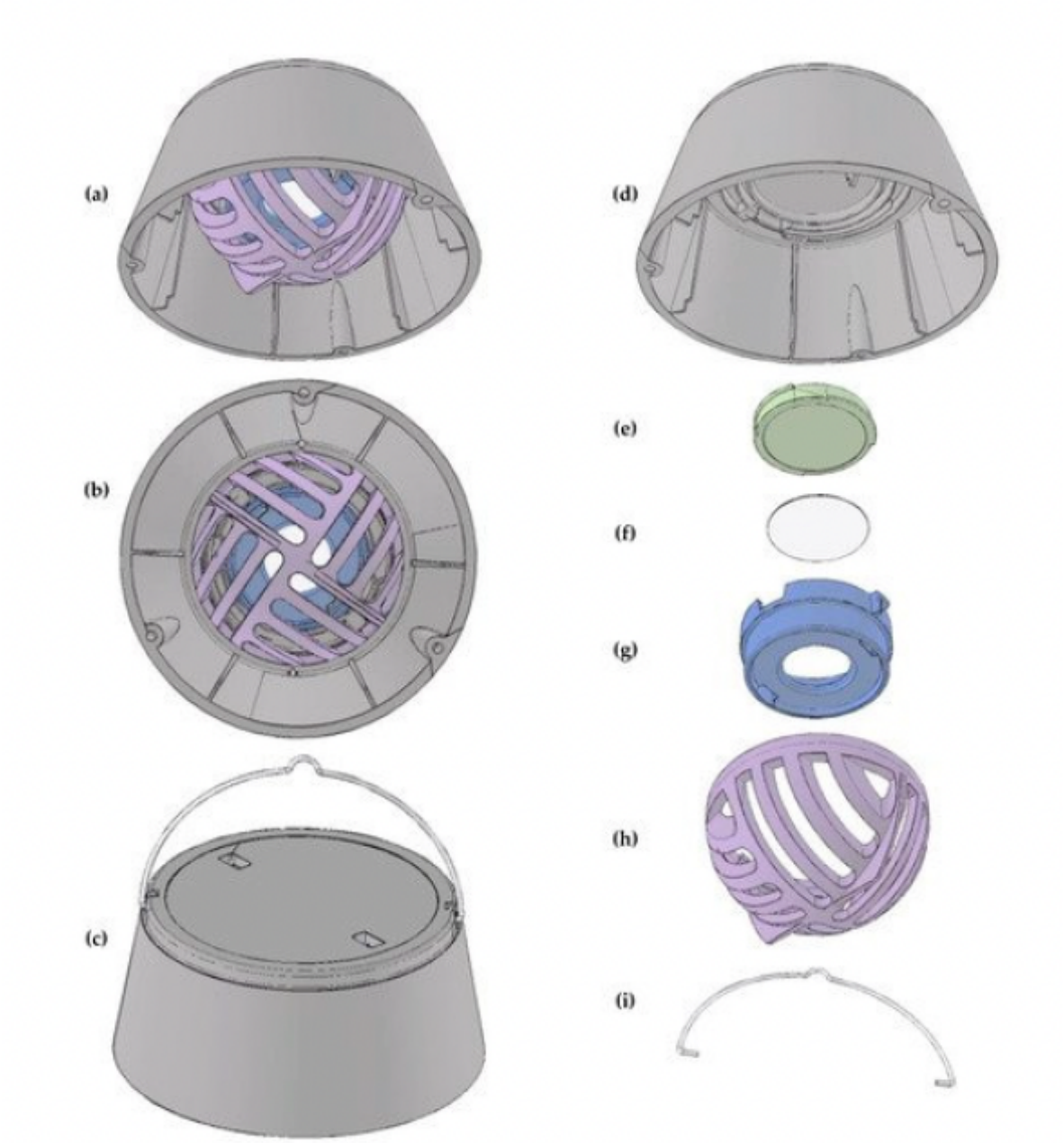

Figure C.1: The assembled low-cost passive sampler, shown from (a) side, (b) bottom, and (c) top, and its components, including the (d) cap, (e) base for paper filter exposure surface, (f) paper filter exposure surface, (g) clamp for paper filter exposure surface, (h) protective cage, and (i) wire for hanging sampler. Reproduced from Clark et al. (2020) with permission [167].

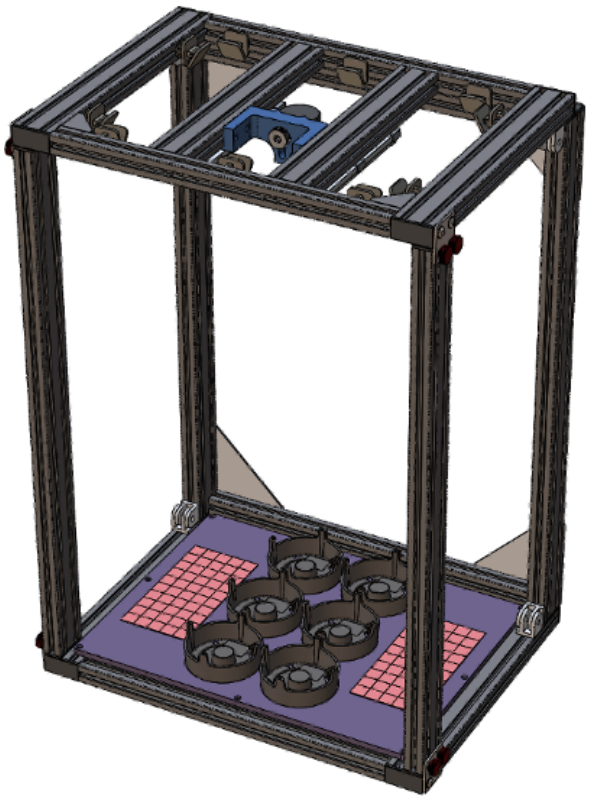

Figure C.2: Photobox design where WPS is photographed before and after deployment to estimate the pixel intensity difference.

Table C.1: Deployment and sample details.

Deployment	Dates of deployment	Number of WPS in each household	Number of UPAS in each household	Number of PurpleAir in each household	Number of successful sample (EC-LAC)
1	12/20/2021 - 01/15/2021	2	2	1	2
2	01/15/2021 - 02/10/2021	4	2	1	6
3	02/10/2021 - 03/13/2021	6	2	1	5
4	03/13/2021 - 04/14/2021	8	2	1	8

Table C.2: Inter-laboratory comparisons using thermal-optical methods for the determination of EC concentrations.

Study	Number of samples	Number of labs	Protocol	Relative Standard deviation EC (%)
Birch (1998)	5	5	NIOSH5040	6–26
Birch (2002)	50	3	NIOSH5040	10
Schauer et al. (2003)	11	8	ACE-ASIA model	13–21
Emblico et al. (2012)	14	16	EUSAAR 2, NIOSH	20–25
Chai et al. (2012)	4	7	NIOSH5040	7–9
Chiappini et al. (2014)	3	5	NIOSH5040, EUSAAR 2	6.8–19.2
Panteliadis et al. (2015)	5	17	EUSAAR 2, NIOSH-870	20

Chapter 5

Conclusion and Contributions

This dissertation reflects my effort to address some of the pressing gaps in air quality research by developing tools, methodologies, and low-cost solutions that can be used for effective air quality management. The work integrates approaches that aim to make air quality research more accessible, efficient, and relevant to both policymakers and researchers. This dissertation aims to contribute to the broader field of air quality management in meaningful ways by combining practical tools with advanced modeling techniques. Below, I summarize the main contributions, acknowledge the limitations of the work, and outline directions for future efforts.

5.1 Contributions to Air Quality Management Tools

This dissertation introduced several tools and methodologies aimed at enhancing air quality research. One of the key contributions is the development and application of the Robust Differences methodology, which provides a practical way to estimate baseline air pollution concentrations. By applying this method to ambient air pollution concentrations recorded during the Covid-19 pandemic, I was able to quantify the effects of stay-at-home orders on air quality and demonstrate how different analytical approaches can influence the outcomes of accountability studies. Another contribution is the updated InMAP Source Receptor Matrix (ISRM 2.0). This modeling tool offers high-resolution insights into source-receptor relationships across over 86,000 grid cells, focusing on primary $PM_{2.5}$ and its key precursors. With its computational efficiency, ISRM 2.0 allows for faster policy scenario analyses, making it a valuable tool for researchers and policymakers who may lack access to more complex air quality models. Additionally, I developed the Washington Passive Sampler (WPS), an ultra-low-cost tool designed to monitor black carbon in resource-constrained settings. The WPS is straightforward to use, costs between $5 and $15, and requires no electricity, making it suitable for citizen science projects and community-based monitoring. Initial validation has shown that the WPS performs well under typical conditions, providing a practical solution for household air pollution studies and intervention assessments. Each of these contributions is designed to make air quality research more accessible, whether through tools like the WPS that communities can deploy themselves or models like ISRM 2.0 that can be used in college classrooms to teach students about policy scenario analysis. I hope that these tools will not only serve academic and policy communities but also engage individuals and organizations working to improve air quality at the local level.

5.2 Limitations

While I am proud of the contributions this dissertation makes, it is important to acknowledge the limitations of this work. The Robust Differences methodology relies on the availability of historical monitoring data, which may not always be available in regions with limited monitoring networks. There are other, more significant limitations, including that only a modest number of monitors had sufficient data for analysis, and those monitors did not cover all U.S. states. Consequently, they likely do not reflect all possible outcomes across the U.S., including differences in emission-change levels, underlying chemistry and meteorology, and resulting concentrations. Additionally, various locations exhibited widely varying levels of adherence to stay-at-home orders, an important aspect that this dataset did not allow us to investigate.

The ISRM 2.0, though computationally efficient, simplifies atmospheric processes to achieve reduced complexity. This results in loss of precision compared to more comprehensive models. Moreover, ISRM 2.0 focuses on a limited set of pollutants, excluding many important pollutants such as ozone and ultrafine particles. The use of static meteorological conditions also limits its ability to reflect temporal variability (for the version employed here: annual-average concentrations only).

The WPS, while offering a low-cost solution for monitoring black carbon, has lower precision compared to regulatory-grade instruments. Its performance under extreme environmental conditions, such as high humidity or temperature, has not yet been fully tested. Its focus on black carbon means that it cannot measure other important pollutants, limiting its broader applicability in air quality assessments. It is a passive device, and each measurement is a temporal average; no information is given on temporal variability.

These limitations highlight areas where further refinement and validation are needed. By addressing these challenges, future efforts can build on this work to improve the robustness and applicability of the tools and methodologies developed here.

5.3 Future Directions

Looking ahead, there are several ways to expand and refine the contributions of this dissertation. First, adapting InMAP and ISRM to other countries, particularly low- and middle-income nations, could help address localized air quality challenges. Developing country-specific models that incorporate additional pollutants and dynamic meteorological conditions would enhance their relevance in diverse policy contexts.

The WPS offers significant potential for scalability and broader application. Ongoing feasibility studies in Mongolia and Nigeria will provide insights into its utility for household air pollution monitoring. Expanding its use to citizen science projects could empower communities to collect and analyze air quality data, fostering public awareness and engagement. Combining WPS data with health impact assessments could also support more comprehensive evaluations of interventions, such as stove or fuel transitions.

Targeted emission reduction strategies remain another important area for future work. For example, developing technologies for manure management and optimized fertilizer application could help address emissions from the agriculture sector. In the transportation and industrial sectors, further adoption of electric vehicles and carbon capture technologies could drive additional reductions.

Future work could focus on enhancing the accuracy and global applicability of reduced-complexity air quality models like InMAP by integrating machine learning and fostering international collaborations. Machine learning methods, such as neural networks or random forests, could refine source-receptor relationships and improve the accuracy of pollutant dispersion predictions without compromising computational efficiency. These enhanced models could then be adapted to diverse regions through collaborative efforts to incorporate localized emissions, meteorology, and demographic data.

Finally, the tools and methodologies developed here are adaptable to global contexts. By collaborating with local universities and institutions, future efforts could focus on capacity building to train researchers and students in air quality management. International collaborations could also help standardize methodologies and share best practices, broadening the impact of these tools.

5.4 Final Thoughts

As I reflect on this work, I am humbled by the opportunity to contribute to the field of air quality research. While this dissertation addresses some critical gaps, it is only a step in a larger journey. By continuing to refine these tools and engaging with diverse communities, I hope this work can support more equitable and effective air quality management, ultimately contributing to healthier and more sustainable environments.

Bibliography

[1] E.T. Jacobs, J.L. Burgess, and M.B. Abbott. The Donora Smog Revisited: 70 Years After the Event That Inspired the Clean Air Act. *American Journal of Public Health*, 108, 2018.

[2] Health Effects Institute. State of global air 2019. Technical report, Health Effects Institute, 2019. Available at: http://www.stateofglobalair.org/sites/default/files/soga$_2$019$_r$*eport.pdf*.

[3] Andrea Pozzer, Susan C. Anenberg, Subhrendu Dey, Andy Haines, Jos Lelieveld, and Sourangsu Chowdhury. Mortality Attributable to Ambient Air Pollution: A Review of Global Estimates. *GeoHealth*, 7(1), 2023.

[4] United Nations Environment Programme. The First Global Assessment of Air Pollution Legislation. United Nations Environment Programme, 2021. Available at: https://www.unep.org/resources/assessment/first-global-assessment-air-pollution-legislation.

[5] K. Kuklinska, L. Wolska, and J. Namiesnik. Air quality policy in the U.S. and the EU - A review. *Atmospheric Pollution Research*, 6(1), 2015.

[6] United States Congress. *Clean Air Act*, volume 42 of *United States Code*. Government Printing Office, Washington, D.C., 1970. Codified as Title 42, Chapter 85 of the United States Code.

[7] U.S. Environmental Protection Agency. Air Quality Management Process Cycle. *Environmental Protection Agency*, 2017. Available at: https://www.epa.gov/air-quality-management-process.

[8] United States Code. 42 U.S.C. 7409 - National Ambient Air Quality Standards (NAAQS). Title 42 - The Public Health and Welfare, Chapter 85 - Air Pollution Prevention and Control, Subchapter I - Programs and Activities, Part A - Air Quality and Emission Limitations, 1970.

[9] U.S. Environmental Protection Agency. Air Quality System (AQS). US Environmental Protection Agency, 2019. Available at: https://www.epa.gov/aqs.

[10] K. W. Appel, S. L. Napelenok, K. M. Foley, H. O. T. Pye, C. Hogrefe, D. J. Luecken, J. O. Bash, S. J. Roselle, J. E. Pleim, H. Foroutan, W. T. Hutzell, G. A. Pouliot, G. Sarwar, K. M. Fahey, B. Gantt, R. C. Gilliam, N. K. Heath, D. Kang, R. Mathur, D. B. Schwede, T. L. Spero, D. C. Wong, and J. O. Young. Description and evaluation of the Community Multiscale Air Quality (CMAQ) modeling system version 5.1. *Geoscientific Model Development*, 10(4), 2017.

[11] Environmental Protection Agency. The Benefits and Costs of the Clean Air Act, 1970 to 1990. Retrospective study, Environmental Protection Agency, October 1997. Available at: https://www.epa.gov/sites/default/files/2015-06/documents/contsetc.pdf.

[12] United States Environmental Protection Agency. Evolution of the Clean Air Act Clean Air Act of 1970. *The United States Environmental Protection Agency*, 2017.

[13] Environmental Protection Agency. The Benefits and Costs of the Clean Air Act from 1990 to 2020, Final Report, Revision A, April 2011. *U.S. Environmental Protection Agency Office of Air and Radiation*, (April 2011), 2011.

[14] X. Liu, C. Guo, Y. Wu, C. Huang, K. Lu, Y. Zhang, L. Duan, M. Cheng, F. Chai, F. Mei, and H. Dai. Evaluating cost and benefit of air pollution control policies in China: A systematic review. *Journal of Environmental Sciences (China)*, 123, 2023.

[15] J. Miller and C. Façanha. Cost-Benefit Analysis of Brazil's Heavy-Duty Emission Standards (P-8). The International Council on Clean Transportation, March 2016. Available at: https://theicct.org/sites/default/files/publications/ICCT$_B$*razilHDV* − *EmissionStandards*$_2$0160301*.pdf*.

[16] A.S. Voorhees, S. Araki, R. Sakai, and H. Sato. An ex-post cost-benefit analysis of the nitrogen dioxide air pollution control program in Tokyo. *Journal of Air and Waste Management Association*, 50(3):391–410, March 2000.

[17] A. Kiziltan and M. Kiziltan. Cost–benefit analysis of road-transport policy options to combat air pollution in Turkey. *Environment, Development and Sustainability*, 25(10), 2023.

[18] J.A. Bonilla, C. Aravena, and R. Morales-Betancourt. Assessing Multiple Inequalities and Air Pollution Abatement Policies. *Environmental and Resource Economics*, 84(3), 2023.

[19] California Air Resources Board. Cost-Benefit Analysis of the California Air Resources Board's (CARB) Incentive Programs. Technical report, California Air Resources Board, 2021. Available at: https://www.arb.ca.gov/incentives-programs-cost-benefit-analysis.

[20] Washington Department of Ecology. Final Cost Benefit Analysis: Air Quality Fee Rule, Ch. 173-455 WAC. Report 11-02-016, Washington Department of Ecology, May 2011. Available at: https://apps.ecology.wa.gov/publications/SummaryPages/1102016.html.

[21] C.A. Pope, A.J. Cohen, and R.T. Burnett. Cardiovascular disease and fine particulate matter lessons and limitations of an integrated exposure-response approach. *Circulation Research*, 122(12), 2018.

[22] C.A. Pope, R.T. Burnett, M.J. Thun, E.E. Calle, D. Krewski, K. Ito, and G.D. Thurston. Lung cancer, cardiopulmonary mortality, and long-term exposure to fine particulate air pollution. *Journal of the American Medical Association*, 287(9), 2002.

[23] C. A. Pope, N. Coleman, Z. A. Pond, and R. T. Burnett. Fine particulate air pollution and human mortality: 25+ years of cohort studies. *Environmental Research*, 183, 2020.

[24] D.W. Dockery, C.A. Pope, X. Xu, J.D. Spengler, J.H. Ware, M.E. Fay, B.G. Ferris, and F.E. Speizer. An Association between Air Pollution and Mortality in Six U.S. Cities. *New England Journal of Medicine*, 329(24), 1993.

[25] M. Ezzati C. A. Pope and D. W. Dockery. Fine-Particulate Air Pollution and Life Expectancy in the United States. *New England Journal of Medicine*, 360(4), 2009.

[26] United States Environmental Protection Agency. List of designated reference and equivalent methods. Technical report, Center for Environmental Measurements & Modeling, Air Methods & Characterization Division, June 2024. Available at: https://www.epa.gov/air-research/list-designated-reference-and-equivalent-methods.

[27] C. A. Noble, R. W. Vanderpool, T. M. Peters, F. F. McElroy, D. B. Gemmill, and R. W. Wiener. Federal reference and equivalent methods for measuring fine particulate matter. *Aerosol Science and Technology*, 34(5), 2001.

[28] S. Kotthaus, J.A. Bravo-Aranda, M. Collaud Coen, J.L. Guerrero-Rascado, M.J. Costa, D. Cimini, E.J. O'Connor, M. Hervo, L. Alados-Arboledas, M. Jiménez-Portaz, L. Mona, D. Ruffieux, A. Illingworth, and M. Haeffelin. Atmospheric boundary layer height from ground-based remote sensing: a review of capabilities and limitations. *Atmospheric Measurement Techniques*, 16(2), 2023.

[29] S. He, H. S. Shin, S. Xu, and A. Tsourdos. Distributed estimation over a low-cost sensor network: A Review of state-of-the-art. *Information Fusion*, 54, 2020.

[30] C. Tong, C. Zhang, and C. Liu. Investigation on the relationship between satellite air quality measurements and industrial production by generalized additive modeling. *Remote Sensing*, 13(16), 2021.

[31] F. Mao, K. Khamis, S. Krause, J. Clark, and D.M. Hannah. Low-Cost Environmental Sensor Networks: Recent Advances and Future Directions, 2019.

[32] K.P. Messier, S.E. Chambliss, S. Gani, R. Alvarez, M. Brauer, J.J. Choi, S.P. Hamburg, J. Kerckhoffs, B. Lafranchi, M.M. Lunden, J.D. Marshall, C.J. Portier, A. Roy, A.A. Szpiro, R.C.H. Vermeulen, and J.S. Apte. Mapping Air Pollution with Google Street View Cars: Efficient Approaches with Mobile Monitoring and Land Use Regression. *Environmental Science and Technology*, 52(21), 2018.

[33] D. Byun and K. L. Scherer. Review of the governing equations, computational algorithms, and other components of the Model-3 Community Multiscale Air Quality (CMAQ) Modeling System. *Applied Mechanics Reviews*, 59(2):51–77, 2006.

[34] ENVIRON International Corporation. *User's Guide to the Comprehensive Air Quality Model with Extensions (CAMx) Version 2.00.* 101 Rowland Way, Suite 220, Novato, California 94945-5010, 1998.

[35] I. Bey, D. J. Jacob, R. M. Yantosca, J. A. Logan, B. D. Field, A. M. Fiore, Q. Li, H. Y. Liu, L. J. Mickley, and M. G. Schultz. Global modeling of tropospheric chemistry with assimilated meteorology: Model description and evaluation. *Journal of Geophysical Research*, 106(D19):23073–23095, 2001.

[36] S. E. Peckham, G. A. Grell, S. A. McKeen, R. Ahmadov, K. Y. Wong, M. Barth, G. Pfister, C. Wiedinmyer, J. D. Fast, W. I. Gustafson, et al. WRF-Chem version 3.8.1 user's guide. Technical Report NOAA technical memorandum OAR GSD; 48, Earth System Research Laboratory (U.S.), Global Systems Division, 2017.

[37] A. Venkatram J. C. Weil R. J. Paine R. B. Wilson R. F. Lee W. D. Peters A. J. Cimorelli, S. G. Perry and R. W. Brode. AERMOD: A dispersion model for industrial source applications. Part I: General model formulation and boundary layer characterization. *Journal of Applied Meteorology and Climatology*, 44(5):682–693, 2005.

[38] R. R. Draxler and G. D. Hess. Description of the HYSPLIT_4 modeling system. Technical report, NOAA Air Resources Laboratory, 1997.

[39] A. Patton, D. N. Politis, and H. White. Correction to automatic block-length selection for the dependent bootstrap by D. Politis and H. White. *Econometric Reviews*, 28:372–375, 2009.

[40] J. Alcamo, R. Shaw, and L. Hordijk, editors. *The RAINS Model of Acidification: Science and Strategies in Europe.* Kluwer Academic Publishers, Dordrecht, Netherlands, 1990.

[41] M. Amann and M. Lutz. The revision of the air quality legislation in the European Union related to ground-level ozone. *Journal of Hazardous Materials*, 78(1-3):41–62, 2000.

[42] U.S. Environmental Protection Agency. *Environmental Benefits Mapping and Analysis Program - Community Edition (BenMAP-CE).* Office of Air Quality Planning and Standards, 2018. Version 1.5.0.0. Available at: https://www.epa.gov/benmap.

[43] C.W. Tessum, J.D. Hill, and J.D. Marshall. InMAP: A model for air pollution interventions. *PLoS ONE*, 12(4), 2017.

[44] J. Heo, P.J. Adams, and H. Gao. Reduced-form modeling of public health impacts of inorganic PM2.5 and precursor emissions. *Atmospheric Environment*, 137:80–89, 2016.

[45] N.Z. Muller and R.M. Mendelsohn. The Air Pollution Emission Experiments and Policy Analysis Model (APEEP) Technical Appendix. Technical report, School of Forestry and Environmental Studies, Yale University, New Haven, CT, December 2006.

[46] C.A. Pope, J.S. Lefler, M. Ezzati, J.D. Higbee, J.D. Marshall, S.Y. Kim, M. Bechle, K.S. Gilliat, S.E. Vernon, A.L. Robinson, and R.T. Burnett. Mortality risk and fine particulate air pollution in a large, representative cohort of U.S. adults. *Environmental Health Perspectives*, 127(7), 2019.

[47] H.K. Im, M.L. Stein, and V.R. Kotamarthi. A new approach to scenario analysis using simplified chemical transport models. *Journal of Geophysical Research Atmospheres*, 110(24), 2005.

[48] J.S. Fu, F.L. Yeh, C.J. Jang, R.J.C. Chen, and M.T. Chuang. Air quality modeling: An investigation of the merits of CMAQ in the analysis of transboundary air pollution from continents to small islands. *International Journal of Environmental Technology and Management*, 10(2), 2009.

[49] R. Mathur, S. Roselle, J. Young, and D. Kang. Representing the Effects of Long-Range Transport and Lateral Boundary Conditions in Regional Air Pollution Models. *NATO Science for Peace and Security Series C: Environmental Security*, 137, 2013.

[50] C.Y. Lim, M. Stein, J. Ching, and R. Tang. Statistical properties of differences between low and high resolution CMAQ runs with matched initial and boundary conditions. *Environmental Modelling and Software*, 25(1), 2010.

[51] J. Pleim, J. Young, D. Wong, R. Gilliam, T. Otte, and R. Mathur. Two-way coupled meteorology and air quality modeling. In *NATO Science for Peace and Security Series C: Environmental Security*. 2008.

[52] A. L. Goodkind, C. W. Tessum, J. S. Coggins, J. D. Hill, and J. D. Marshall. Fine-scale damage estimates of particulate matter air pollution reveal opportunities for location-specific mitigation emissions. *PNAS*, 116(18):8775–8780, 2019.

[53] J. S. Coggins J. D. Hill A.L. Goodkind, C. W. Tessum and J. D. Marshall. Fine-scale damage estimates of particulate matter air pollution reveal opportunities for location-specific mitigation of emissions. *Proceedings of the National Academy of Sciences of the United States of America*, 116(18), 2019.

[54] C.W. Tessum, D.A. Paolella, S.E. Chambliss, J.S. Apte, J.D. Hill, and J.D. Marshall. PM2.5 polluters disproportionately and systemically affect people of color in the United States. *Science Advances*, 7(18), 2021.

[55] C.W. Tessum, J.S. Apte, A.L. Goodkind, N.Z. Muller, K.A. Mullins, D.A. Paolella, S. Polasky, N.P. Springer, S.K. Thakrar, J.D. Marshall, and J.D. Hill. Inequity in consumption of goods and services adds to racial-ethnic disparities in air pollution exposure. *Proceedings of the National Academy of Sciences of the United States of America*, 116(13), 2019.

[56] S.K. Thakrar, A.L. Goodkind, C.W. Tessum, J.D. Marshall, and J.D. Hill. Life cycle air quality impacts on human health from potential switchgrass production in the United States. *Biomass and Bioenergy*, 114, 2018.

[57] S.K. Thakrar, S. Balasubramanian, P.J. Adams, I.M.L. Azevedo, N.Z. Muller, S.N. Pandis, S. Polasky, C.A. Pope, A.L. Robinson, J.S. Apte, C.W. Tessum, J.D. Marshall, and J.D. Hill. Reducing Mortality from Air Pollution in the United States by Targeting Specific Emission Sources. *Environmental Science and Technology Letters*, 7(9), 2020.

[58] S.K. Thakrar, C.W. Tessum, J.S. Apte, S. Balasubramanian, D.B. Millet, S.N. Pandis, J.D. Marshall, and J.D. Hill. Global, high-resolution, reduced-complexity air quality modeling for PM2.5 using InMAP (Intervention Model for Air Pollution). *PLoS ONE*, 17(5 May), 2022.

[59] Y. Wang, J.S. Apte, J.D. Hill, C.E. Ivey, R.F. Patterson, A.L. Robinson, C.W. Tessum, and J.D. Marshall. Location-specific strategies for eliminating US national racial-ethnic PM2.5 exposure inequality. *Proceedings of the National Academy of Sciences of the United States of America*, 119(44), 2022.

[60] Y. Wang, J.S. Apte, J.D. Hill, C.E. Ivey, D. Johnson, E. Min, R. Morello-Frosch, R. Patterson, A.L. Robinson, C.W. Tessum, and J.D. Marshall. Air quality policy should quantify effects on disparities. *Science*, 381(6655), 2023.

[61] M.W. Tessum, S.C. Anenberg, Z.A. Chafe, D.K. Henze, G. Kleiman, I. Kheirbek, J.D. Marshall, and C.W. Tessum. Sources of ambient PM2.5 exposure in 96 global cities. *Atmospheric Environment*, 286, 2022.

[62] M.P.S. Thind, G. Heath, Y. Zhang, and A. Bhatt. Characterization factors and other air quality impact metrics: Case study for PM2.5-emitting area sources from biofuel feedstock supply. *Science of the Total Environment*, 822, 2022.

[63] C.L. Gallagher, T. Holloway, C.W. Tessum, C.M. Jackson, and C. Heck. Combining Satellite-Derived PM2.5 Data and a Reduced-Form Air Quality Model to Support Air Quality Analysis in US Cities. *GeoHealth*, 7(5), 2023.

[64] E. Gakidou, A. Afshin, A.A. Abajobir, K.H. Abate, C. Abbafati, K.M. Abbas, F. Abd-Allah, A.M. Abdulle, S.F. Abera, and V. Aboyans. Global, regional, and national comparative risk assessment of 84 behavioral, environmental and occupational, and metabolic risks or clusters of risks, 1990–2016: A systematic analysis for the Global Burden of Disease Study 2016. *Lancet*, 390:1345–1422, 2017.

[65] J. Volckens, C. Quinn, D. Leith, J. Mehaffy, C.S. Henry, and D. Miller-Lionberg. Development and evaluation of an ultrasonic personal aerosol sampler. *Indoor Air*, 27:409–416, 2017.

[66] PurpleAir. PurpleAir: Real-Time Air Quality Monitoring. Available at: https://www2.purpleair.com, 2022.

[67] IQAir. AirVisual Pro, 2021. Available at: https://www.iqair.com/air-quality-monitors/airvisual-pro.

[68] Uhoo. Uhoo Indoor Air Sensor, 2021. Available at: https://uhooair.com/.

[69] Temtop. Temtop M2000C Air Quality Monitor, 2021. Available at: https://www.temtopus.com/products/temtop-m2000c-air-quality-monitor.

[70] Atmotube. Atmotube Pro Portable Air Quality Monitor, 2021. Available at: https://atmotube.com/products/atmotube-pro.

[71] Sensirion. SPS30 Particulate Matter Sensor, 2021. Available at: https://www.sensirion.com/en/environmental-sensors/particulate-matter-sensors-pm25/.

[72] T.C. Bond and R.W. Bergstrom. Light absorption by carbonaceous particles: An investigative review. *Aerosol Science and Technology*, 40:27–67, 2006.

[73] C.A. Pope, M.R. Ransom, and J. Schwartz. Daily mortality and pm10 pollution in Utah Valley. *Archives of Environmental Health*, 47(3), 1992.

[74] C.A. Pope. Mortality from Copper Smelter Emissions: Pope Responds. *Environmental Health Perspectives*, 115(9), 2007.

[75] Y. Hu, M.T. Odman, and A.G. Russell. Re-examination of the 2003 North American electrical blackout impacts on regional air quality. *Geophysical Research Letters*, 33(22), 2006.

[76] L. Clancy, P. Goodman, H. Sinclair, and D.W. Dockery. Effect of air pollution control on death rates in Dublin, Ireland: an intervention study. *Lancet*, 360(9341):1210–1214, 2002.

[77] F. Kelly, H.R. Anderson, B. Armstrong, R. Atkinson, B. Barratt, S. Beevers, D. Derwent, D. Green, I. Mudway, P. Wilkinson, et al. The Impact of the Congestion Charging Scheme on Air Quality in London. *Health Effects Institute*, 155:5–71, 2011.

[78] M.S. Friedman, K.E. Powell, and L. Hutwagner. Impact of changes in transportation and commuting behaviors during the 1996 Summer Olympic Games in Atlanta on air quality and childhood asthma. *JAMA*, 285(7):897–905, 2001.

[79] J.L. Peel, M. Klein, W.D. Flanders, J.A. Mulholland, and P.E. Tolbert. Impact of Improved Air Quality During the 1996 Summer Olympic Games in Atlanta on Multiple Cardiovascular and Respiratory Outcomes. *Health Effects Institute*, 148:3–23, 2010.

[80] D.Q. Rich, H.M. Kipen, and W. Huang. Association between changes in air pollution levels during the Beijing Olympics and biomarkers of inflammation and thrombosis in healthy young adults. *JAMA*, 307(19):2068–2078, 2012.

[81] L. Li, P. Tang, and D.R. Cocker. Instantaneous nitric oxide effect on secondary organic aerosol formation from m-xylene photooxidation. *Atmospheric Environment*, 119:144–155, 2015.

[82] C.A. III Pope, D.L. Rodermund, and M.M. Gee. Mortality effects of a copper smelter strike and reduced ambient sulfate particulate matter air pollution. *Environmental Health Perspectives*, 115(5):679–683, 2007.

[83] Y. Hu, M.T. Odman, and A.G. Russell. Re-examination of the 2003 North American electrical blackout impacts on regional air quality. *Geophysical Research Letters*, 33(22), 2006.

[84] S. Henschel, R. Atkinson, A. Zeka, A. Le Tertre, A. Analitis, K. Katsouyanni, O. Chanel, M. Pascal, B. Forsberg, S. Medina, and P.G. Goodman. Air pollution interventions and their impact on public health. *International Journal of Public Health*, 57(5):757–768, 2012.

[85] L.R.F. Henneman, C. Liu, J.A. Mulholland, and A.G. Russell. Evaluating the effectiveness of air quality regulations: a review of accountability studies and frameworks. *Journal of the Air & Waste Management Association*, 67(2):144–172, 2016.

[86] A. Tobias, C. Carnerero, C. Reche, J. Massague, M. Via, M.C. Minguillon, A. Alastuey, and X. Querol. Changes in air quality during the lockdown in Barcelona (Spain) one month into the SARS-CoV-2 epidemic. *Science of The Total Environment*, 726:138540, 2020.

[87] G. He, Y. Pan, and T. Tanaka. The short-term impacts of COVID-19 lockdown on urban air pollution in China. *Nature Sustainability*, 2020.

[88] Y. Kambalagere. A study on air quality Index (AQI) of Bengaluru, Karnataka during lockdown period to combat coronavirus disease (Covid-19): air quality turns 'Better' from 'Hazardous'. *Science of The Total Environment*, 732:139281, 2020.

[89] Z.S. Venter, K. Aunan, S. Chowdhury, and J. Lelieveld. COVID-19 lockdowns cause global air pollution declines with implications for public health risk. *PNAS*, 117(32):18984–18990, 2020.

[90] N. Anjum. Good in the worst: Covid-19 restrictions and ease in global air pollution. *Preprints*, 2020.

[91] S. Mahato and K.G. Ghosh. Effect of lockdown amid COVID-19 pandemic on air quality of the megacity Delhi, India. *Science of The Total Environment*, 730:139086, 2020.

[92] A. Shrestha, U. Shrestha, R. Sharma, S. Bhattarai, H. Tran, and M. Rupakheti. Lockdown Caused by COVID-19 Pandemic Reduces Air Pollution in Cities Worldwide. EarthArXiv, 2020.

[93] M. Bauwens, S. Compernolle, T. Stavrakou, J.F. Muller, J. van Gent, H. Eskes, P.F. Levelt, A.R. van der, J.P. Veefkind, J. Vlietinck, H. Yu, and C. Zehner. Impact of coronavirus outbreak on NO2 pollution assessed using TROPOMI and OMI observations. *Geophysical Research Letters*, 47(11), 2020.

[94] K. Xu, K. Cui, L. Young, Y. Hsieh, Y. Wang, J. Zhang, and S. Wan. Impact of the COVID-19 event on air quality in central China. *Aerosol and Air Quality Research*, 20:5, 2020.

[95] F. Dutheil, J.S. Baker, and V. Navel. COVID-19 as a factor influencing air pollution, journal = Environmental Pollution. 263, 2020.

[96] R. Alfarra, J. Allan, K. Alzahrani, S. Alzahrani, H. Coe, C. Jay, N. Marsden, G. McFiggans, E. Reyes-Villegas, H. Rickets, J. Taylor, D. Topping, and T. Wu. Contribution to the aqeg/defra call for evidence. *Centre for Atmospheric Sciences and Computer Science*, 2020.

[97] R. Tanzer-Gruener, J. Li, S.R. Eilenberg, A. Robinson, and A. Presto. Impacts of modifiable factors on ambient air pollution: a case study of COVID-19 shutdowns. *Environmental Science & Technology Letters*, 7(8):554–559, 2020.

[98] J.D. Berman and K. Ebisu. Changes in U.S air pollution during the COVID-19 pandemic. *Science of The Total Environment*, 739:139864, 2020.

[99] D. L. Goldberg, S. C. Anenberg, D. Griffin, C. A. McLinden, Z. Lu, and D. G. Streets. Disentangling the impact of the COVID-19 lockdowns on urban NO2 natural variability. *Geophysical Research Letters*, 47(17), 2020.

[100] J. Xiang, E. Austin, T. Gould, T. Larson, J. Shirai, J. Marshall, and E. Seto. Impacts of the COVID-19 responses on traffic-related air pollution in a Northwestern US city. *Science of The Total Environment*, 747:141325, 2020.

[101] G. Dantas, B. Siciliano, B.B. Franca, and C.M. da Silva. The Impact of COVID-19 partial lockdown on the air quality of the city of Rio de Janeiro, Brazil. *Science of The Total Environment*, 729:139085, 2020.

[102] R. Bao and A. Zhang. Does lockdown reduce air pollution? Evidence from 44 cities in northern China. *Science of The Total Environment*, 731:139052, 2020.

[103] A. Kerimray, N. Baimatova, O.P. Ibragimova, B. Bukenov, B. Kenessov, P. Plotitsyn, and F. Karaca. Assessing air quality changes in large cities during COVID-19 lockdowns: the impacts of traffic-free urban conditions in Almaty, Kazakhstan. *Science of The Total Environment*, 730:139179, 2020.

[104] S. Sharma, M. Zhang, Anshika, J. Gao, H. Zhang, and S.H. Kota. Effect of restricted emissions during COVID-19 on air quality in India. *Science of The Total Environment*, 728:138878, 2020.

[105] K. Chen, M. Wang, C. Huang, P.L. Kinney, and P.T. Anastas. Air pollution reduction and mortality benefit during the COVID-19 outbreak in China. *Lancet*, 4:6, 2020.

[106] S. Kugel and R. Feeser. How the Pandemic is Changing Air Pollution. CBS News, April 2020. Available at: https://www.cbsnews.com/news/coronavirus-air-pollution-how-the-pandemic-is-changing-air-quality/.

[107] H. Regan. Lockdowns Lead to Air Pollution Drops in Major Cities. CNN, April 2020. Available at: https://edition.cnn.com/videos/world/2020/04/22/air-quality-cities-coronavirus-lon-orig-mrg.cnn.

[108] S. Lewis. Before-and-after Photos Show Dramatic Decline in Air Pollution Around the World During Coronavirus Lockdown. CBS News, April 2020. Available at: https://www.cbsnews.com/news/air-pollution-decline-photos-before-after-coronavirus-lockdown/.

[109] S. Hoeller. Before-and-after Photos Show the Dramatic Effect Lockdowns Are Having on Pollution Around the World. Insider, April 2020. Available at: https://www.insider.com/coronavirus-lockdowns-before-and-after-photos-of-pollution-2020-4.

[110] A. Freedman and L. Tierney. The Silver Lining to Coronavirus Lockdowns: Air Quality Is Improving. The Washington Post, April 2020. Available at: https://www.washingtonpost.com/climate-environment/2020/04/09/air-quality-improving-coronavirus/.

[111] P. Monks. Here's How Lockdowns Have Improved Air Quality Around the World. World Economic Forum, 2020. April 20.

[112] S. Mervosh, D. Lu, and V. Swales. See Which States and Cities Have Told Residents to Stay at Home. The New York Times, April 2020. Available at: https://www.nytimes.com/2020/04/20/us/coronavirus-stay-at-home-orders.html.

[113] Cal Fire. 2020 Statewide Fire Summary, 2020. Available at: https://www.fire.ca.gov/incidents/2020/.

[114] T. Fuller and J. Healy. As Wildfires Burn Out of Control, the West Coast Faces the Unimaginable. The New York Times, September 2020. Available at: https://www.nytimes.com/2020/09/13/us/wildfires-west-coast.html.

[115] M. Brauer, C. Lencar, L. Tamburic, M. Koehoorn, P. Demers, and C. Karr. A Cohort Study of Traffic-Related Air Pollution Impacts on Birth Outcomes. *Environmental Health Perspectives*, 116(5):680–686, 2008.

[116] M.A. Bravo, M. Fuentes, T. Zhang, M.J. Burr, and M.L. Bell. Comparison of Exposure Estimation Methods to Pollutants: Ambient Monitoring Data and Region Quality Simulation. *Environmental Research*, 116:1–10, 2012.

[117] J.D. Marshall. Environmental inequality: air pollution exposure in California's South Coast Air Basin. *Atmospheric Environment*, 42:5499–5503, 2008.

[118] H. Hersbach, B. Bell, P. Berrisford, G. Biavati, A. Horányi, J. Muñoz Sabater, J. Nicolas, C. Peubey, R. Radu, I. Rozum, D. Schepers, A. Simmons, C. Soci, D. Dee, and J.-N. Thépaut. ERA5 hourly data on single levels from 1979 to present. Copernicus Climate Change Service (C3S) Climate Data Store (CDS), 2018. Available at: https://cds.climate.copernicus.eu.

[119] B.J. Finlayson-Pitts and J.N. Pitts Jr. Atmospheric chemistry of tropospheric ozone formation: scientific and regulatory implications. *Air Waste*, 43(8):1091–1100, 1993.

[120] E. Badger and A. Parlapiano. Government Orders Alone Didn't Close the Economy. They Probably Can't Reopen It. The New York Times, May 2020. Available at: https://www.nytimes.com/2020/05/07/upshot/pandemic-economy-government-orders.html.

[121] Y. Quan, L.R.F. Henneman, J.A. Mulholland, and A.G. Russell. Empirical development of ozone isopleths: applications to Los Angeles. *Environmental Science & Technology*, 6(5):294–299, 2019.

[122] J.H. Seinfeld and S.N. Pandis. *Atmospheric Chemistry and Physics - From Air Pollution to Climate Change*. Wiley, 2016.

[123] S. Kim, M. Bechle, S. Hankey, L. Sheppard, A.A. Szpiro, and J.D. Marshall. Concentrations of criteria pollutants in the contiguous U.S. 1979-2015: role of prediction model parsimony in integrated empirical geographic regression. *PLoS ONE*, 15(2), 2020.

[124] M. Bechle, D.B. Millet, and J.D. Marshall. National spatiotemporal exposure surface for NO2: monthly scaling of a satellite-derived land-use regression, 2000–2010. *Environmental Science & Technology*, 49(20):12297–12305, 2015.

[125] E.V. Novotny, M.J. Bechle, D.B. Millet, and J.D. Marshall. National satellite-based land-use regression: NO2 in the United States. *Environmental Science & Technology*, 45(10):4407–4414, 2011.

[126] B. Feenstra, V. Papapostolou, S. Hasheminassab, H. Zhang, B. Der Boghossian, D. Cocker, and A. Polidori. Performance evaluation of twelve low-cost PM2.5 sensors at an ambient air monitoring site. *Atmospheric Environment*, 216:116946, 2019.

[127] C. Malings, R. Tanzer, A. Hauryliuk, P.K. Saha, A.L. Robinson, A.A. Presto, and R. Subramanian. Fine particle mass monitoring with low-cost sensors: corrections and long-term performance evaluation. *Aerosol Science and Technology*, 54(2):160–174, 2020.

[128] L.P. Clark, D.B. Millet, and J.D. Marshall. National patterns in environmental injustice and inequality: outdoor NO2 air pollution in the United States. *PLoS ONE*, 9(4), 2014.

[129] L.P. Clark, D.B. Millet, and J.D. Marshall. Changes in transportation-related air pollution exposure by race-ethnicity and socioeconomic status: outdoor nitrogen dioxide in the United States in 2000 and 2010. *Environmental Health Perspectives*, 125(9), 2017.

[130] Y. Zhao, A.T. Lambe, R. Saleh, G. Saliba, and A. Robinson. Secondary organic aerosol production from gasoline vehicle exhaust: effects of engine technology, cold start, and emission certification standard. *Environmental Science & Technology*, 52(3):1253–1261, 2018.

[131] A.W.H. Chan, K.E. Kautzman, P.S. Chhabra, J.D. Surratt, M.N. Chan, J.D. Crounse, A. Kurten, P.O. Wennberg, R.C. Flagan, and J.H. Seinfeld. Secondary organic aerosol formation from photooxidation of naphthalene and alkyl naphthalenes: implications for oxidation of intermediate volatility organic compounds (VOCs). *Atmospheric Chemistry Physics*, 9(9):2039–2060, 2009.

[132] C. Song, K. Na, and D.R. Cocker. Impact of the hydrocarbon to NOx ratio on secondary organic aerosol formation. *Environmental Science & Technology*, 39(9):3143–3149, 2005.

[133] N.L. Ng, J.H. Kroll, A.W.H. Chan, P.S. Chhabra, R.C. Flagan, and J.H. Seinfeld. Secondary organic aerosol formation from m-xylene, toluene, and benzene. *Atmospheric Chemistry and Physics*, 7(14):3909–3922, 2007.

[134] R. Bahreini, A.M. Middlebrook, J.A. de Gouw, C. Warneke, M. Trainer, C.A. Brock, H. Stark, S.S. Brown, W.P. Dube, J.B. Gilman, K. Hall, J.S. Holloway, W.C. Kuster, A.E. Perring, A.S.H. Prévôt, J.P. Schwarz, J.R. Spackman, S. Szidat, N.L. Wagner, R.J. Weber, P. Zotter, and D.D. Parrish. Gasoline emissions dominate over diesel in the formation of secondary organic aerosol mass. *Geophysical Research Letters*, 39:6, 2012.

[135] L.C. Marr and R.A. Harley. Spectral analysis of weekday-weekend differences in ambient ozone, nitrogen oxide, and non-methane hydrocarbon time series in California. *Atmospheric Environment*, 36(14):2327–2335, 2002.

[136] J. Apte, M. Brauer, A.J. Cohen, M. Ezzati, and C.A. Pope III. Ambient pm2.5 reduces global and regional life expectancy. *Environmental Science & Technology Letters*, 5(9):546–551, 2018.

[137] World Health Organization. Total Burden of Disease from Household and Ambient Air Pollution. World Health Organization, 2021. Available at: https://www.who.int/data/gho/data/themes/air-pollution.

[138] S.K. Thakrar, S. Balasubramanian, P.J. Adams, I.M.L. Azevedo, N.Z. Muller, S.N. Pandis, S. Polasky, C.A. III Pope, A.L. Robinson, J.S. Apte, C.W. Tessum, J.D. Marshall, and J.D. Hill. Reducing Mortality from Air Pollution in the United States by Targeting Specific Emission Sources. *Environmental Science & Technology Letters*, 7(9), 2020.

[139] Google Cloud Platform. *Google Cloud Kubernetes*. Google. Available at: https://cloud.google.com/kubernetes-engine.

[140] K.M. Foley, G.A. Pouliot, A. Eyth, M.F. Aldridge, C. Allen, K.W. Appel, J.O. Bash, M. Beardsley, J. Beidler, D. Choi, C. Farkas, R.C. Gilliam, J. Godfrey, B.H. Henderson, C. Hogrefe, S.N. Koplitz, R. Mason, R. Mathur, C. Misenis, N. Possiel, H.O.T. Pye, L. Reynolds, M. Roark, S. Roberts, D.B. Schwede, K.M. Seltzer, D. Sonntag, K. Talgo, C. Toro, J. Vukovich, J. Xing, and E. Adams. 2002-2017 Anthropogenic Emissions Data for Air Quality Modeling over the United States. *Data in Brief*, page 109022, 2023.

[141] M. M. Nasari, M. Szyszkowicz, H. Chen, D. Crouse, M. C. Turner, M. Jerrett, C. A. Pope, B. Hubbell, N. Fann, A. Cohen, S. M. Gapstur, W. R. Diver, D. Stieb, M. H. Forouzanfar, S. Y. Kim, C. Olives, D. Krewski, and R. T. Burnett. A class of non-linear exposure-response models suitable for health impact assessment applicable to large cohort studies of ambient air pollution. *Air Quality, Atmosphere & Health*, 9(8):961–972, 2016.

[142] R. Burnett, H. Chen, M. Szyszkowicz, N. Fann, B. Hubbell, C.A. Pope, J.S. Apte, M. Brauer, A. Cohen, S. Weichenthal, J. Coggins, Q. Di, B. Brunekreef, J. Frostad, S.S. Lim, H. Kan, K.D. Walker, G.D. Thurston, R.B. Hayes, C.C. Lim, M.C. Turner, M. Jerrett, D. Krewski, S.M. Gapstur, W.R. Diver, B. Ostro, D. Goldberg, D.L. Crouse, R.V. Martin, P. Peters, L. Pinault, M. Tjepkema, A. van Donkelaar, P.J. Villeneuve, A.B. Miller, P. Yin, M. Zhou, L. Wang, N.A.H. Janssen, M. Marra, R.W. Atkinson, H. Tsang, T.Q. Thach, J.B. Cannon, R.T. Allen, J.E. Hart, F. Laden, G. Cesaroni, F. Forastiere, G. Weinmayr, A. Jaensch, G. Nagel, H. Concin, and J.V. Spadaro. Global estimates of mortality associated with long-term exposure to outdoor fine particulate matter. *Proceedings of the National Academy of Sciences of the United States of America*, 115(38):9592–9597, 2018.

[143] D. Krewski, M. Jerrett, R. T. Burnett, R. Ma, E. Hughes, Y. Shi, M. C. Turner, C. A. III Pope, G. Thurston, and E. E. Calle. Extended follow-up and spatial analysis of the American Cancer Society study linking particulate air pollution and mortality. *Research Report - Health Effects Institute*, 140:5–136, 2009.

[144] U.S. Environmental Protection Agency. Acid Rain Program. U.S. Environmental Protection Agency, 1990. Available at: https://www.epa.gov/acidrain/acid-rain-program.

[145] U.S. Environmental Protection Agency. Cross-State Air Pollution Rule (CSAPR), 2011. Available at: https://www.epa.gov/csapr.

[146] Internal Revenue Service. Investment Tax Credit (ITC), 2006. Available at: https://www.energy.gov/eere/solar/federal-solar-investment-tax-credit-itc.

[147] U.S. Environmental Protection Agency. Tiered Vehicle Emission Standards (Tier 1, Tier 2, and Tier 3), 1994. Available at: https://www.epa.gov/regulations-emissions-vehicles-and-engines/final-rule-control-air-pollution-new-motor-vehicles-tier-3.

[148] U.S. Environmental Protection Agency. Clean Truck Program, 2008. Available at: https://www.epa.gov/regulations-emissions-vehicles-and-engines/clean-trucks-plan.

[149] U.S. Environmental Protection Agency. Diesel Emission Reduction Act (DERA), 2005. Available at: https://www.epa.gov/dera.

[150] Internal Revenue Service. Plug-In Electric Drive Vehicle Credit (EV Tax Credit), 2008. Available at: https://www.irs.gov/credits-deductions/individuals/plug-in-electric-drive-vehicle-credit-section-30d.

[151] U.S. Department of Agriculture, Natural Resources Conservation Service. Environmental Quality Incentives Program (EQIP), 1996. Available at: https://www.nrcs.usda.gov/wps/portal/nrcs/main/national/programs/financial/eqip/.

[152] U.S. Department of Agriculture, Economic Research Service. Precision Agriculture in the U.S., 2016. Available at: https://www.ers.usda.gov/topics/farm-practices-management/precision-agriculture/.

[153] World Health Organization. Household air pollution attributable DALYs. Available at: https://www.who.int/data/gho/data/indicators/indicator-details/GHO/household-air-pollution-attributable-dalys.

[154] M. Bentayeb, V. Wagner, M. Stempfelet, M. Zins, M. Goldberg, M. Pascal, S. Larrieu, P. Beaudeau, S. Cassadou, D. Eilstein, et al. Association between long-term exposure to air pollution and mortality in France: A 25-year follow-up study. *Environ. Int.*, 85:5–14, 2015.

[155] K.R. Smith. Indoor air pollution in developing countries: Recommendations for research. *Indoor Air*, 12:198–207, 2002.

[156] S.S. Lim, T. Vos, A.D. Flaxman, G. Danaei, K. Shibuya, H. Adair-Rohani, M. Amann, H.R. Anderson, K.G. Andrews, M. Aryee, et al. A comparative risk assessment of burden of disease and injury attributable to 67 risk factors and risk factor clusters in 21 regions, 1990–2010: A systematic analysis for the Global Burden of Disease Study 2010. *Lancet*, 380:2224–2260, 2012.

[157] E.D. Van Vliet, K. Asante, D.W. Jack, P.L. Kinney, R.M. Whyatt, S.N. Chillrud, L. Abokyi, C. Zandoh, and S. Owusu-Agyei. Personal exposures to fine particulate matter and black carbon in households cooking with biomass fuels in rural Ghana. *Environ. Res.*, 127:40–48, 2013.

[158] S.E. Bartington, I. Bakolis, D. Devakumar, O.P. Kurmi, J. Gulliver, G. Chaube, D.S. Manandhar, N.M. Saville, A. Costello, D. Osrin, et al. Patterns of domestic exposure to carbon monoxide and particulate matter in households using biomass fuel in Janakpur, Nepal. *Environ. Pollut.*, 220:38–45, 2016.

[159] A. Emmelin and S. Wall. Indoor air pollution: A poverty-related cause of mortality among the children of the world. *Chest*, 132:1615–1623, 2007.

[160] O.P. Kurmi, K.B. Lam, and J.G. Ayres. Indoor air pollution and the lung in low- and medium-income countries. *Eur. Respir. J.*, 40:239–254, 2012.

[161] M.L. Clark, J.L. Peel, K. Balakrishnan, et al. Health and household air pollution from solid fuel use: The need for improved exposure assessment. *Environ. Health Perspect.*, 121:1120–1128, 2013.

[162] N. Ramanathan, M. Lukac, T. Ahmed, et al. A cellphone-based system for large-scale monitoring of black carbon. *Atmos. Environ.*, 45:4481–4487, 2011.

[163] J.J. Caubel, T.E. Cados, and T.W. Kirchstetter. A new black carbon sensor for dense air quality monitoring networks. *Sensors*, 18(738), 2018.

[164] V. Jagatha, A. Klausnitzer, M. Chacón-Mateos, et al. Calibration method for particulate matter low-cost sensors used in ambient air quality monitoring and research. *Sensors*, 21:3960, 2021.

[165] M.R. Giardano, C. Malings, S.N. Pandis, et al. From low-cost sensors to high-quality data: A summary of challenges and best practices for effectively calibrating low-cost particulate matter mass sensors. *J. Aerosol Sci.*, 158:105833, 2021.

[166] E. Anastasiou, M.J.R. Vilcassim, J. Adragna, et al. Feasibility of low-cost particle sensor types in long-term indoor air pollution health studies after repeated calibration, 2019–2021. *Sci. Rep.*, 12:14571, 2022.

[167] L.P. Clark, V. Sreekanth, B. Bekbulat, M. Baum, S. Yang, P. Baylon, T.R. Gould, T.V. Larson, E.Y.W. Seto, and J.D. Marshall. Developing a Low-Cost Passive Method for Long-Term Average Levels of Light-Absorbing Carbon Air Pollution in Polluted Indoor Environments. *Sensors*, 20:3417, 2020.

[168] J.G. Watson, J.C. Chow, and L. Wa. Summary of organic and elemental carbon/black carbon analysis methods and intercomparisons. *Aerosol Air Qual. Res.*, 5:65–102, 2005.

[169] A. Karanasiou, M.C. Minguillon, M. Viana, A. Alastuey, J.P. Putaud, W. Maenhaut, P. Panteliadis, G. Mocnik, O. Favez, and T.A.J. Kuhlbusch. Thermal-optical analysis for the measurement of elemental carbon (EC) and organic carbon (OC) in ambient air—a literature review. *Atmos. Meas. Tech. Discuss.*, 8:9649–9712, 2015.

[170] L. Chippiani, S. Verlhac, R. Aujay, W. Maenhaut, J.P. Putaud, J. Sciare, L. Jaffrezo, C. Liousse, C. Galy-Lacaux, and L.Y. Alleman. Clues for a standardized thermal-optical protocol for the assessment of organic and elemental carbon within ambient air particulate matter. *Atmos. Meas. Tech.*, 7:1649–1661, 2014.

[171] G.A. Allen, J. Lawrence, and P. Koutrakis. Field validation of a semi-continuous method for aerosol black carbon (Aethalometer) and temporal patterns of summertime hourly black carbon measurements in southwestern PA. *Atmos. Environ.*, 33:817–823, 1999.

[172] R. Hitzenberger, A. Petzold, H. Bauer, P. Ctyroky, P. Pouresmaeil, L. Laskus, and H. Puxbaum. Intercomparison of thermal and optical measurement methods for elemental carbon and black carbon at an urban location. *Environ. Sci. Technol.*, 40:6377–6383, 2006.

[173] V. Lalchandani, S.N. Tripathi, E.A. Graham, N. Ramanathan, J.J. Schauer, and T. Gupta. Recommendations for calibration factors for a photo-reference method for aerosol black carbon concentrations. *Atmos. Pollut. Res.*, 7:75–81, 2016.

[174] D.A. Lack, H. Moosmüller, G.R. McMeeking, R.K. Chakrabarty, and D. Baumgardner. Characterizing elemental, equivalent black, and refractory black carbon aerosol particles: A review of techniques, their limitations and uncertainties. *Anal. Bioanal. Chem.*, 406:99–122, 2014.

[175] M.R. Olson, E. Graham, S. Hamad, P. Uchupalanun, N. Ramanathan, and J.J. Schauer. Quantification of elemental and organic carbon in atmospheric particulate matter using color space sensing—hue, saturation, and value (HSV) coordinates. *Sci. Total Environ.*, 548–549:252–259, 2016.

[176] T. Sayahi, A. Butterfield, and K.E. Kelly. Long-term field evaluation of the Plantower PMS low-cost particulate matter sensors. *Environmental Pollution*, 245:932–940, 2019.

[177] K. Ardon-Dryer, Y. Dryer, J.N. Williams, and N. Moghimi. Measurements of $PM_{2.5}$ with PurpleAir under atmospheric conditions. *Atmospheric Measurement Techniques*, 13:5441–5458, 2020.

[178] I. Stavroulas, G. Grivas, P. Michalopoulos, E. Liakakou, A. Bougiatioti, P. Kalkavouras, K.M. Fameli, N. Hatzianastassiou, N. Mihalopoulos, and E. Gerasopoulos. Field Evaluation of Low-Cost PM Sensors (Purple Air PA-II) Under Variable Urban Air Quality Conditions, in Greece. *Atmosphere*, 11(926), 2020.

[179] J. Tryner, C. L'Orange, J. Mehaffy, D. Miller-Lionberg, J.C. Hofstetter, A. Wilson, and J. Volckens. Laboratory evaluation of low-cost PurpleAir PM monitors and in-field correction using co-located portable filter samplers. *Atmospheric Environment*, 220:117067, 2020.

[180] B.I. Magi, C. Cupini, J. Francis, M. Green, and C. Hauser. Evaluation of $PM_{2.5}$ measured in an urban setting using a low-cost optical particle counter and a Federal Equivalent Method Beta Attenuation Monitor. *Aerosol Science and Technology*, 54:147–159, 2020.

[181] T. K. Koo and M. Y. Li. A guideline of selecting and reporting intraclass correlation coefficients for reliability research. *Journal of Chiropractic Medicine*, 15:155–163, 2016.

[182] N. Good, A. Molter, J. Peel, and J. Volckens. An accurate filter loading correction is essential for assessing personal exposure to black carbon using aethalometer. *J. Expo. Sci. Environ. Epidemiol.*, 27:409–416, 2017.

[183] T.W. Kirchstetter and T. Novakov. Controlled generation of black carbon particles from a diffusion flame and applications in evaluating black carbon measurement methods. *Atmospheric Environment*, 41:1874–1888, 2007.

[184] A.T. Weakley J. Giacomo X. Zhang N. Hyslop A.M. Dillner M. Shupler M. Jeronimo, Q. Steward and M. Brauer. Analysis of black carbon on filters by image-based reflectance. *Atmospheric Environment*, 223:117300, 2020.

[185] M. E. Birch. Analysis of carbonaceous aerosols: Interlaboratory comparison. *Analyst*, 123:851–857, 1998.

[186] M. E. Birch. Analytical instrument performance criteria: Occupational monitoring of particulate diesel exhaust by NIOSH method 5040. *Applied Occupational and Environmental Hygiene*, 17:400–405, 2002.

[187] J. T. Deminter G. Heidemann M. S. Bae J. H. Seinfeld R. C. Flagan R. A. Cary D. Smith B. J. Huebert J. J. Schauer, B. T. Mader et al. ACE-Asia inter-comparison of a thermal-optical method for the determination of particle-phase organic and elemental carbon. *Environmental Science & Technology*, 37:993–1001, 2003.

[188] L. Emblico, F. Cavalli, T. Hafkenscheid, and A. Borowiak. Results of the First EC/OC Comparison Exercise for EU National Air Quality Reference Laboratories (AQUILA). Technical report, JRC Technical Reports, Publications Office of the European Union, 2012.

[189] R. Aujay W. Maenhaut J.P. Putaud J. Sciare L. Jaffrezo C. Liousse C. Galy-Lacaux L. Chippiani, S. Verlhac and L.Y. Alleman. Clues for a standardized thermal-optical protocol for the assessment of organic and elemental carbon within ambient air particulate matter. *Atmos. Meas. Tech.*, 7:1649–1661, 2014.

[190] M. E. Birch M. Chai and G. Deye. Organic and elemental carbon filter sets: Preparation method and interlaboratory results. *Annals of Occupational Hygiene*, 56:959–967, 2012.

[191] P. Panteliadis, T. Hafkenscheid, B. Cary, E. Diapouli, A. Fischer, O. Favez, P. Quincey, M. Viana, R. Hitzenberger, R. Vecchi, et al. ECOC comparison exercise with identical thermal protocols after temperature offset correction—Instrument diagnostics by in-depth evaluation of operational parameters. *Atmospheric Measurement Techniques*, 8:779–792, 2015.

[192] X. Liu, R. Jayaratne, P. Thai, T. Kuhn, I. Zing, B. Christensen, R. Lamont, M. Dunbabin, S. Zhu, J. Gao, et al. Low-cost sensors as an alternative for long-term air quality monitoring. *Environmental Research*, 185:109438, 2020.

[193] R. A. Fisher. A mathematical examination of the methods determining the accuracy of observation by the mean error, and by the mean square error. *Monthly Notices of the Royal Astronomical Society*, 80:758–770, 1920.

[194] M. Zusman, C. S. Schumacher, A. J. Gassett, E. W. Spalt, E. Austin, T. V. Larson, G. Carvlin, E. Seto, J. D. Kaufman, and L. Sheppard. Calibration of low-cost particulate matter sensors: Model development for a multi-city epidemiological study. *Environmental International*, 134:105329, 2020.

[195] H. Khreis, J. Johnson, K. Jack, B. Dadashova, and E.S. Park. Evaluating the Performance of Low-Cost Air Quality Monitors in Dallas, Texas. *International Journal of Environmental Research and Public Health*, 19(1647), 2022.